Report Prepared by :

Lianfang Li
Alberto A. Sagüés

METALLURGICAL EFFECTS ON CHLORIDE ION CORROSION THRESHOLD OF STEEL IN CONCRETE

State Job 99700-3373-010, WPI 0510806
Contract No. BA501
Final Report to Florida Department of Transportation

Alberto A. Sagüés
Principal Investigator
Department of Civil and Environmental Engineering
November 30, 2001

University of South Florida
Tampa, FL, 33620

Technical Report Documentation Page

1. Report No.	2. Government Accession No.	3. Recipient's Catalog No.
WPI 0510806		

4. Title and Subtitle

METALLURGICAL EFFECTS ON CHLORIDE ION CORROSION THRESHOLD OF STEEL IN CONCRETE

5. Report Date
November, 2001

6. Performing Organization Code

8. Performing Organization Report No.

7. Author's

Lianfang Li, Alberto A. Sagüés,

9. Performing Organization Name and Address

Department of Civil and Environmental Engineering
University of South Florida
Tampa, FL 33620

10. Work Unit No. (TRAIS)

11. Contract or Grant No.
BA501

13. Type of Report and Period Covered

Final Report
August 1995 - April 2001

12. Sponsoring Agency Name and Address

Florida Department of Transportation
605 Suwannee Street
Tallahassee, FL 32399-0450

14. Sponsoring Agency Code

15. Supplementary Notes
Prepared in cooperation with the U.S. Department of Transportation and the Federal Highway Administration

16. Abstract

The chloride-induced corrosion of reinforcing steel bars (rebar) in concrete seriously limits durability of reinforcing concrete structures. This investigation examines key issues in pitting corrosion and chloride corrosion threshold of rebar in alkaline solutions ($[Cl^-]_T$).The effect of rebar surface condition on $[Cl^-]_T$ values was evaluated using the open-circuit immersion method (OCI). Results indicate that sandblasted rebar had higher $[Cl^-]_T$ values than as-received or prerusted rebar. The threshold chloride-to-hydroxide ratio (CR_T) increased with pH, suggesting that the intrinsic inhibiting effect of hydroxide ions was stronger at higher $[OH^-]$ levels. Ranges of total chloride threshold in concrete (C_{TT}) were estimated based on $[Cl^-]_T$ from liquid solution measurements and on available chloride binding data, and were found to be consistent with values observed in practice. The effect of several important factors ($[Cl^-]$, pH, rebar surface finish, polarization scan rate, passive film maturity, specimen size) on pitting (E_p) and repassivation (E_r) potentials in alkaline solutions (pH11.6 to 13.6) was investigated with the cyclic polarization technique (CYP). It was found that E_p was not a unique function of the test condition and that its variability tended to increase with decreasing chloride-to-hydroxide ratio. The average value of E_p in replicate tests decreased with solution $[Cl^-]$, specimen size, and steel surface roughness but increased with solution $[OH^-]$ and passive film maturity. In contrast, E_r was nearly insensitive to those parameters. The functional form of the distribution of E_p for a given solution and steel surface condition was not clearly apparent. The dependence of E_p on specimen size was explained using stochastic pitting initiation theory. The passivation behavior of rebar steel in alkaline solutions (pH 8.2 to 13.6) was also explored. Recomendations included: incorporating a C_{TT} variability term in future service life predicition procedures; using a representatively large exposed steel surface area for future testing to determine C_{TT}; performing exploratory cost/benefit analyses to assess possible use of sandblasted rebar surfaces and performing corresponding tests in concrete; careful assessment of effect of lowering pore water pH in new concrete formulations, and taking into consideration potential dependence of C_{TT} in future durability models.

17. Key Words	18. Distribution Statement
Reinforcing Steel, Corrosion, Chlorides, Pitting, Threshold, Potential, Concrete	No restrictions. This document is available to the public through the National Technical Information Service, Springfield, VA 22161

19. Security Classif.(of this report)	20. Security Classif. (of this page)	21. No. of Pages	22. Price
Unclassified	Unclassified	119	

Form DOT F 1700.7 (8-72)

TABLE OF CONTENTS

NOTICE

The opinions, findings and conclusions expressed in this publication are those of the authors and not necessarily those of the State of Florida Department of Transportation or the U.S Department of Transportation.

Prepared in cooperation with the State of Florida Department of Transportation and the U.S. Department of Transportation.

EXECUTIVE SUMMARY

FDOT uses the chloride ion corrosion threshold as a key parameter in assessing the time to corrosion initiation in marine substructure, and to compare against the amount of chloride contamination that may exist in other cementitious media such as the grout surrounding post-tensioned high strength steel strands. This investigation obtained in-depth understanding of the fundamental causes of corrosion initiation in alkaline media, focusing on the effect of the condition of the metal surface and the statistical nature of the processes involved.

Open-circuit immersion tests investigated the effect of metal surface condition on the chloride corrosion threshold ($[Cl^-]_T$). Removing mill scale or any rust from the rebar surface by sandblasting elevated $[Cl^-]_T$ to about twice the value of as-received or prerusted steel. The threshold chloride-to-hydroxide ratio increased with pH, suggesting that the intrinsic inhibiting effect of hydroxide ions is stronger at higher concentration of those ions. Ranges of total chloride threshold in concrete (C_{TT}) were estimated based on the liquid solution measurements and on available chloride binding data. The values thus estimated were consistent with those observed in practice in concrete.

The effects of chloride content, pH, steel surface finish, scan rate, and passive film maturity on the distribution of pitting and repassivation potentials were examined with the cyclic polarization technique. The value of the pitting potential was found not to be a unique function of solution composition or steel surface condition, so a statistical approach was used to analyze results. The variability tended to decrease at high values of the chloride-to-hydroxide ratio. The average value of the pitting potential for a series of replicate tests decreased with chloride content and steel surface roughness but increased with hydroxide ion content and passive film maturity. In contrast, the repassivation potential was nearly independent of solution composition and steel surface finish but found to depend on the severity of corrosion that took place during the return scan of the polarization cycle.

For most of the conditions examined, the average pitting potential was found to decrease significantly as the nominal specimen surface area increased. Neither the relative variability of the pitting potential, nor the value of the repassivation potential were strongly affected by the specimen surface area. The experimental observations were in reasonable agreement with the prediction of the stochastic pitting initiation theory. The passivation process of rebar steel in alkaline solutions was found to be gradual and in agreement with the observation that the pitting potential increased with prepassivation time. The steady-state corrosion current density of passive rebar steel in alkaline solutions was estimated to be 0.01~0.001 $\mu A/cm^2$.

Recomendations based on the findings of this investigtion included: incorporating a C_{TT} variability term in future service life predicition procedures; using a representatively large exposed steel surface area for future testing to determine C_{TT}; performing exploratory cost/benefit analyses to assess possible use of sandblasted rebar surfaces and performing corresponding tests in concrete; performing careful assessment of effect of lowering pore water pH in new concrete formulations, and taking into consideration potential dependence of C_{TT} in future durability models.

CHAPTER 1: LITERATURE REVIEW

1.1 Background

Steel reinforced concrete has been in extensive use for over a century because it is normally a versatile, economical and durable construction material. Embedding reinforcing steel bars (rebar) in concrete not only renders the structure with optimal strength but also provides the rebar with a protective environment. The highly alkaline environment of concrete (normally with pore water pH>13) results in the formation of a dense, metal-adherent oxide film on the rebar surface and hence maintains its corrosion rate at a negligible level. However, carbonation of concrete (by reducing pore water pH below ~9) can induce loss of passivity and cause the steel to corrode at significant rates. Chloride ion contamination is even more detrimental in breaking down passivity.

Corrosion of steel in concrete has received increasing attention in the last three decades because of its widespread occurrence and the high cost of repairs. The corrosion of steel reinforcement has been widely observed in marine structures, chemical manufacturing plants, bridge decks, parking structures, underground pipes, etc. According to a Transportation Research Board Report (1991), the annual cost of bridge deck repairs due to deicing salts only was estimated to be $50 to $200 million, with substructures and other components requiring $100 million a year and a further $50 to $150 million a year on multistory car parks.

Chloride ions are the major cause for the corrosion of steel reinforcement in concrete. There are several ways by which chlorides can be introduced into concrete. Chlorides may exist at small levels within the mix ingredients of concrete (e.g. aggregates), or may be introduced by using a chloride-containing admixture (e.g. calcium chloride as an accelerator) or saline water as mixing water where fresh water is not available. However, chlorides in concrete most often come from the service environment to which the concrete structure is exposed, such as deicing salt or marine environment.

Investigations on the chloride-induced corrosion of reinforcing steel in concrete have been widely documented. However, there are two important issues still unresolved. First, does the chloride have to reach a critical level (often called “chloride threshold”) for steel in concrete to corrode? Secondly, if there is such a chloride threshold, how can that threshold be quantified and how is that affected by the condition of the steel itself and by the surrounding environment? Before a detailed discussion of these two issues, a basic review of the concrete chemistry and the corrosion process of steel in concrete is warranted.

1.2 The Structure and Chemistry of Concrete and Cement Paste

1.2.1 Hydration Products

Concrete is a composite material of coarse granular material (the aggregate or filler) embedded in a hard matrix of material (the cement or binder) that fills the space between the aggregate particles and bonds them together (Mindness and Young, 1981). The aggregate phase is predominantly responsible for the unit weight, elastic modulus, and dimensional stability of concrete. Those properties of concrete are determined mainly by the physical rather

than chemical characteristics of the aggregate structure. On the other hand, the hardened cement (most often 'Portland cement') paste, is a porous material that not only affects the physical properties but also the chemical properties of the concrete.

The hydration products of Portland cement consist mainly of calcium silicate hydrates (abbreviated for C-S-H) and calcium hydroxide ($Ca(OH)_2$). The C-S-H is poorly crystallized and is not a well-defined compound; its C/S ratio varies between 1.5 to 2.0 and its structural water content varies even more. The C-S-H makes up 50 to 60 percent of the solid volume in a completely hydrated paste and is, therefore, the most important constituent in determining the properties of the paste (Mehta and Monteiro, 1993). However, C-S-H does not control the pore water chemistry because of its nearly insoluble nature.

On the other hand, calcium hydroxide is well crystallized and has a definite stoichiometry. It constitutes 20% to 25% of the solid volume in the cement paste. Considering the large availability of $Ca(OH)_2$ and the limited pore volume, the concrete pore water is often saturated with $Ca(OH)_2$. In the absence of other soluble species, the pH of the saturated $Ca(OH)_2$ solution (hereafter denoted by SCS) at 25 ºC is ~12.4 (CRC, 1973).

1.2.2 Hydroxide Concentration in the Pore Water

Interestingly, the pore water pH is most often not determined by $Ca(OH)_2$, but by the small quantity (normally less than 1%) of alkalis existing in the cement clinker. Those alkalis are expressed analytically in terms as K_2O and Na_2O but are actually present either as alkali sulfates or alkali-calcium sulfates, or in solid solution within certain compounds of the cement. Much of the alkali content, especially that present as alkali sulfate, is readily soluble in the mixing water. The reaction can be expressed (Bakker, 1988) as

$$Na_2SO_4 + Ca(OH)_2 \rightarrow CaSO_4 + 2\ NaOH \qquad (1.1)$$

$$K_2SO_4 + Ca(OH)_2 \rightarrow CaSO_4 + 2\ KOH \qquad (1.2)$$

As a result of the above reactions, a large amount of Na^+, K^+, and OH^- ions are released into pore water. Table 1.1 gives a typical composition of pore solution expressed from cement paste with a water-to-cement ratio (w/c) of 0.5 (Constantiner et al. 1997).

From Table 1.1, it can be seen that Na^+ and K^+ ions are the main cations and OH^- ions are the main anions. The concentration of Ca^{2+} ions is normally very low. The $[OH^-]$ in the pore water is mainly controlled by the alkali content in the cement and the w/c of the mixing material. The $[OH^-]$ is nearly balanced by the $[Na^+]$ and $[K^+]$. Table 1.2 gives experimental data from the literature showing the $[Na^+]$, $[K^+]$, and $[OH^-]$ in the pore water of cement paste or mortar prepared using cement of various alkali contents and w/c ratios. In Figure 1.1, the pore water $[OH^-]$ is plotted against the normalized equivalent Na_2O content in the cement, which is obtained by dividing the total equivalent Na_2O content ($=Na_2O\%+0.66K_2O\%$) by the w/c ratio. It is clearly seen that the pore water $[OH^-]$ is approximately in linear relationship with the normalized equivalent Na_2O content. In other words, the higher the equivalent Na_2O content in the cement (and/or the lower the w/c ratio), the higher will be the pore water $[OH^-]$. The typical

pH of concrete pore water is about 13, and pH as high as 13.5 has been reported for concrete in Florida (Li et al., 1999 a).

1.2.3 Chloride Concentration in the Pore Water

Actually not all the alkali ions present in the cement are dissolved into the pore water, otherwise the pore water [OH^-] would be much higher. The same is true of chlorides in concrete. Only a part of the total amount of chlorides (often called "total chloride", denoted as C_T hereafter, given as the weight percentage of cement in a mix) exists in the pore water, with the remaining chlorides being chemically or physically bound with the cement paste (often called "bound chloride", denoted as C_B). The chloride present in the pore water is called "free chloride", and its concentration will be denoted as $[Cl^-]_f$ (in mol/L). The tricalcium aluminate ($3CaO{\cdot}Al_2O_3$, abbreviated for C_3A) and tetra-calcium aluminoferrite ($4CaO{\cdot}Al_2O_3{\cdot}Fe_2O_3$, abbreviated for C_4AF) in the cement are believed to be mainly responsible for the binding of chlorides by the formation of the insoluble "Friedel's salt, $3CaO{\cdot}Al_2O_3{\cdot}CaCl_2{\cdot}10H_2O$, and its ferrite analogue, ($3CaO{\cdot}Fe_2O_3{\cdot}CaCl_2{\cdot}10H_2O$), respectively (Rasheeduzzafar et al.,1992). The binding capability of the concrete mainly depends on the composition and content of the cement in the mix. However, there is no unique relationship between C_T and $[Cl^-]_f$. By regression analysis of chloride binding data in the literature, Larsen (1998) proposed a numerical relationship between total chloride and the average $[Cl^-]_f$ as follows:

$$C_{Cl,T} = 19.34 \cdot [Cl^-]_f^{0.56} \qquad (1.3)$$

where $C_{Cl,T}$ is the total chloride content in grams per kilogram of cement. If the total chloride content is expressed as C_T, Eq.(1.3) can be expressed as:

$$C_T = 1.934 \cdot [Cl^-]_f^{0.56} \qquad (1.4)$$

According to Eq.(1.4), when C_T=2%, the pore water free chloride concentration is likely to be close to 1.0M. However, Eq.(1.3) is only valid for $[Cl^-]_f \leq 1.0M$ and mainly represents water-saturated concrete. The actual $[Cl^-]_f$ in concrete mixes with same C_T can be significantly different from that calculated with Eq.(1.3) either due to differences in cement chemical composition or in environment humidity.

1.3 Corrosion of Steel in Concrete
1.3.1 Sequence of Corrosion

The corrosion sequence of steel in concrete can be appropriately described by the model proposed by Tuutti (1982), which is schematically shown in Figure 1.2. The first stage is called the initiation period. During that period, steel is mainly in the passive condition with negligible corrosion rate. The second period is called the propagation stage. During that stage, corrosion of steel proceeds at a significant rate until the stress build-up from the accumulation of corrosion products causes the cracking or even spalling of the concrete cover. At the end of the propagation period, replacement or repair of the concrete structure is necessary.

1.3.2 Mechanism of Chloride-Induced Corrosion Propagation

The chloride-induced corrosion of steel in concrete is often localized. The corrosion process then involves two separate, but coupled electrochemical reactions which take place simultaneously at different sites on the steel surface. Figure 1.3 schematically illustrates that process. After pitting is initiated, the dissolution of iron inside the corrosion pit can be described with the following anodic reaction:

$$Fe \rightarrow Fe^{2+} + 2\,e^{-} \qquad (1.5)$$

The electrons produced per Eq.(1.5) will be transported to the passive zone of the steel surface (where the potential is more positive than inside the pit) where they are consumed by the oxygen reduction reaction as:

$$\tfrac{1}{2}\,O_2 + H_2O + 2\,e^{-} \rightarrow 2\,OH^{-} \qquad (1.6)$$

It can be seen that oxygen and water are essential to the corrosion process. Since concrete is a porous material, there usually is (except for concrete immersed in water or buried in humid soil or silt) fast enough oxygen transport for reaction (1.6) to proceed. Another significant factor is that the area of anodic reaction (Fe dissolution) is much smaller than the area for the cathodic reaction (oxygen reduction). Consequently, a small amount of oxygen inside the concrete may enable the steel to corrode at very severe local rates. Finally, for the whole corrosion process to be sustained, ionic transport inside the concrete (more accurately, inside the pore water) is required so that the flow of current is completed. Since concrete pore water is a strong electrolyte (even stronger in the presence of chloride), normally there is no difficulty in supplying the ionic current by the transport of soluble species. The corrosion product is formed by the reaction of Fe^{2+} with OH^{-} and O_2 followed by precipitation after transport to the outside of the pit. The corrosion product is porous and hence ionic species such Cl^{-} can usually pass through this layer without difficulty.

The above localized corrosion process can also be illustrated with a simplified Evans diagram (Figure 1.4). When there is no chloride, the anodic polarization of iron can be represented by curve A; steel maintains passivity in a wide potential range. When pitting corrosion initiates due to chloride ions, the anodic polarization curve is represented by curve B, showing the active dissolution of iron inside the pit (for simplicity, the difference in area between anodic and cathodic regions is not addressed in these diagrams). In either condition, oxygen reduction is the main cathodic process as represented by curve C. When there is no (or not enough) chloride in the concrete, curves A and C intersect at point 1, which indicates that steel is passive with a very low corrosion rate (i_{corr1}) and a noble corrosion potential (E_{corr1}). However, when pitting corrosion takes place, curves B and C intersect at point 2, which means that steel corrodes at a much faster rate (i_{corr2}) and a more active potential (E_{corr2}). During the actual localized corrosion of steel in concrete, the ionic current flow in concrete is often accompanied by a significant IR drop (also called ohmic drop) because of the high resistivity of concrete. Consequently, the potential of the anodic zone (E_{corr3a}) will be different from that of the cathodic zone (E_{corr3c}), as shown in Fig.1.4. For that reason, the active corrosion zone of the steel in concrete can be easily differentiated from the passive zone by

simply mapping the corrosion potential of the steel structure. The IR drop also results in the corrosion current density drop from i_{corr2} to i_{corr3}. From that point of view, an increase of the concrete resistivity can reduce the corrosion rate and hence extend the service life of concrete structure because the propagation period will be effectively augmented. This beneficial effect has already been put into practical usage. For example, concrete structures exposed to severe environments are now often made using a concrete mix design which has very low w/c ratio, and using fly ash and/or silica fume as cement replacement to reduce the porosity of concrete. These changes in mix design not only increase the concrete resistivity, but also extend the initiation period by delaying the transport of chlorides from outside environment.

1.4 The Total Chloride Corrosion Threshold in Concrete (C_{TT})

The previous section addressed only the steady-state active corrosion process during the propagation stage. What has not been addressed is when and how the passive film on steel surface is broken down, or what is the critical amount of chloride (often called the chloride threshold) needed to initiate pitting corrosion. The above issues are directly related to the initiation period of the corrosion sequence as illustrated in Fig.1.2. The mechanism for pitting initiation (especially for stainless steels in chloride-containing solutions) has received much attention in the last 50 years (Szklarska-Smialowska 1986, Frankel 1998). Although several models have been proposed, a clear picture of the pitting initiation mechanism is still unavailable. This is partly because the passive film on metal surfaces normally has a thickness of only about several nanometers. Thus, an accurate characterization of the structure and composition of the passive film and its breakdown is very difficult. In the case of reinforcing steel in concrete, the thick concrete cover renders the *in situ* study of the passive film and how the chloride breaks down that film almost impossible with the techniques currently available.

Knowledge of the magnitude of the chloride threshold and how that threshold is affected by internal and external factors is of practical significance. Such information not only enables designers to set a guideline as to how much is the allowable chloride content in concrete so that precautions can be taken during the design and making of concrete, but also, if it is known that some factors have detrimental effects, measures may be taken beforehand to avoid or reduce their influence. Conversely, if there exist some factors which raise the threshold, designers may capitalize on those factors to the maximum efficiency so that the service life of a structure can be extended. This investigation seeks to increase the knowledge and understanding of these issues.

It is often observed that corrosion of steel in concrete (both field structures and laboratory specimens) only seems to start when C_T reaches a certain level. Figure 1.5 shows a typical example (Thomas, 1996) concerning the relationship between rebar mass loss and C_T at the bar location for reinforced concrete prisms after one to four years of field exposure. It can be seen that the corrosion was negligible when $C_T \leq$ ~0.4%. Similar observations lead to the concept of a total chloride threshold (denoted as C_{TT}).

Glass and Buenfeld (1997) have reviewed the C_{TT} values reported for steel embedded in concrete structures in the field and for steel in concrete and mortar specimens exposed to laboratory and outdoor environments, with results presented in Table 1.3. From this table, it

can be seen that a universal, well-defined C_{TT} value does not appear to exist. The lowest limit of C_{TT} was ~0.2% whereas the highest was ~2.5%, a difference of more than 10 times. C_{TT} has been found to be affected by many factors, the most important of which are listed in Figure 1.6. For example, corrosion initiation can be directly affected by the chemical composition of rebar itself. It has been reported that the iron and manganese sulfide inclusions in the steel pose a high risk for pitting initiation (Szklarska-Smialowska, 1972). Reinforcing steel is usually made of scrap metals, and the ASTM A615/A615M specification for reinforcing steel only prescribes that the phosphorus content be less than 0.05% whereas the contents of other elements are not restricted as long as the tensile strength and ductility of the steel are satisfied. The rebar surface finish is also expected to affect C_{TT} since the more homogeneous the surface is, both chemically and physically, the higher the pitting potential (Szklarska-Smialowska, 1986). Consequently, agreement between C_{TT} obtained from specimens using the as-received, mill scale covered rebar (often called “black bar”) and C_{TT} obtained from specimens using highly surface finished rebar (sometimes polished to a mirror-like finish (Thanggavel, 1998)) is unlikely.

Externally, corrosion initiation is controlled by the chemistry of both the concrete and its exposure environment. Any significant change in some of the factors listed in Fig. 1.6 can affect the pore solution chemistry and hence C_{TT}. For example, a difference in the type of cement used or a significant variation in the alkali content of the same type of cement can greatly affect the alkalinity of the concrete. The type of chloride-bearing salt (NaCl vs. $CaCl_2$) is directly related to the pore solution pH and chloride concentration and hence C_{TT}. As a result of these and other influences, treating C_{TT} as a universal parameter to quantify the corrosion threshold is inappropriate. Another important issue is whether even for specific exposure and materials conditions the threshold is a precisely defined value or it should be viewed instead in statistical terms.

Nevertheless, as a matter of practice, most specifications and guidelines usually consider a universal and deterministic value of C_{TT} to set the allowable chloride limit. It is commonly recommended that C_T be lower than ~ 0.2% (Bentur et al., 1997), as is for example the limit for internal chloride set by the British Standard Institution (1985) for concrete made with cement complying with BS 4027 and BS 4208. The present specifications for chloride content recommended by the American Concrete Institute (ACI 1999) are listed in Table 1.4, which sets a more stringent limit for prestressed concrete than for conventionally reinforced concrete.

1.5 The $[Cl^-]$ to $[OH^-]$ Ratio Threshold (CR_T)
1.5.1 Behavior of Steel in Alkaline Solutions

It is generally believed that the free chloride in the concrete pore solution is responsible for the corrosion initiation whereas the hydroxide ions in the pore solution play an opposing role and tend to stabilize the passive film. Therefore, the chloride-to-hydroxide ratio (defined as $CR = [Cl^-]/[OH^-]$) is an important parameter in evaluating the behavior of steel. However, it is difficult to accurately determine the $[Cl^-]$ and $[OH^-]$ in concrete pore solution, especially at the rebar level. To gain insight on the relative proportions leading to corrosion initiation, several laboratory investigations of the effect of OH^- and Cl^- on the corrosion behavior of reinforcing

steel have been carried out in model alkaline solutions such as saturated $Ca(OH)_2$ (SCS), pure NaOH or KOH solution, and simulated concrete pore solutions (SPS). A literature review of the behavior of pure iron and carbon steel (mostly reinforcing steel) in alkaline solutions (pH 10 to 14) is presented in Table 1.5. For reasons that have been emphasized earlier, the most important experimental conditions (e.g. specimen size and surface finish, experimental techniques), if available, are also included in that table.

It is difficult to compare the results of the different investigations listed in Table 1.5, because of the different experimental conditions used. A quantitative and graphical presentation of those results will be nevertheless helpful to yield some insight on the effect of the $[Cl^-]$ and $[OH^-]$. For that purpose, the following assumptions and conversions are made:

1) The condition of steel is in one of three states: passive, corrosion, or non-sustained corrosion. (The "non-sustained corrosion" state is assigned to steel which was passive for most of the experimental period but its E_{corr} and i_{corr} infrequently fluctuated in the active direction.)

2) Passive steel in concrete exposed to humid environment normally develops an open circuit potential (E_{oc}) rarely higher than 0V/SCE (Schiessl 1988). Therefore, if tests were performed with potentiodynamic polarization instead of open-circuit immersion, the steel is assumed to be passive if its pitting potential (E_p) was nobler than 0V/SCE. Otherwise, the steel is assumed to have been under active corrosion.

3) Results from Dawson (1988) and Joiret et al. (1999) were interpreted as meaning the steel was passive, although the authors suggested otherwise. The passive current densities in their experiments were slightly higher than in chloride-free solutions. However, no definite pitting potential or hysteresis loop due to pitting initiation was observed on their cyclic polarization curves, which strongly suggests that the steel had not corroded.

4) When the testing temperature was not reported, it is assumed that tests were conducted at 25ºC, so that the water dissociation constant (k_w) was assumed to be 10^{-14}.

5) When $[OH^-]$ was not given, it was calculated using k_w and assuming the activity coefficient of OH^- (γ) to be 0.7(CRC 1973). (Although γ of a pure pH 11 NaOH solution is closer to 1 than to 0.7, it could be much lower than unity as the solution ionic strength increases due to the presence of chlorides.)

6) If $CaCl_2$ was used as a source of chlorides but the solution pH or the equilibrium $[OH^-]$ of that solution was not given, $[OH^-]$ was evaluated by employing the solubility product of $Ca(OH)_2$.

7) Differences in the surface area and surface condition of specimens were not taken into account.

Based on the above assumptions and conversions, the experimental results summarized in Table 1.5 were plotted into Figure 1.7, where the steel behavior is directly

related to the $[Cl^-]$ and $[OH^-]$ in the solutions. From Fig.1.7, it can be seen that, at a fixed $[OH^-]$, steel changed from the passive to the active state as $[Cl^-]$ increased. At a fixed $[Cl^-]$, the passive to active transition took place as $[OH^-]$ decreased. Thus for a given $[OH^-]$, a critical chloride concentration threshold (denoted by $[Cl^-]_T$) could be envisioned as the value of $[Cl^-]$ above which the steel depassivates. More generally, the "passive" and "active" state observations can be roughly separated by the dashed line which corresponds to a fixed value of $[Cl^-]/[OH^-]$. This observation suggests that the onset of corrosion can be related to exceeding a threshold value of CR (denoted by CR_T). The results indicate CR_T ~1, although with considerable variability.

1.5.2 Variability in the Reported CR_T Values

In Fig. 1.7, the chloride concentration thresholds as a function of solution $[OH^-]$ reported by Hausmann(1967), Gouda(1970), and Breit(1998) are also represented. It can be seen that Hausmann's results approached the CR_T=1 line, whereas results from Gouda and Breit significantly deviated from that line. For clarity, the CR_T values for the above three authors were calculated (see Appendix A) and presented as a function of solution pH (Fig.1.8). The CR_T from these authors showed three different patterns. Hausmann's CR_T increased from ~0.35 (at pH11.6) to ~1.1 (at pH13.2). Breit's CR_T values also increased with pH, but were about one order of magnitude lower than those of Hausmann's. Gouda's CR_T values were comparable with Hausmann's at pH11.7, but decreased with increasing pH (CR_T = ~0.1 at pH 13.9).

Significant deviation of CR_T from unity has also been reported by other investigators. Yonezawa et al.(1987) found that sustained active corrosion was not observed on steel in solution with 0.6M $[OH^-]$ and 2.84 M $[Cl^-]$ (corresponding to CR=4.7). Ratliff's(1975) result yielded a CR_T value as high as ~10 in a pH 13 solution. On the other hand, Kitowski's (1997) data yielded a CR_T value in SCS as low as ~0.2 (even lower than that estimated from Gouda's results). Consequently, the literature data suggest that CR_T values spread over a two orders of magnitude range.

1.5.3 Causes for the Variability in CR_T Values

In contrast to the heterogeneous environment of concrete, bulk liquid solutions used for corrosion tests are usually homogeneous and the chemical species in solution are often uniformly distributed. Thus, less variation of chloride corrosion threshold values from liquid solution tests (CR_T) should be expected than from those in concrete (C_{TT}). However, the literature data (Table 1.3) suggested that the variation of CR_T values is even larger than that of C_{TT} values. Many possible causes can contribute to this large variation of CR_T. Some of the most likely factors affecting CR_T are discussed in the following.

1.5.3.1 Influence of pH

Accurate measurement of solution pH or $[OH^-]$ is very important because, as noted above, the threshold appears to be directly affected by those values. Unfortunately, confusion exists regarding the pH values reported in the literature. Even for the same type of solution,

reported pH values often vary. For example, Hausmann (1967) reported the pH of SCS (at an unreported testing temperature) to be 12.40, which is in agreement with the value listed in CRC(1973) for T=25ºC. However, Gouda, reported that the pH of SCS was only 12.10. If γ is approximately the same, the $[OH^-]$ of a pH 12.4 solution is twice that of pH12.1 solution. Consequently, the threshold CR_T will be affected accordingly. If the pH value of 12.1 for SCS reported by Gouda was accurate, it would mean Gouda's experiment was conducted at a temperature much higher than normal room temperature, since the solubility of $Ca(OH)_2$ (and hence the pH of SCS) decreases with temperature. However, Gouda did not report the test temperature either. Nevertheless, the pH of SCS reported by most of the investigators was between 12.4 and 12.6, and it was reported to decrease with the addition of NaCl.

Secondly, when the alkalinity of a solution is very high ($[OH^-]$>0.1M), a direct pH measurement using a glass electrode often involves significant "alkaline error" (Bates,1973). On the other hand, if the solution alkalinity is low, carbonation of the test solution could take place, especially when a corrosion experiment lasts for a long period. If carbonation of solution is not properly prevented, the solution pH at the time of corrosion initiation may be substantially lower than its initial value. Unfortunately, this potential problem is sometimes neglected.

According to its definition (Bates1973), pH can be calculated as follows:

$$pH = -\log(a_{H^+}) = -\log\left(\frac{K_w}{\gamma[OH^-]}\right) = \log[OH^-] + \log\gamma - \log K_w \qquad (1.7)$$

where a_H+ is the activity of H^+ ions. According to Eq(1.7), pH depends not only on $[OH^-]$, but also on γ (a function of solution ionic strength) and K_w (a strong function of temperature). Therefore, any simplifying assumption (e.g. by assuming that γ =1 and/or $K_w = 10^{-14}$) during the calculation of pH form $[OH^-]$ (or calculation of $[OH^-]$) can introduce significant error.

1.5.3.2 Influence of Specimen Parameters

Specimen parameters such as size, surface condition, and chemical composition can be of great importance when threshold results are compared. The effect of steel composition has already been addressed briefly in section 1.4. The effect of specimen size and surface finish on CR_T will be discussed here. From Table 1.5, it can be seen that the specimen size ranged from very small (~0.2cm^2 exposed surface area) to relatively large (~70cm^2) bars. The specimen surface condition also varied significantly; some had a rough as-received mill scale whereas others were ground with 600 grit emery paper or even polished to a 1µm finish. It has been shown that steel surface finish has a significant effect on pitting susceptibility (Szklarska-Smialowska, 1986). For example, Mammoliti et al.(1996) reported that the pitting potential of reinforcing steel in SCS containing NaCl was raised dramatically by reducing the steel surface roughness. A similar effect of surface finish on pitting potential has also been reported by Manning et al.(1979) for single phase 304L stainless steel in a 1M NaCl solution. Therefore, the surface finish could be one of the most important factors in the variability of the reported CR_T values. The specimen surface area may also have a strong effect on CR_T. Shibata (1982) reported that E_p of 304L stainless steel in 3.5% NaCl solution was more negative for larger specimens. This observation can be related to the theory that pitting corrosion initiates

preferentially at weak spots (e.g. sulfide inclusions, grain boundary defects, etc.) on the steel surface. Therefore, the likelihood of developing a stable pit is higher on a very large specimen than on a very small one.

1.5.3.3 Influence of Experimental Procedures and Techniques

The initiation of pitting on steel in alkaline solutions is directly related to the condition of the passive film, which is then expected to influence CR_T. Important properties of passive film include its composition, structure and thickness, which are often affected by the experimental procedures and techniques used. From Table 1.5 it can be seen that in most instances steel was immediately exposed to chloride-containing test solutions (designated here as Case A). In other experiments (Case B), steel was first pre-passivated in a chloride-free solution for a certain period then tested in chloride-containing solutions. This difference in the way the chlorides are introduced may strongly affect CR_T. In Case A, if the CR value of a solution is sufficiently high, a passive film may never be able to build up before steel corrodes. Even if CR is low, the passive film formed on steel surface would be less stable or mature than that formed in Case B, where the passive layer is allowed to build up in a chloride-free solution first. A stable, chloride-free passive layer may yield a higher CR_T, or at least lead to a longer pitting initiation time.

The above issue can be even more complicated by the experimental techniques used. For example, consider a case where the anodic polarization technique is employed to determine the pitting potential of steel in a chloride-containing solution. The properties of the passive film before pitting initiation are expected to be related to the anodic polarization scan rate, since the scan rate directly controls the duration of time that the steel exists in the passive state (before reaching E_p). For the same reason, the starting potential of anodic polarization can also affect the passive film. Therefore, if E_p is a strong function of the passive film maturity, it is expected that these parameters can affect the experimental measured E_p (and hence CR_T) values.

1.5.3.4 Criteria to Define the Threshold

The $[Cl^-]_T$ values (hence CR_T) obtained using different experimental methods depend on the criterion used to define the threshold in each method. When tested at open-circuit condition, corrosion initiation on an individual specimen is often manifested by a sudden open circuit potential (E_{oc}) drop or corrosion current density (i_{corr}) rise as $[Cl^-]$ is above a certain level, although that $[Cl^-]$ level may vary from specimen to specimen. Therefore, if the $[Cl^-]$ level for pitting initiation has small variability, $[Cl^-]_T$ for the open-circuit test condition can be obtained directly. However, pitting initiation of steel not only depends on $[Cl^-]$, but also on the potential applied to the steel. When experiments are carried out using electrochemical techniques such as cyclic polarization (CYP), potentiodynamic polarization (PDP), potentiostatic polarization (PSP), etc., the $[Cl^-]$ level for pitting initiation is a function of potential. Therefore, a criterion is needed to obtain $[Cl^-]_T$. By taking into account that passive steel in concrete or alkaline solutions normally achieves an open circuit potential no higher than 0V/SCE, $[Cl^-]_T$ can be defined as the maximum $[Cl^-]$ at which the E_p of steel is no lower than 0V/SCE. The $[Cl^-]_T$ value

thus obtained for CYP, PDP or PSP can then be compared with that obtained directly with the open-circuit test method.

However, the same criterion can not be applied to the galvanostatic polarization (GSP) method. Using GSP, Gouda (1970) defined $[Cl^-]_T$ as the maximum $[Cl^-]$ in a solution at which steel was able to remain passive when an anodic current density of $10\mu A/cm^2$ was applied. That anodic current density causes the steel to reach a noble potential near the oxygen evolution potential (denoted as E_{OE}). Therefore, the criterion used by Gouda actually implies that $[Cl^-]_T$ is the maximum $[Cl^-]$ at which E_p is above E_{OE} (~0.6V/SCE), instead of ~0V/SCE as assumed elsewhere. Breit (1998) defined $[Cl^-]_T$ in a similar way, although the experiment was performed using a stepwise potentiostatic polarization method. Evidently, the criterion adopted by Gouda and Breit is more stringent than that used for the other methods. This difference in the threshold definition could explain why the $[Cl^-]_T$ (or CR_T) values from Gouda and Breit were significantly lower than most of the other investigators, as can be seen from Fig 1.7 and Fig.1.8. In addition, the oxygen evolution reaction may cause the depletion of OH^- at the steel/solution interface and hence significant error in CR_T may be involved when CR_T is simply assigned the CR value of the bulk solution.

1.5.3.5 Reproducibility and Probability

The broad range of reported CR_T values may be partially due to the nature of the pitting corrosion process itself. It has been widely observed that pitting corrosion normally initiates randomly on steel surface and E_p is often poorly reproduced. Shibata and Takeyama (1977) found that the E_p values of 304 and 316 stainless steels in 3.5% NaCl solution were significantly scattered and approximately normally distributed. Hausmann (1967, 1998) suggested that the behavior of steel (corrosion or passivation) in chloride-containing SCS could be estimated in a probabilistic approach. Preliminary results in this laboratory (Li and Sagüés, 1999b and 1999c) also revealed that E_p of reinforcing steel in chloride-containing alkaline solutions showed large variability. All these observations imply that the pitting corrosion of steel can be best understood from a statistical standpoint. A deterministic chloride corrosion threshold may not exist. In that case, a reasonable estimate of chloride threshold should be based on multiple tests. Unfortunately, most of the reported data in the literature have been based only on a very limited number of repeated tests.

1.6 Objectives

In view of the unresolved issues for chloride corrosion threshold presented above, this investigation was focused on the study of the passivation and corrosion of reinforcing steel in alkaline solutions. The objectives of this research include the following:

1) Determine the effect of rebar surface condition on the chloride corrosion threshold in alkaline solutions

2) Determine the pitting potentials (E_p) and repassivation potentials (E_r) of rebar steel in alkaline solutions and evaluate how E_p and E_r are affected by the following factors:
   (a) $[Cl^-]$ and $[OH^-]$

(b) rebar surface finish condition
(c) anodic polarization scan rate
(d) specimen size
(e) passive film maturity

2) Evaluate the steady-state passive current density of steel in alkaline solutions

3) Examine the underlying causes for the variation of CR_T

3) Estimate and validate the concrete total chloride threshold (C_T) using results from solution tests

1.7 Approach

The investigation primarily focused on the objectives specified in Section 1.6. The first objective was addressed with an open circuit immersion (OCI) experiment. Specimens of three surface conditions (as-received with mill scale, sandblasted to remove mill scale and any rusts on surface, and pre-rusted in a 3.5% NaCl solution for three days) were used. OCI tests were conducted in three types of solutions (pH 12.6 saturated $Ca(OH)_2$ solution (SCS), and simulated concrete pore solutions (pH 13.3 SPS1 and pH13.6 SPS2). The base solutions were chloride-free initially to allow the specimens to passivate, then [Cl^-] was raised stepwisely to corrode the steel. E_{corr} of each specimen was monitored periodically. Electrochemical impedance spectroscopy (EIS) was also performed on selected specimens.

Much of the research work was focused on the second objective. To determine E_p and E_r, the cyclic polarization technique (CYP) was employed. Tests were mainly conducted in two types of base solutions: pH 12.6 SCS and pH 13.6 SPS2, with [Cl^-] between 0.001M and 3.0M. Anodic polarization scan rates (v_f) ranging from 0.0033mV/sec to 10mV/sec were used to explore the E_p dependence on v_f. To explore the surface finish effect, steel surface was either sandblasted or ground with grinding paper to a final finish of 60, 120, 320, and 600 grit. The area effect was studied by using specimens with surface area differed by three orders of magnitude (from 0.005 cm^2 to 60 cm^2).

The passivation process of rebar steel was investigated in four types of alkaline solutions: pH13.6 SPS2, pH 12.6 SCS, pH 11.4 NCS (0.1M Na_2CO_3), and pH 8.2 NHS (0.2M $NaHCO_3$). E_{oc} was measured and EIS was performed periodically for a testing period of over 100 days. Pre-passivated specimens were also tested in chloride-containing SCS and SPS2 for E_p using CYP.

Table 1.1 Ion concentrations (N) in pore solution obtained for ASTM Type I portland cement paste specimens (w/c=0.5)

	Na^+	K^+	Ca^{2+}	SO_4^{2-}	OH^-	$\Sigma+$	$\Sigma-$
Type A	0.070	0.389	0.0035	0.0154	0.468	0.436	0.483
Type B	0.181	0.358	0.0038	0.0330	0.523	0.543	0.556

Table 1.2 Data from literature showing relationship between the total alkali content in cement and the total alkaline ion content in pore water

Reference	Material	w/c	Na_2O (%)	$[Na^+]$ (M)	$[K^+]$ (M)	$[OH^-]$ M)
Diamond (1981)	paste	0.40	0.72	0.2	0.4	0.6
Arya et al. (1995)	paste	0.50	0.54	N.A.	N.A.	0.53
Page et al.(1983)	paste	0.50	1.19	0.27	0.63	0.83
Constantiner (1997)	paste	0.50	0.50	0.07	0.40	0.45
Constantiner (1997)	paste	0.50	0.85	0.187	0.39	0.53
Diamond (1983)	paste	0.50	0.72	N.A.	0.33	0.52
Tritthart (1989)	paste	0.60	0.79	N.A.	N.A.	0.51
Kawamura (1988)	mortar	0.45	0.38	N.A.	N.A.	0.20
Kayyali et al.(1990)	mortar	0.48	0.38	N.A.	N.A.	0.18
Larbi et al.(1990)	paste	0.40	0.75	0.17	0.39	0.52
Larbi et al.(1990)	paste	0.45	0.75	0.14	0.38	0.48
Larbi et al.(1990)	paste	0.56	0.75	0.11	0.29	0.38
Duchesne (1994)	paste	0.50	1.06	0.85 (total)		N.A.
Li & Sagüés (2000a)	mortar	0.45	0.37	N.A.		0.284
Li & Sagüés (2000a)	concrete	0.50	0.37	N.A.		0.2

Table 1.3 Chloride levels required to initiate the corrosion of steel reviewed by Glass and Buenfeld (1997)

C_{TT} (wt.%)	$[Cl^-]_f$ (M)	CR_T	Exposure	Sample	Reference
0.17-1.4			Outdoors	structure	Stratful et al. (1975)
0.2-1.5			Outdoors	structure	Vassie (1984)
0.5-0.7			Outdoors	concrete	Thomas (1996)
0.25-0.5			Laboratory	Mortar	Elsener and Böhni(1986)
0.3-0.7			Outdoors	Structure	Henriksen (1993)
0.32-1.9			Outdoors	Concrete	Treadaway et al. (1989)
0.4			Outdoors	Concrete	Bamforth at al. (1994)
0.4	0.11	0.22	Laboratory	Paste	Page et al. (1986)
0.4-1.6			Laboratory	Mortar	Hansson et al. (1990)
0.5-2			Laboratory	Concrete	Schiessl et al. (1990)
0.5			Outdoors	Concrete	Thomas et al. (1990)
0.5-1.4			Laboratory	Concrete	Tuutti (1993)
0.6			Laboratory	Concrete	Locke and Siman (1980)
1.6-2.5		3-20	Laboratory	concrete	Lambert at al. (1991)
1.8-2.2			Outdoors	structure	Lukas (1985)
	0.14-0.18	2.5-6	Laboratory	paste/mortar	Pettersson (1993)
		0.26-0.8	Laboratory	solution	Goni and Andrade (1990)
		0.3	Laboratory	paste/solution	Diamond (1986)
		0.6	Laboratory	solution	Hausmann (1967)
		1-40	Laboratory	mortar/solution	Yonezawa et al. (1988)

Table 1.4 Maximum chloride ion content (percent by weight of cement) for corrosion protection of reinforcement

Types of member	Chloride limit
Prestressed concrete	0.06
Reinforced concrete exposed to chloride in service	0.15
Reinforced concrete that will be dry or protected from moisture in service	1.00
Other reinforced concrete construction	0.15

Table 1.5 Behavior of iron and carbon steel in chloride-containing alkaline solutions

References	Solution	Specimen	Experimental Technique	Results
Venu *et al.* (1965)	0.01N, 0.1N NaOH NaCl added	ϕ0.24mm Fe wire and ϕ0.4mm mild steel wire(cross-section exposed), 3/0 emery paper polished	potentiokinetic at 3.33mv/s or galvanostatic at 15μA for Fe specimens	In 0.1N NaOH: when $[Cl^-] \leq 0.1N$ passive up to 1.0V/SHE when $[Cl^-] \geq 1N$ corroded at E>-0.2V In 0.01N NaOH: when $[Cl^-] \leq 0.01N$ passive up to ~1.7V when $[Cl^-]=0.1N$ corroded at E_p=~0V In 0.1N NaOH (galvanostatic): when $[Cl^-] \leq 0.1N$ passive, corroded at $[Cl^-]=1.0N$
Hausmann (1967)	pH12.4 $Ca(OH)_2$, pH11.6, 13.2 NaOH, NaCl added, bubbled with O_2	ϕ9.5×228mm mild steel, burnished to bright finish with emery paper (of unknown grade)	open-circuit immersion, monitored E_{corr}~t for at least 2 weeks	Corrosion defined by probability(%): pH11.6: 0.002M $[Cl^-]$ (8%), 0.003M $[Cl^-]$ (67%) pH12.4: 0.02M $[Cl^-]$ (0%), 0.04M $[Cl^-]$ (67%) pH13.2: 0.25M $[Cl^-]$ (0%) suggested activity ratio threshold: $[Cl^-]/[OH^-]$~0.6
Gouda (1970)	pH12.1 $Ca(OH)_2$, pH13.95, 13.3, 12.6, 12.1,11.75 NaOH NaCl added, N_2 deaerated	ϕ6mm reinforcing steel rod (unknown length) mechanically polished	galvanostatic at 10μA/cm^2, Immersion E_{corr}~t, visual inspection	pH11.75: passive $[Cl^-] \leq 0.0034M$ pH12.1: passive $[Cl^-]$ NaCl≤0.007M pH12.6: passive $[Cl^-]$NaCl≤0.014M pH13.30: passive $[Cl^-] \leq 0.085M$ pH13.95: passive when $[Cl^-] \leq 0.115M$ suggested threshold: $pH=0.83\log[Cl^-]+K$
	Same solution as above without NaCl	same as above	same as above	when pH>11.5 passive when pH≤11.5 corroded
Berman (1975)	Saturated $Ca(OH)_2$, naturally aerated, NaCl added after prepassivation	steel drill rod (unknown size) polished with emery paper (finer than #100)	open-circuit partial immersion E_{corr}~t	when $[Cl^-] \leq 0.02N$ passive when $[Cl^-] \geq 0.03N$ corroded
Ratliff (1975)	pH 11, 12, 13 NaOH naturally aerated NaCl added	ϕ~8mm×12.7mm grade 40 reinforcing rod, grit 400 emery paper grinding	E_{oc}, and i_{corr} measured 0.5hr after immersion	pH 11: NaCl=0.1% corroded pH 12: NaCl ≤0.1% passive; NaCl≥1% corroded pH 13: NaCl ≤6% passive; NaCl≥10% corroded

(Continued on next page)

Table 1.5 (Continued)

References	Solution	Specimen	Experimental Technique	Results
Oranowska *et al.* (1981)	Saturated $Ca(OH)_2$ deaerated, $CaCl_2$ added	Armco iron , 0.2cm^2, 1µm finish	potentiokinetic at 1V/min, polarization started at –0.8V/NHE	when $[Cl^-]$=0.02M passive up to E_{OE}(0.8V) when $[Cl^-]$=0.1M corroded at E_p=-0.25V
Page *et al.* (1982)	Saturated $Ca(OH)_2$ $CaCl_2{\cdot}2H_2O$ added	Mild steel Specimen (size and surface condition unknown)	potentiokinetic at 1mV/s, polarization started at –1V/SCE	0.1% $CaCl_2{\cdot}2H_2O$: passive up to 0.5V (E_{OE}) 0.25% $CaCl_2{\cdot}2H_2O$: Ep=~0.1V/SCE 0.5% $CaCl_2{\cdot}2H_2O$: Ep=~0.1V/SCE
Alvarez and Galvele (1984)	pH 10 to 12 NaOH N_2 deaerated	99.999% pure Fe, 0.13cm^2, #600 SiC paper abraded then polished electrolytically	potentiostatic surface scratching technique, galvanostatic at 150µA/cm^2	At pH=10, 0.01-1.0M NaCl : Ep=-0.364-0.064log$[Cl^-]$ At pH=10-12, 1.0M NaCl : Ep=-0.560+0.020pH
Zakroczymski *et al.* (1985)	0.05M NaOH NaCl added, deaerated	pure Fe,0.32cm^2 exposed area, polished to 1µm	potentiokinetic at several scan rates (PSR) then potentiostatic at 0.55V/SHE	PSR=10mV/s: $[Cl^-]$=0.005M passive $[Cl^-]$=0.05M corroded PSR=1mV/s : $[Cl^-]$=0.05M passive
Berke (1986)	saturated $Ca(OH)_2$ NaCl added, N_2 deaerated	ϕ12.5×12.5mm 1045 steel rod, 600 grit finish	cyclic polarization at scan rate of 0.056mV/s, polarization started at –0.85V/SCE	0.01M$[Cl^-]$ E_n=0.49V 0.05M$[Cl^-]$ E_n=0.11V 0.1M $[Cl^-]$ E_n=-0.18V
Dawson & Langford (1988)	pH13.3 to 13.5 extracted pore water with NaCl, aerated	600 grit small mild steel electrode (unknown size)	cyclic polarization at 18mV/min, started from –1.25V/SCE	when $[Cl^-]/[OH^-]$=3.2 passive at E_{OE}(~0.5V) (results misinterpreted by the investigators)
Yonezawa *et al.* (1988)	Saturated $Ca(OH)_2$, 0.4MKOH+0.2M NaOH, NaCl added, Aerated	ϕ8×60mm (grade 250 mild steel reinforcing bar) polished to 800 grade emery paper	open-circuit immersion E_{corr}, i_{corr} (measured from LRP)	In $Ca(OH)_2$, when $[Cl^-]$=0.52M and 2.84M corroded In SPS, when $[Cl^-]$=0.52M passive, when $[Cl^-]$=2.84M,.E_{corr} fluctuated
Goñi and Andrade (1990)	$Ca(OH)_2$ with 0, .2M, 0.5M KOH, 0.1, 0.5, 0.75,1M $[Cl^-]$ from NaCl or $CaCl_2$	steel bar, 4.2cm^2 exposed area, unknown surface condition	open-circuit immersion E_{corr}, i_{corr}~t, potentiodynamic polarization (1.67mV/s) started at –0.9 V/SCE	i_{corr} was $[Cl^-]/[OH^-]$ dependent: log(i_{corr})=-0.43+0.62 log($[Cl^-]/[OH^-]$) breakdown potential was pH dependent: pH=12.5+0.016E_b

(Continued on next page)

Table 1.5 (Continued)

References	Solution	Specimen	Experimental Technique	Results
Gonzáalez *et al.* (1993)	Saturated $Ca(OH)_2$ NaCl added, deaerated	low carbon steel rotating disc electrode (unknown size and surface finish)	potentiodynamic @ 0.5mV/s started at unknown potential	breakdown potential: when $[Cl^-]$=0.01M E_b>0.2V/SCE when $[Cl^-]\geq$0.25M E_b< 0V/SCE
Mammoliti *et al.* (1996)	Saturated $Ca(OH)_2$, NaCl added	cross-section of deformed rebar (order of ~1cm^2) with grit 240 and grit 600 or 6µm polish	cyclic polarization at 1mV/s started from –1V/SCE	pitting potential depended on surface finish: 600grit: E_p=0.3V at 4%Cl^- 240grit: E_p=0.25V at 2% Cl- 6µm: No pitting up to 0.5V at 3% Cl^-
Kitowski & Wheat (1997)	Sat'd $Ca(OH)_2$, SPS (0.6MKOH+ 0.2M NaOH+$Ca(OH)_2$), NaCl added	grade 60 reinforcing steel rod, ϕ15..9mm×102 mm) With as-received mill scale and deformation	open circuit immersion, E_{corr}~t, R_p initially chloride free,	SPS: passive even when $[Cl^-]$=21,000 ppm $Ca(OH)_2$: passive when $[Cl^-]\leq$200ppm, corroded when≥400ppm
Breit (1998)	pH 12 to 14 alkaline solutions (SPS)	reinforcing steel rod, ϕ10mm×100mm, as-received condition	stepwise (50mV/12hr) anodic polarization from E_{oc} to E_{OE}	Critical $[Cl^-]$: $\log[Cl^-]_{crit}=1.5\cdot\log[OH^-]-0.245$
Videm (1999)	0.3M KOH 0.1M NaCl added open to air	Mild steel 6~8 cm^2, pickled in 10%wt. HCl for 2min	open circuit immersion for 44 months, E_{corr}~t, EIS	E_{corr} fluctuated, final E_{corr} =-0.214V/SCE, EIS suggested passivation at final stage, active corrosion not sustained
Joiret *et al.* (1999)	1M NaOH, deaerated with N_2 NaCl added	ϕ5mm Fe rod (cross-section exposed), unknown finish	cyclic polarization at 0.5mV/s started from –1.2V vs. Hg/HgO	no pitting up to E_{OE} (0.5V) at 0.34M NaCl

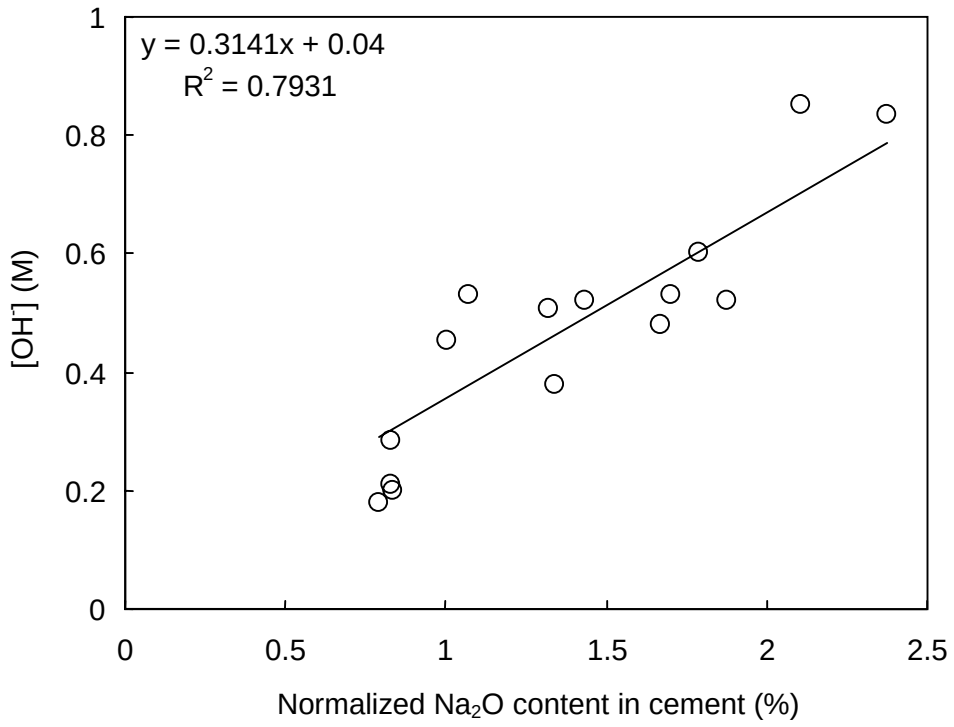

Figure 1.1 Relationship between pore solution [OH^-] and normalized alkali content in cement

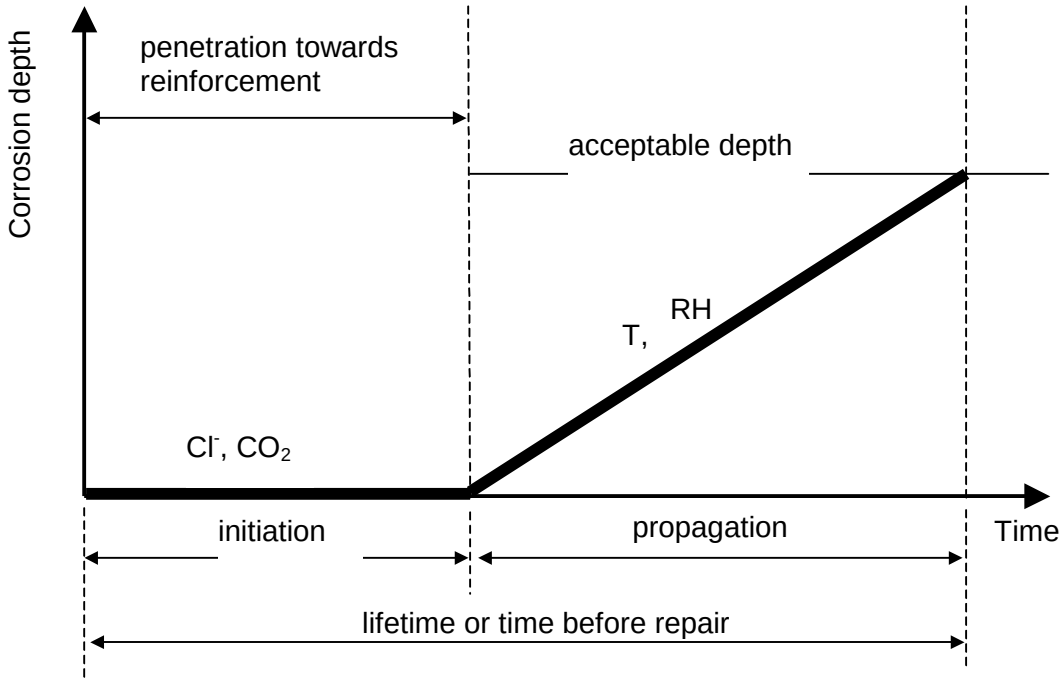

Figure 1.2 Schematic sketch of steel corrosion sequence in concrete (Tuuitti 1982)

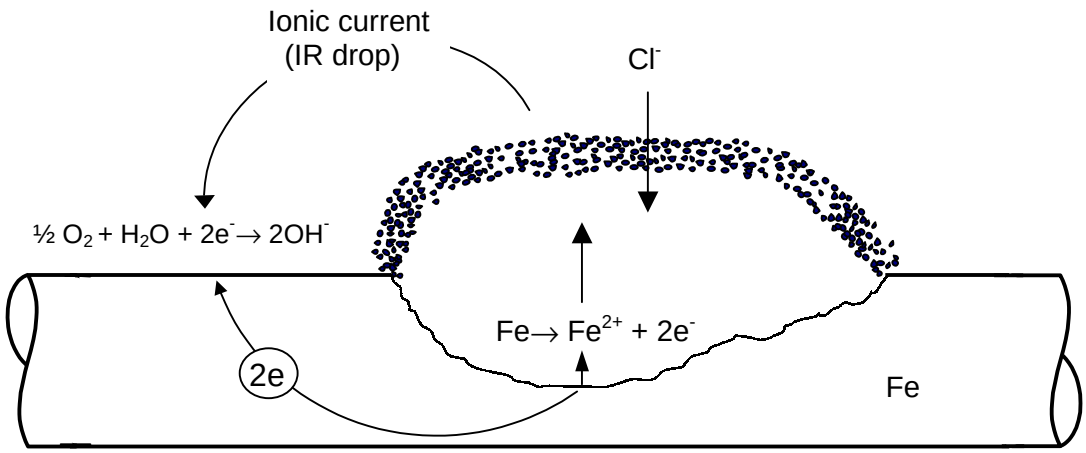

Figure 1.3 Schematic graph showing the localized corrosion process (the marked direction of ionic current is the direction of the flow of positive charges in the electrolytes.)

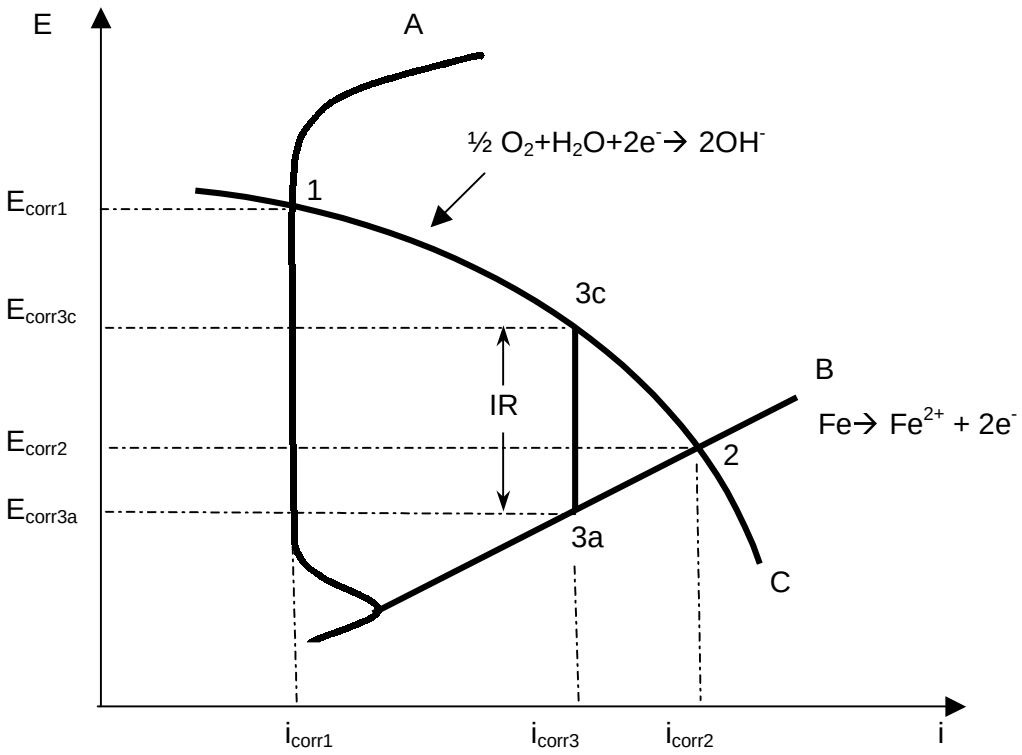

Figure 1.4 An Evans diagram showing the corrosion potential and corrosion current density for steel in concrete

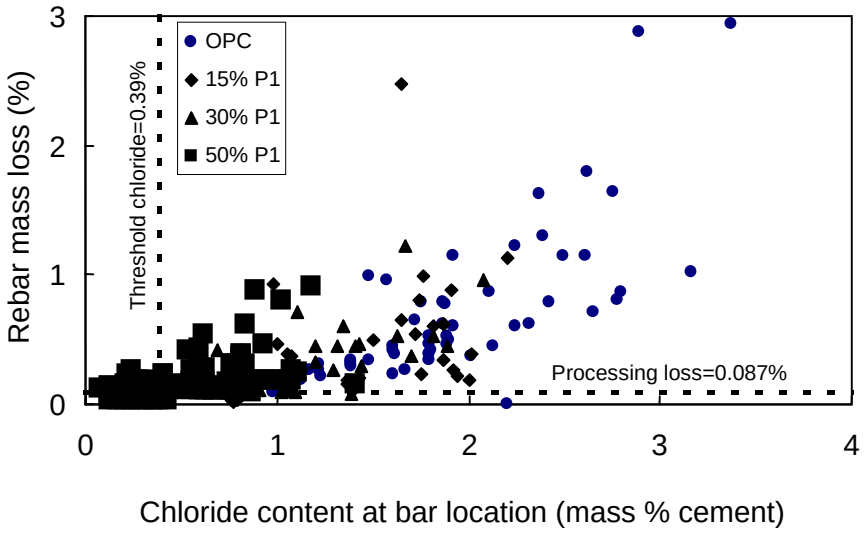

Figure 1.5 Rebar mass loss vs. chloride content for all mixes (Thomas 1996)

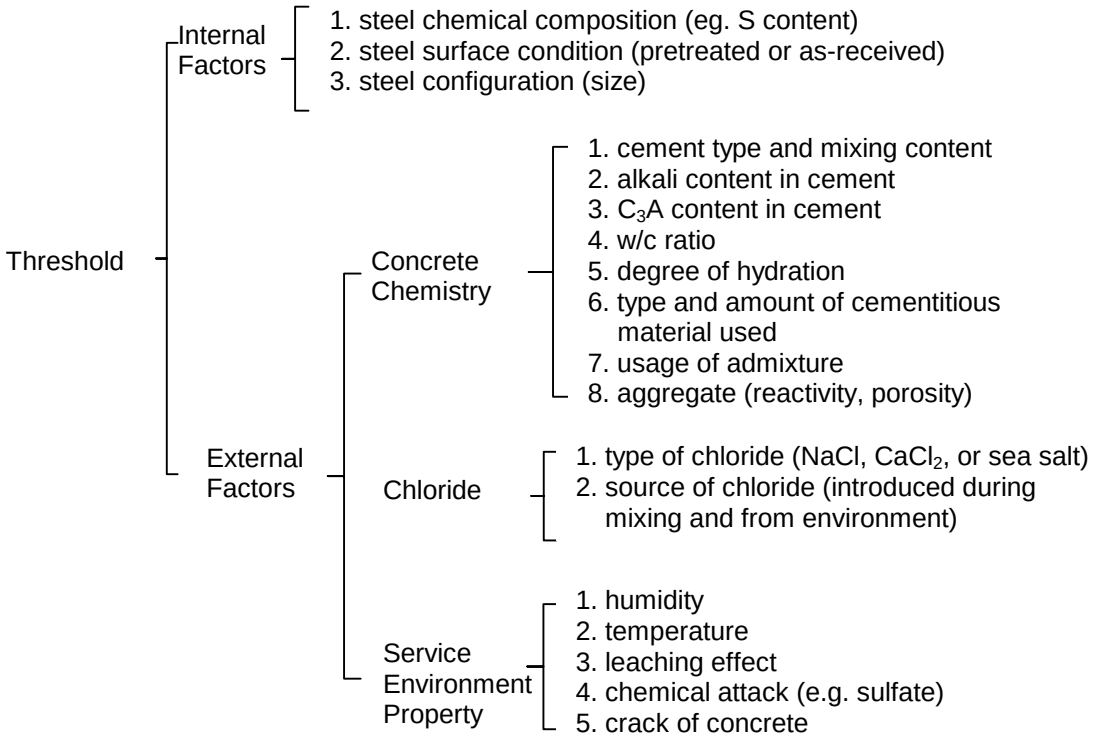

Figure 1.6 Internal and external factors that may affect the corrosion initiation of steel in concrete

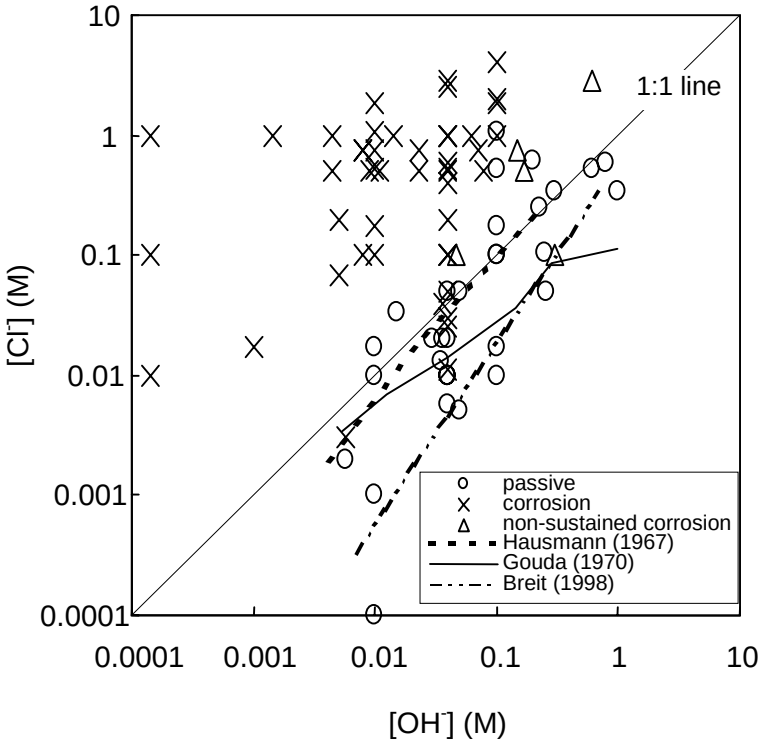

Figure 1.7 Behavior of carbon steel and pure iron in alkaline solutions (pH10 to 14) as a function of $[Cl^-]$ and $[OH^-]$

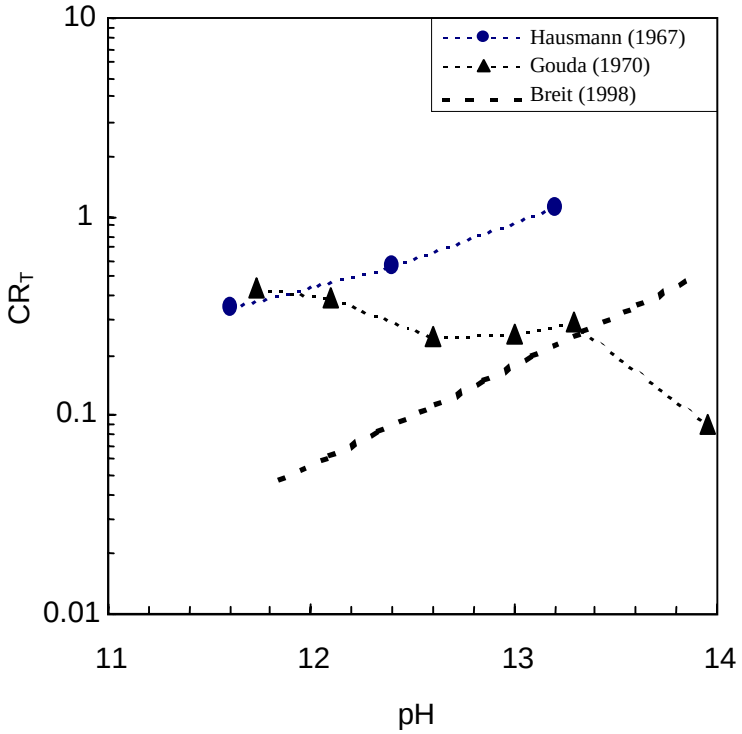

Figure 1.8 A comparison of CR_T values from the work of Hausmann, Gouda, and Breit

CHAPTER 2: Effect of Metal Surface Condition on Chloride Corrosion Threshold

2.1 Introduction

It is widely known that chlorides can induce corrosion of reinforcing steel in concrete by causing breakdown of the passive film on the steel surface. It has also been found that corrosion in non-carbonated concrete only takes place when the chloride concentration reaches a certain threshold level, although this threshold level shows much variability (Glass and Buenfeld 1997). To better understand the corrosion mechanism of steel in concrete, studies of chloride-induced corrosion have often been carried out in liquid solutions. Chloride-containing saturated calcium hydroxide solution (pH=~12.6) and other simulated concrete pore solutions with higher pH have been employed by many investigators to simulate the concrete environment. However, agreement between the chloride threshold results obtained from different laboratories has been poor. For example, Hausmann (1967) reported that the critical activity ratio of chloride ion to hydroxide ion was between 0.5 to 0.83 and increased with solution pH. However, Gouda's results (1970), after being reevaluated by Diamond (1986), indicated that the critical chloride-to-hydroxide ratio was between 0.6 to 0.1 and decreased with increasing solution pH. A study by Yonezewa et al. (1987) in a high pH solution found a critical chloride-to-hydroxide ratio of ~4.7. Yet another more recent investigation by Breit (1998) suggested critical chloride-to-hydroxide ratios even much lower than those of Gouda's, over a very wide pH range. It is important to understand why the reported threshold chloride to hydroxide ratios varied so much.

Another issue is that most of the experiments carried out in alkaline solutions used steel free of thick iron oxide and with a highly smooth surface finish, whereas steel used in concrete structures often has a rough surface and is covered with a layer of mill scale. Sometimes red rust is present after natural weathering including exposure to a marine environment. The surface condition may affect the extent to which localized corrosion nucleates and develops on the steel, thus possibly affecting the value of the threshold. If procedures such as sandblasting could substantially increase the value of the threshold, the resulting increase in the time to corrosion initiation may represent a significant improvement in material durability. Therefore, the present investigation focused not only on the effect of the solution composition on the chloride corrosion threshold, but also on the effect of steel surface condition.

2.2 Experimental

Specimens ~150mm long were cut from ordinary A-615 reinforcing steel bars (size #4, diameter ~12mm) with diamond-pattern surface deformations. The chemical composition of the rebar steel used is shown in Table 2.1. Specimens were divided into three groups according to their surface conditions. In the first group, specimens were used in the as-received condition, with a black mill scale and some red rust spots on the bar surface due to natural weathering. In the second group, specimens were sandblasted to remove all the mill scale and rust on their surfaces before being put into the test solutions. In the third group, specimens with mill scale were immersed in agitated aerated 3.5% NaCl solution for three days to produce a prerusted condition on the steel surface. The groups will be denominated as-received, sandblasted, and prerusted, respectively. A conical bevel at one end of each specimen was then ground with

emery paper to a 600 grit finish. All the specimens were finally assembled as shown schematically in Figure 2.1. The purpose of this arrangement was to prevent crevice corrosion from happening near the tip, since it has been shown that pitting initiation is relatively more difficult on smoother than on coarser surfaces (Mammoliti et al. 1996) (trial tests using specimens with epoxy mounting often failed due to crevice corrosion at edges). The acrylic washer shown in Fig. 2.1 was very tightly pressed against the tip of the specimen with a screw. A fast curing epoxy was finally used to seal the acrylic washer to the bottom (also made of acrylic) so that the specimens could stand upright on a stable base. There were five specimens in each group. Each specimen had a nominal surface area of about 60 cm^2.

Each test cell was a 20L PVC container holding 15L of one of the three types of test solutions (SCS, SPS1, and SPS2) with base compositions listed in Table 2.2. These solutions were intended to cover a range of pH values representative of concrete pore water conditions. The higher pH simulated pore solution (SPS1 and SPS2) contained K^+ and Na^+ ions in proportions comparable to those often reported for concrete and mortar (Diamond, 1981). Chloride content in the test solutions was adjusted by adding reagent grade sodium chloride (NaCl). NaCl crystals were first dissolved with part of the test solution then mixed thoroughly with the bulk of solution inside the test cell. Generally, chloride concentration was adjusted stepwise about every two weeks. All containers were normally sealed from the outside environment to minimize carbonation of the test solution, but calcium hydroxide was nevertheless periodically added into the SCS container to make up for any possible carbonation losses. The stagnant air (~5L) within the containers was enough to sustain the corrosion process, but fresh air was also supplied when the seal of the container was removed to add NaCl and mix the solution. The test cells were at ambient room temperature, 21±2ºC.

Fifteen specimens (five in each group) sat upright in each cell. These specimens shared one stainless counter electrode placed around them and one activated titanium reference (ATR) electrode (Castro et al., 1996) placed in the center of the cell. The open circuit potential of each specimen was measured, with a multimeter of 200MΩ input resistance, with respect to a saturated calomel electrode (SCE) momentarily placed in the liquid. (Unless specified, all the potentials reported here will be given on the SCE scale.) E_{oc} and $\underline{E}_{oc}$ will designate the open circuit potential of each individual specimen, and the average of a group at a given time, respectively. Electrochemical impedance spectroscopy (EIS) in the frequency range from 100kHz to 1mHz was also performed periodically on selected specimens, using the ATR as the reference electrode. The EIS spectra were analyzed with the equivalent circuit shown in Fig. 2.2 to obtain the values of R_p, R_s, Y_o and n with the best fit in the frequency range between 1mHz to 0.1Hz. The R_p values were used to calculate the nominal corrosion current density (i_{corr}) using the Stern-Geary equation (Stern and Geary, 1957):

$$i_{corr} = B / R_p \qquad (2.1)$$

where B is the Stern-Geary constant, assumed to be 26mV (Stern and Geary, 1957).

2.3 Results

2.3.1 Rebar in pH 13.6 Simulated Concrete Pore Solution (SPS2)

Figure 2.3 illustrates the time evolution of the $\underline{E}_{oc}$ of each specimen group in pH 13.6 SPS2 as the chloride concentration increased. When no chloride was present in the solution, the $\underline{E}_{oc}$ of all the specimens evolved similarly with time. Immediately after immersion, $\underline{E}_{oc}$ (not shown) reached a value between about –300 mV (for as-received and sandblasted steel) and –400 mV (for pre-rusted steel). After that, $\underline{E}_{oc}$ shifted anodically and reached a steady state value of about –150 mV in two weeks, an indication that all the specimens had been passivated.

The $\underline{E}_{oc}$ of the sandblasted group stayed at about –160 mV when $[Cl^-] \leq 1.5M$. However, when $[Cl^-]$ was 2.0 M or higher, the $\underline{E}_{oc}$ of this group fluctuated between ~-400mV (active corrosion) and –200 mV (passive). Fluctuations of this magnitude in E_{oc} suggest that sustained active corrosion of steel was not taking place. The $\underline{E}_{oc}$ of the other two specimen groups behaved similarly, but the $\underline{E}_{oc}$ fluctuation started at a lower $[Cl^-]$ level (1.0M). Clearly, under these conditions, both pitting and repassivation processes were taking place.

The above observations were in good agreement with EIS results. Figure 2.4 shows Nyquist plots obtained for one sandblasted specimen at 84, 117, 261, and 732 days in SPS2 with 3.0M NaCl. The projected R_p at day 84 (E_{oc} = -242 mV) was very large, indicating passive behavior. However, by day 117 (E_{oc} = -404 mV) R_p was much smaller, on the order of 10 $k\Omega \cdot cm^2$, consistent with active corrosion. With continued immersion, the same steel specimen returned to a passive condition as indicated by the data for days 261 (E_{oc} = -211 mV) and 732 (E_{oc} = -162 mV).

2.3.2 Rebar in pH 13.3 Simulated Concrete Pore Solution (SPS1)

Figure 2.5 presents the time evolution of the $\underline{E}_{oc}$ of each specimen group in pH13.3 SPS1. The $\underline{E}_{oc}$ of the sandblasted specimen group stayed at ~-170mV with up to 0.8M NaCl, after which there was a sudden $\underline{E}_{oc}$ drop due to onset of active corrosion of some of the specimens. In the as-received and pre-rusted specimen groups, $\underline{E}_{oc}$ was affected by the presence of 0.2M NaCl and it continued to drop gradually with increasing $[Cl^-]$. When $[Cl^-] > 0.8M$, all three specimen groups were experiencing active corrosion. At 2.0M NaCl addition, the sandblasted steel group showed the most negative $\underline{E}_{oc}$ among the three groups.

Figure 2.6 shows the time evolution of the Nyquist plots of a sandblasted specimen in SPS1. There was no significant difference between results for day 16 ($[Cl^-]$ = 0.0 M, E_{oc}= -169mV), day 41($[Cl^-]$ = 0.4 M, E_{oc} = -175 mV), day 55 ($[Cl^-]$ = 0.6 M, E_{oc} = -179 mV), and day 63 ($[Cl^-]$ = 0.8M, E_{oc} = -162 mV). Very high R_p values (~1 $M\Omega \cdot cm^2$) were projected from those diagrams suggesting that the steel was passive during that period. However, by day 74 ($[Cl^-]$ = 1.0M, E_{oc} = -321 mV), the diagram was significantly depressed. It was further depressed at day 91 ($[Cl^-]$ = 1.0M, E_{oc} = -507 mV) with an estimated R_p of ~10 $k\Omega \cdot cm^2$, suggestive of a comparatively high corrosion rate at that time.

2.3.3 Rebar in pH 12.6 SCS

The time evolution of $\underline{E}_{oc}$ of each specimen group in SCS (Figure 2.7) was very similar to that in SPS1, but the chloride concentration level needed to cause $\underline{E}_{oc}$ shifts was much lower. The sandblasted specimens maintained a passive $\underline{E}_{oc}$ of ~-100mV when $[Cl^-] \leq 0.02M$ and started active corrosion when $[Cl^-] = 0.04M$. For the as-received and prerusted groups, $\underline{E}_{oc}$ dropped by ~150mV with only 0.01M NaCl addition and continued to drop with increasing NaCl addition. As in the SPS1 tests, the sandblasted steel had the most negative $\underline{E}_{oc}$ once all the specimens were actively corroding.

2.4 Discussion

2.4.1 Relationship between i_{corr} and E_{oc}

Figure 2.8 presents the E_{oc} as a function of the nominal corrosion current density (i_{corr}) for each type of specimen in SPS1, SPS2, and SCS. There was clear differentiation between the passive and active behavior of the sandblasted steel. When passive, the sandblasted steel had a low i_{corr} between $0.003\mu A/cm^2$ and $0.1\mu A/cm^2$, and E_{oc} nobler than ~-250mV, but when active, i_{corr} was much larger (between 1 $\mu A/cm^2$ and 4.5 $\mu A/cm^2$) and E_{oc} was ~-500mV. In the case of as-received and prerusted steel, the differentiation between the passive and active states was present but less pronounced. Interestingly, the largest i_{corr} value observed for the as-received and prerusted steels was ~1 $\mu A/cm^2$, which was several times lower than that for the sandblasted steel. This is consistent with the latter having the most negative E_{oc}.

In general, E_{oc} appears to be well correlated with i_{corr}, with a roughly linear relationship between E_{oc} and $\log(i_{corr})$. A simple numerical regression yields a slope of –145mV/decade for the as-received and sandblasted steel, and –175mV/decade for the prerusted steel, respectively. This slope can be interpreted as the Tafel slope for the cathodic oxygen reduction reaction (Schiessl, 1988), which is expected to be the main cathodic reaction coupled with the metal dissolution reaction. As the latter shifts from uniform passive dissolution (low total current), to localized active corrosion (high current), the potential should change as observed.

2.4.2 Chloride Concentration Threshold

During the present experiments, the chloride concentration in a given solution was increased stepwise. Therefore, it is more appropriate to give the chloride concentration threshold (denoted as $[Cl^-]_T$ hereafter) as a range. The lower limit of $[Cl^-]_T$ is defined here as the maximum chloride concentration level at which none of the specimens in a given group showed any sign of active corrosion, whereas the upper limit of $[Cl^-]_T$ is defined as the minimum chloride concentration level at which at least one specimen in a given group actively corroded. In the literature (Andrade and Alonso, 1994), steel in concrete is often considered to be active if its i_{corr} value is greater than about $0.1\mu A/cm^2$ to $0.2\mu A/cm^2$. In Fig. 2.8, most of the data for which i_{corr} > ~0.2 $\mu A/cm^2$ corresponded to E_{oc} < ~–350mV. Therefore, for the determination of $[Cl^-]_T$, steel was considered as active if its E_{oc} < -350mV, whether that E_{oc} was observed momentarily or permanently.

Using the potential criterion indicated above, $[Cl^-]_T$ limit values were obtained for each surface condition category and are shown as a function of pH in Figure 2.9. Generally, log($[Cl^-]_T$) increased nearly linearly with pH, which clearly illustrates the inhibiting properties of hydroxide ions in these solutions. The limits for the as-received and prerusted conditions were the same. The $[Cl^-]_T$ limits for sandblasted steel were about twice as high as those for the other two conditions. Therefore, removing the mill scale or other corrosion products from steel surface appears to improve pitting resistance. This effect may be partially attributed to the bare metal surface of the sandblasted steel. Unlike the as-received or prerusted steels (which can be assumed to have had porous and discontinuous film on their surfaces), the sandblasted steel had no thick pre-existing oxides so that a fresh, dense passive film could easily grow on the surface as long as the solution environment was favorable and enough time was allowed for film growth.

Given the beneficial effect of hydroxide ions and the detrimental effect of chloride ions, the corrosion threshold of reinforcing steel in alkaline solutions (and also in concrete) is sometimes expressed as a critical concentration threshold $[Cl^-]/[OH^-]$ ratio (hereafter denoted as CR_T). Figure 2.10 gives the CR_T values from the present investigation (the ratio of the average of the upper and lower limits of $[Cl^-]_T$ to $[OH^-]$) as a function of the solution pH, and also those calculated from the original data reported by Hausmann (1967), Gouda (1970), and Breit (1998), for comparison. To compute the CR_T values, the $[OH^-]$ for Hausmann's and Gouda's work was calculated assuming that the activity coefficient of OH^- ions was 0.7 (CRC, 1973-1974) and the testing temperature (not reported) 25ºC. The CR_T values for Breit's work were directly calculated by using the relationship between $[Cl^-]_T$ and $[OH^-]$ proposed by that author. However, the pH values reported by Breit were corrected assuming an OH^- activity coefficient of 0.7 (see Appendix A).

Fig. 2.10 shows reasonable agreement between the present results for sandblasted steel and those of Hausmann's, considering that in Hausmann's experiment the reinforcing steel specimens were free of mill scale ("burnished to bright steel with emery paper") and tested, as in here, under open circuit conditions. The arrow in Fig. 2.10 indicates that the CR_T at pH 13.2 from Hausmann's results is expected to be a lower limit, since $[Cl^-]_T$ was not reached in those experiments. Both Hausmann's and the present results show that CR_T increased with pH. Breit's CR_T values also increased with pH, but were about one order of magnitude lower. The CR_T values from Gouda's results not only decreased with increasing pH, but also were much lower than Hausmann's and those from the present investigation.

The lower CR_T values from Gouda and Breit can be mainly attributed to the experimental methods employed and the criterion used for $[Cl^-]_T$ determination. In Gouda's experiments, a galvanostatic anodic current density of $10\mu A/cm^2$ was applied to the steel. Since this current density was several orders of magnitude larger than the steady-state passive current density (Andrade and Alonso, 1994), only steel which had a pitting initiation potential (E_p) more noble than the oxygen evolution potential (denoted as E_{OE}, a function of pH, ~0.6V in these solutions) could remain passive. Otherwise the steel would have corroded once its E_p (as long as it was below E_{OE}) was reached during the anodic excursion caused by the polarizing current (Berke, 1986). In other words, the threshold chloride concentration in Gouda's experiments was implicitly defined as the maximum tolerable chloride level at which

steel is able to remain passive when the steel is polarized up to E_{OE}. In Breit's experiments, each specimen was first immersed in a chloride-free solution for 48 hours to reach a steady-state open circuit potential, E_{oc}. After that, NaCl was introduced and stepwise anodic potentiostatic polarization starting at E_{oc} was applied (50mV steps every 12 hours) until E_{OE} was reached. The experiment was conducted with various [Cl^-] levels. At each level, the specimen either pitted or remained passive throughout the test. The $[Cl^-]_T$ was considered to be a value somewhere between the minimum [Cl^-] at which steel pitted during the test and the maximum [Cl^-] at which the steel remained passive. Therefore, the criterion for $[Cl^-]_T$ determination used by Breit was apparently the same as that implicitly adopted by Gouda. Since steel in naturally aerated alkaline solutions or concrete typically only reaches an open circuit potential ≤ ~0V/SCE, or in dry aerated concrete ≤ ~0.2V/SCE (Alonso et al, 1998) (much lower than E_{OE}), the threshold as obtained by Gouda and Breit would appear to be too conservative.

As the criteria used by Gouda and Breit are almost the same, their CR_T values would be expected to be comparable. However, Breit's CR_T values were much lower than Gouda's for most of the investigated pH range. Two major factors may have accounted for that difference. First, specimens used by Breit were tested in the as-received condition (without any surface treatment except cleaning with acetone) whereas those used by Gouda were mechanically polished. As observed here, removing the mill scale or other corrosion products from the steel surface improved pitting resistance, so the CR_T values by Breit would be expected to be the lower ones. A second and perhaps more important factor may directly relate to the oxygen evolution process. Anodic polarization at E_{OE} can reduce the electrolyte pH at the steel/solution interface due to the oxygen evolution reaction as follows:

$$4OH^- \rightarrow O_2\uparrow + 2H_2O + 4e^- \qquad (2.2)$$

The lowering of [OH^-] near the steel surface depends on factors such as the [OH^-] in the bulk solution, the anodic current density, the extent of solution convection, and the duration of the anodic current application. As most of Gouda's galvanostatic tests were finished within an hour while Breit's polarization steps lasted 12 hours each, the [OH^-] decrease at E_{OE} in Breit's experiment would be more significant. Since CR_T is actually related to the [Cl^-]/[OH^-] ratio at the steel surface, using the ratio for the bulk solution under these circumstances may no longer be appropriate and accordingly lead to underestimating CR_T.

An important finding from the present investigation is that the CR_T values were not constant, but increased with solution pH. This is in good agreement with the results from the cyclic polarization tests, in which the CR_T value also significantly increased with pH (Li and Sagüés 1999a, 1999b), and also supported by other sources (Yonezawa et al 1988, Kitowski and Wheat 1997). This observation strongly indicates that the inhibiting effect of the hydroxide ion increases more than linearly with its concentration.

2.4.3 Implications to the Chloride Corrosion Threshold in Concrete

While the present experiments are a very limited simulation of the actual concrete conditions, it is desirable to attempt to relate the CR_T values obtained in solutions to the total

chloride corrosion threshold in concrete (C_{TT}). This quantity, which is often considered in practical design applications (Bentur et al 1997), is commonly expressed in terms of total amount of chloride (C_T) as a percentage of the weight of cement. However, a simple conversion from CR_T to C_{TT} is not possible since the chloride concentration in concrete pore water (also called the free chloride concentration, denoted here as $[Cl^-]_f$) is not a unique function of C_T. For a fixed C_T, $[Cl^-]_f$ also depends on many factors such as the water-to-cement ratio, the cement chemical composition, the degree of hydration, the properties of the aggregates, the presence of admixtures, the relative humidity, etc. The combination of those factors determines how much of the total amount of chloride in the concrete will be present in the pore water (thus accounting for $[Cl^-]_f$) and how much will remain elsewhere (as "bound" chloride). Limited experimental information is available on the partition between free and bound chloride, mostly for cement pastes and mortars and usually under water-saturated conditions. Nevertheless, it is instructive to examine that information for indications of the range of $[Cl^-]_f$ values that may be expected with typical C_T contents. Figure 2.11 is a sampling of observations of $[Cl^-]_f$ as a function of C_T as reported in the literature for several types of nearly water saturated cement pastes, mortars, and concretes (Rasheeduzzafar 1992 , Haque 1995, Tritthart 1989, Andrade 1986, Arya 1995, Suryavanish 1995, Yonezawa 1987, Pereira 1984, Tang 1993, Li & Sagüés 2000a). For a given C_T, $[Cl^-]_f$ showed considerable variability; for example, the $[Cl^-]_f$ value for C_T=2% ranges between ~0.3M and 1.2M. Also, for a given $[Cl^-]_f$ value, C_T varied significantly (e.g., for $[Cl^-]_f$=1.0M, C_T was between 1.7% and 3.2%). Those examples suggest that even if the corrosion initiation of steel in concrete were (for a given pore water pH) a unique function of $[Cl^-]_T$, the variability in chloride binding would preclude a similarly unique relationship for C_{TT}. Instead, a range of possible values for a total chloride threshold should be considered. Based on the experimental results of this work and binding data, that range could be estimated using the following working assumptions:

1) The active or passive condition of steel in concrete is controlled by the chemistry of the concrete pore water, and its composition around the rebar is uniform before pitting initiation.

2) The critical chloride concentration threshold ($[Cl^-]_T$) determined here in the alkaline solution experiments applies to concrete pore water having the same pH.

3) There are no chloride ions initially present in the concrete, so that the steel is passive before chloride contamination starts.

4) The relationships between $[Cl^-]_f$ and C_T shown in Fig. 2.11 are representative for concrete (although much of the data originated from mortar and cement paste), and concrete is assumed to be saturated with water.

Based on the above assumptions, C_{TT} value ranges were obtained from the data in Figs. 2.9 and 2.11. For example, for sandblasted steel in pH 13.3 SPS1, 0.6M<Cl_T<0.8M per Fig. 2.9. In Fig. 2.11, for $[Cl^-]_f$=0.6M, C_T ranged from 1.25% to 2.4%, whereas the corresponding C_T range for $[Cl^-]_f$=0.8M was from 1.5% to 2.8%. Consequently, the C_{TT} under those conditions could easily vary over about 1.25% to 2.8%. Representative ranges of C_{TT}

values for all the other pH and surface conditions examined were similarly estimated and the results are listed in Table 2.3.

Since the ranges of C_{TT} values given in Table 2.3 reflect only the distribution of chloride binding properties encountered in the limited sample of literature data examined, the calculated values should be viewed only as an illustration of the variability expected in actual systems. This variability could be considerably larger than shown in Table 2.3, especially if conditions other than water saturation were considered. Nevertheless, the spread of values indicated there includes the C_{TT} values commonly observed in practice (for example 0.4% for concrete with ordinary portland cement (Thomas, 1996), which often has pore water pH values somewhere between that of saturated calcium hydroxide and SPS1 (Li et al. 1999a)). Moreover, the estimated ranges are also in rough agreement with the C_{TT} range of 0.17% to 2.5% summarized by Glass and Bunefeld (1997) for data from actual concrete structures and laboratory specimens.

Table 2.3 also underscores the strong expected dependence of C_{TT} on the pore solution pH. It should be emphasized that the relevant pore water pH is not that in the bulk of fresh concrete, but rather that reflecting the conditions at the rebar/concrete interface at the moment just before corrosion initiation. Thus, if during the service life prior to chloride buildup the pH of the pore water were to be significantly reduced (for example because of leaching or carbonation), C_{TT} could be reduced accordingly. This consideration may explain why C_{TT} values higher than 3% have rarely been reported, although they may still be possible under the assumptions made. Table 2.3 also shows the possibly beneficial effect of increased C_{TT} in a scale-free rebar surface, a promising finding if confirmed by future work in actual concrete environments. However, detrimental effects could take place during active corrosion of sandblasted steel. As shown in Figs. 2.5, 2.7, and 2.8, once active corrosion started, the sandblasted steel always had a more negative E_{oc} and a larger i_{corr} than those of the as-received and prerusted steel. If the corrosion sequence of steel in concrete is viewed as a two step model (initiation followed by propagation, see Fig. 1.2) as proposed by Tuutti (1982), the beneficial effect of sandblasting by the increase of initiation time could be compromised by a reduction of the propagation time.

The actual conditions leading to corrosion initiation of steel in concrete are much more complicated than those that can be covered in a limited laboratory investigation. The findings discussed above should be considered while recognizing that many other factors can affect the effective threshold for corrosion initiation. For example, the threshold is expected to be a strong function of the open circuit potential before depassivation (Pedeferri, 1996), which may be altered by special exposure conditions (for example in submerged structures). Variations in the water content of the concrete and their effect on pore water composition should also be taken into account. Moreover, as suggested by Glass and Buenfeld (1997), simple initiation of active corrosion may not ensure its continuation in concrete and the presence of a reserve of bound chloride may be as important in defining an effective threshold as the chemistry of the pore water just before corrosion initiation. Finally, the experiments described here did not explore the effects of crevice configurations on corrosion initiation in concrete. Those conditions are a concern in the case of rebar with organic coatings (Sagüés et al. 1991), but have been thought to be potentially important also in the behavior of plain steel (González et al

1993). Another important factor that was not considered in this study was the effect of the specimen size. The threshold values were obtained using specimen areas of only ~60cm^2. However, the total steel area in an actual structure is typically several orders of magnitude larger. The chance of pit generation increases with the surface area of the specimen (Shibata 1982) since the number of "weak" points in the protective oxide film on a specimen increases accordingly (Szklarska-Simalowska 1986). Confirming evidence that an increase in area generally increased the corrosion probability has been documented (Mears and Brown 1937), although in relative few studies. This issue will be addressed in Chapter 4.

2.5 Conclusions

1) The chloride corrosion threshold in alkaline solutions depended strongly on pH. When [Cl^-] exceeded a threshold level, all the rebar specimens actively corroded in pH 12.6 SCS or pH 13.2 SPS1 solutions. In pH 13.6 simulated pore solutions, active corrosion was manifested but not sustained even when the [Cl^-] reached 3.0 M.

2) The threshold expressed as the ratio $CR_T=[Cl^-]_T/[OH^-]$ was not a constant; it increased significantly with pH, suggesting that the inhibiting effect of OH^- ions at high levels was stronger.

3) Estimated ranges of the total chloride corrosion threshold in concrete based on the liquid solution measurements and on available chloride binding data included threshold values observed in practice.

4) The large variability in the reported chloride threshold values in concrete may be attributed to variability of concrete pore water pH and of chloride binding ability.

5) Sandblasting to remove mill scale and other rust on the rebar surface was beneficial in increasing the chloride corrosion threshold in solutions. However, after activation, corrosion in liquid solutions was more severe on sandblasted steel than on steel with the other surface conditions.

Table 2.1 Chemical composition of the rebar steel (wt.%)

C	P	S	Mn	Si	Cr	Ni	Mo	Cu	Fe
0.43	0.007	0.038	1.11	0.22	0.03	0.11	<0.01	0.37	Bal.

Table 2.2 *Base chemical composition and pH values of test solutions (g/L)*

Composition	NaOH	KOH †	$Ca(OH)_2$*	pH
SCS	0	0	2.0	12.6
SPS1	3.70	10.5	2.0	13.3
SPS2	8.33	23.3	2.0	13.6

†Reagent grade KOH had only a purity of 85.3%.

∗ Most of the $Ca(OH)_2$ was not dissolved.

Table 2.3 C_{TT} (%wt of cement) ranges based on working assumptions

Steel surface condition	Concrete pore water pH		
	12.6	13.3	13.6
Sandblasted	0.10~0.65	1.25~2.8	2.7~6*
As-received or prerusted	0.05~0.45	0.6~2.1	1.8~4.2

*The upper limit is less accurate because of the unavailability of chloride binding data at that chloride level.

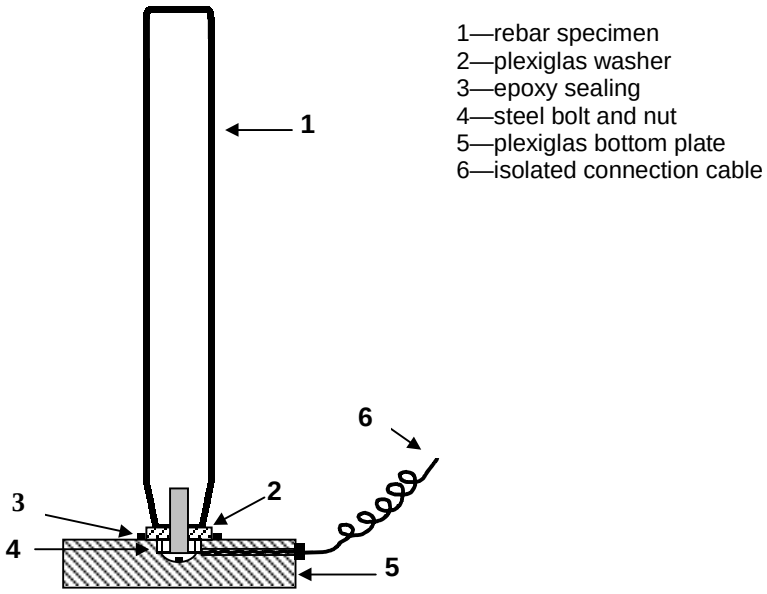

Figure 2.1 Schematic configuration showing specimen assembly

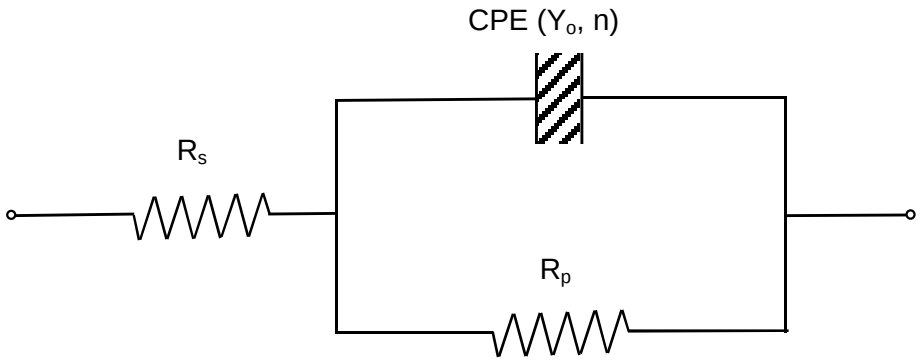

Rs: solution resistance
Rp: polarization resistance
CPE: constant phase-angle element ($Z=Y_o^{-1}(j\omega)^{-n}$)

Figure 2.2 Equivalent circuit used to interpret the EIS results

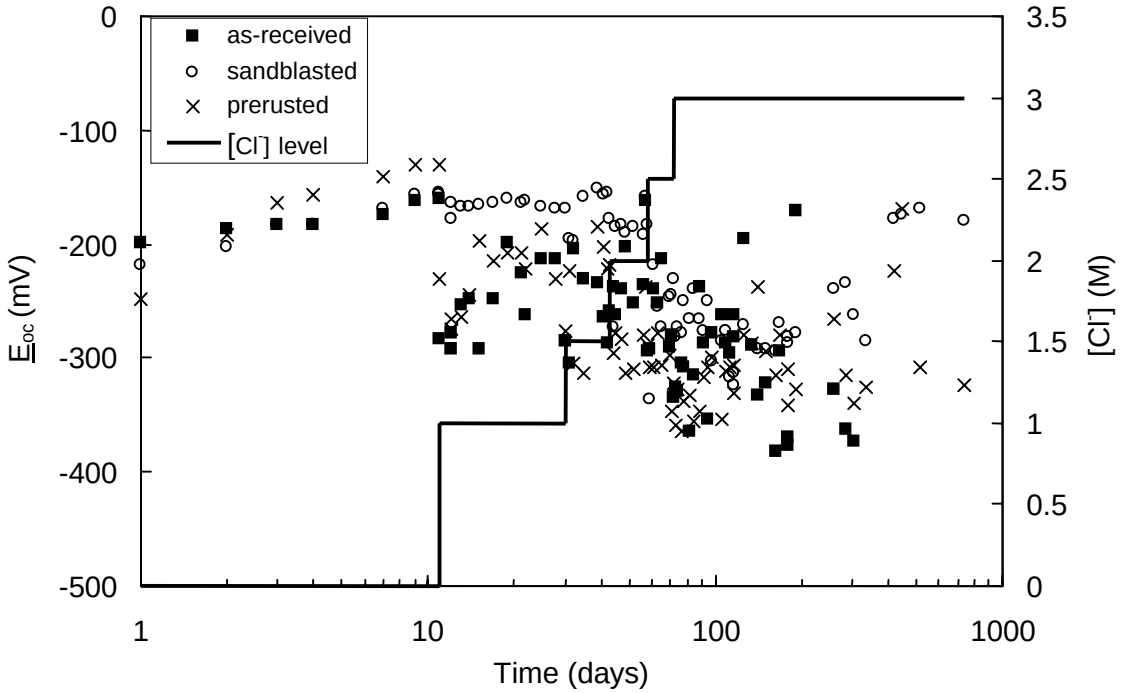

Figure 2.3 Evolution of open circuit potentials (average of five specimens) in pH 13.6 SPS2 solution with different levels of chloride addition

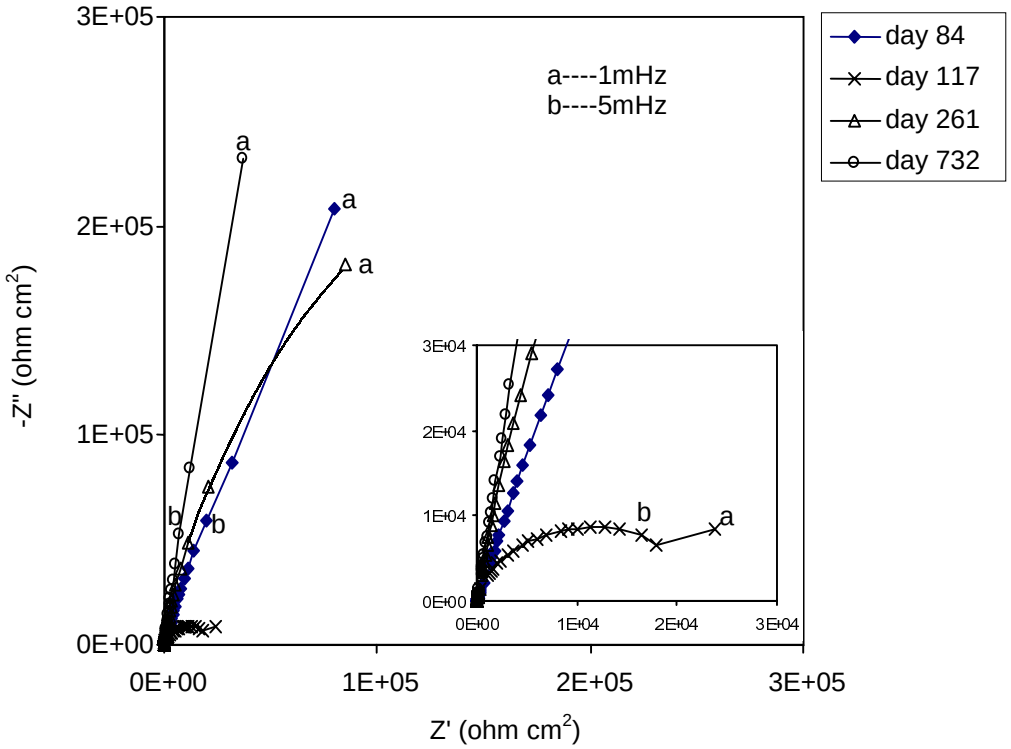

Figure 2.4 Nyquist plots of the EIS response of sandblasted rebar steel in pH 13.6 SPS2 with 3.0M NaCl.

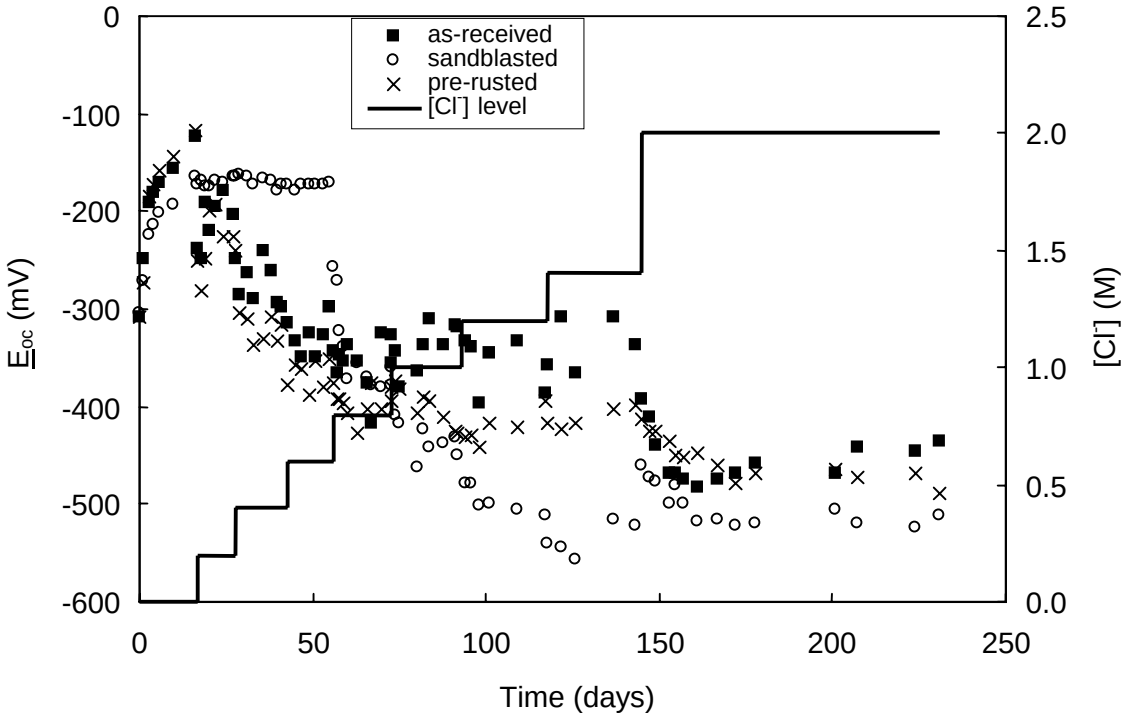

Figure 2.5 Evolution of open circuit potentials (average of five specimens) in pH 13.3 SPS1 solution with different levels of chloride addition

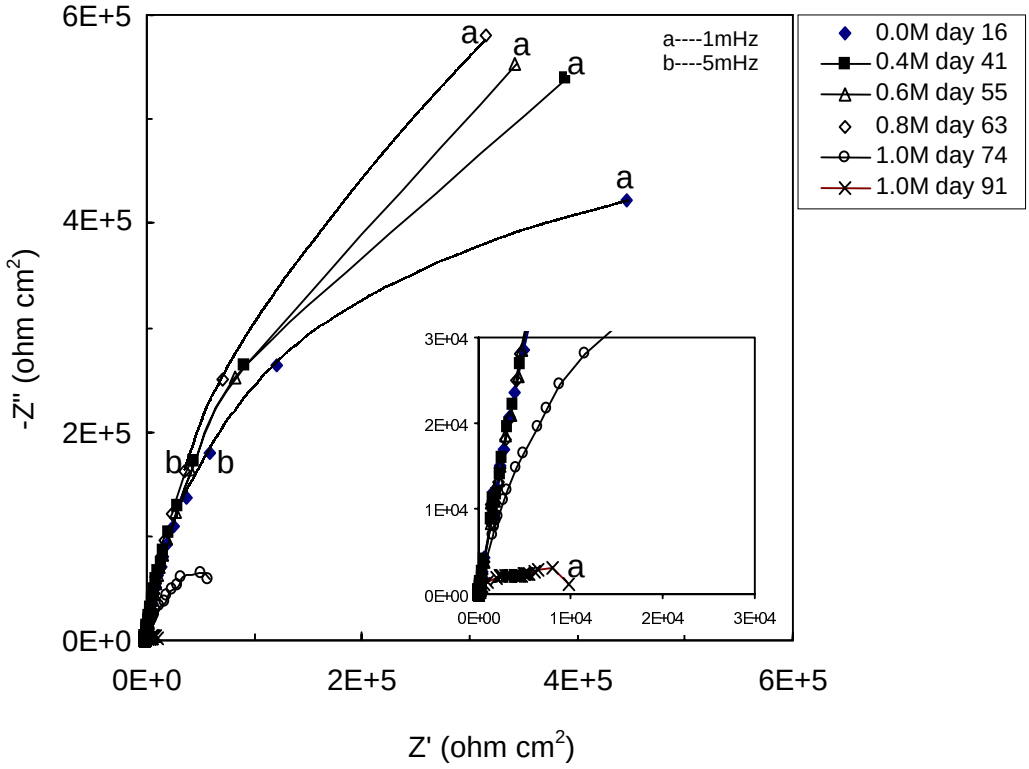

Figure 2.6 Nyquist plots of the EIS response of sandblasted rebar steel in pH 13.3 SPS1 with various levels of NaCl

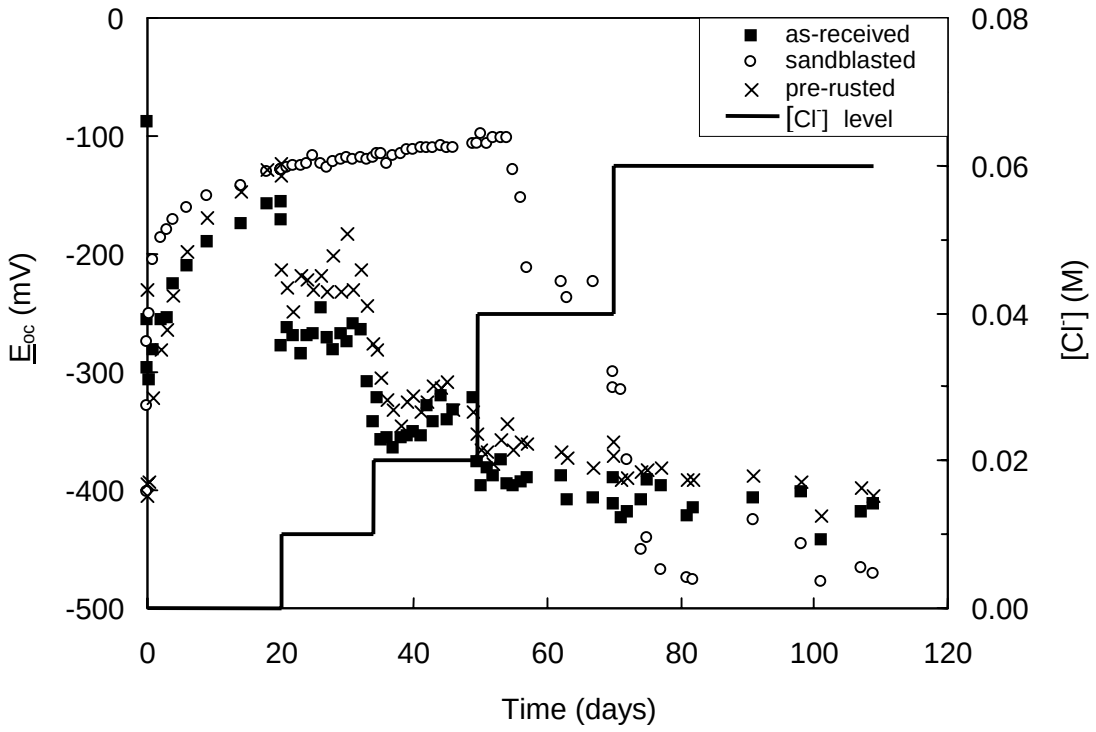

Figure 2.7 Evolution of open circuit potentials (average of five specimens) in pH 12.6 SCS with different levels of chloride addition

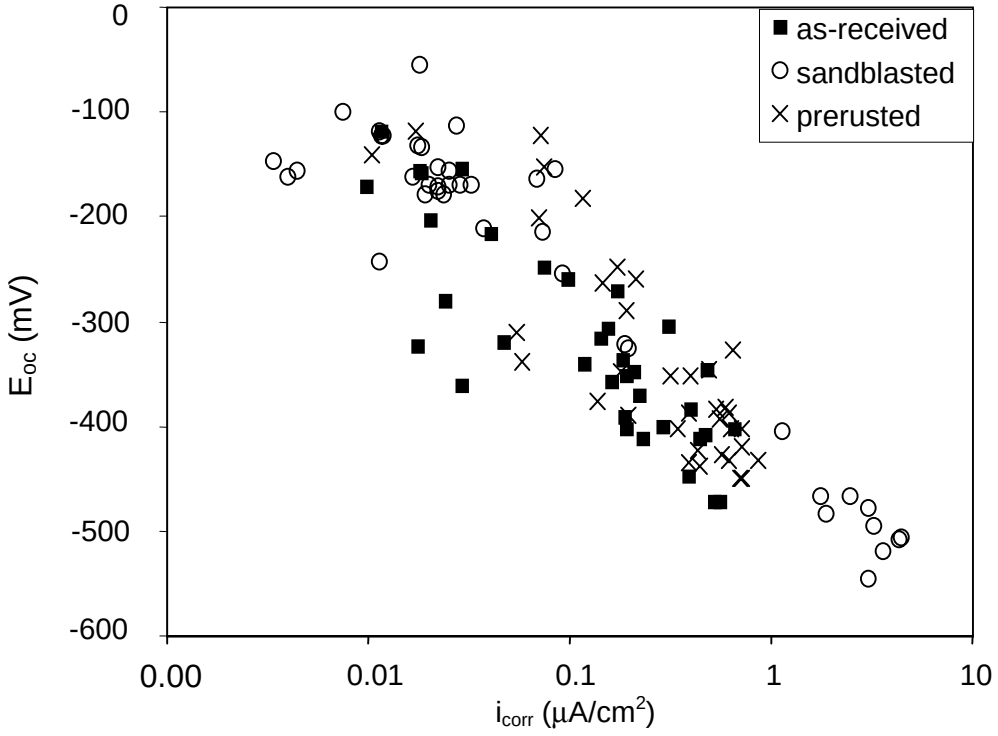

Figure 2.8 Relationship between E_{oc} and i_{corr} in SCS, SPS1, and SPS2

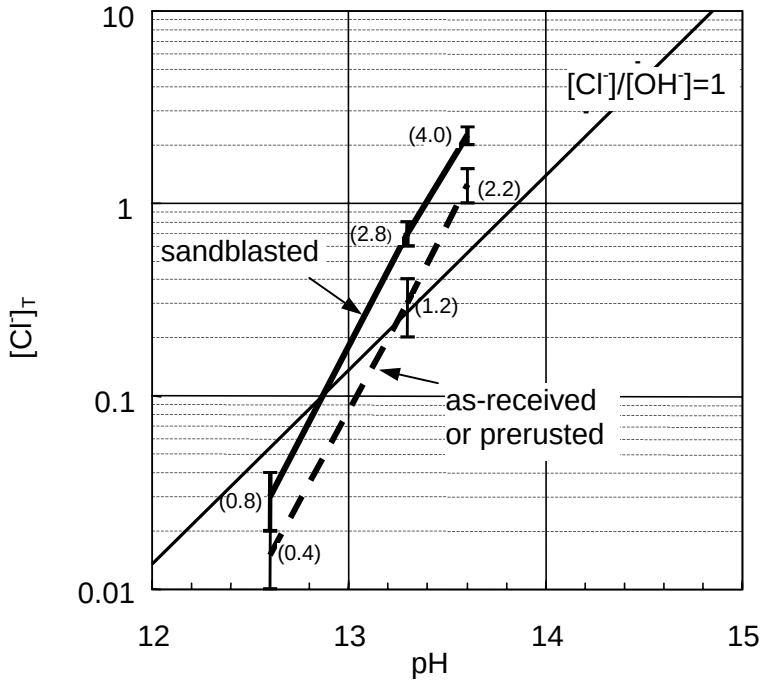

Figure 2.9 Upper and lower limits of the chloride concentration threshold as function of test solution pH (The lines join the average of the upper and the lower limit for each case. The as-received and pre-rusted conditions shared the same limits.)

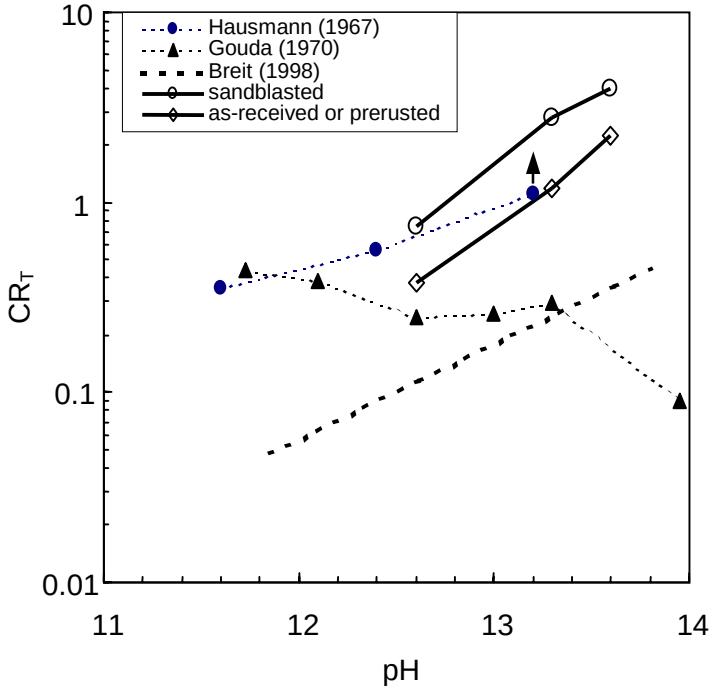

Figure 2.10 Comparison of threshold ratio $CR_T = [Cl^-]/[OH^-]$ from the present investigation and those from Hausmann, Gouda, and Breit

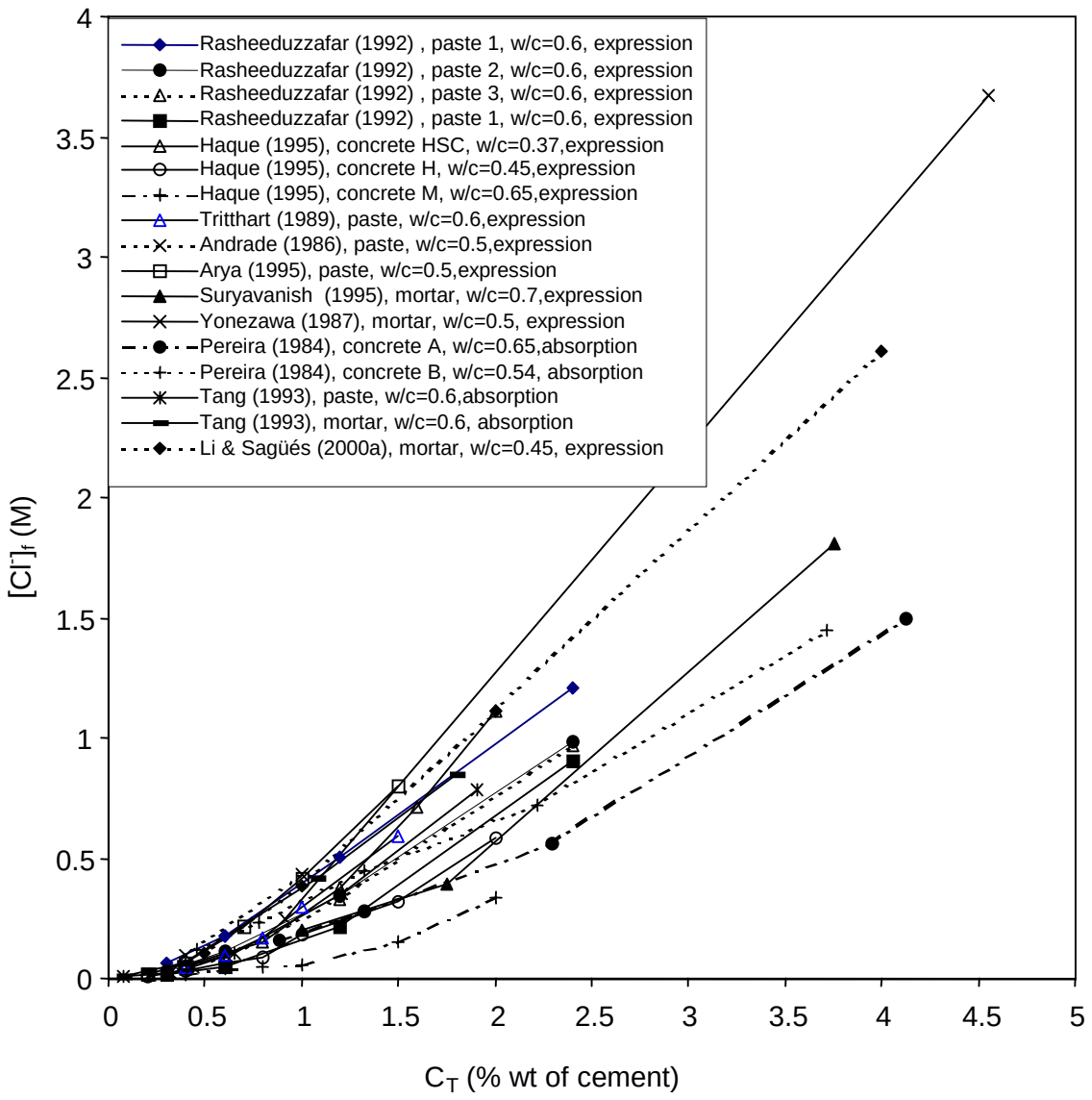

Figure 2.11 Relationship between concrete total chloride content (C_T) and pore water chloride concentration ($[Cl^-]_f$) for a variety of cement pastes, mortars, and concretes reported in the literature

CHAPTER 3: THE DISTRIBUTION OF PITTING AND REPASSIVATION POTENTIALS

3.1 Introduction

Chloride-induced corrosion of reinforcing steel bars (rebars) in concrete begins when the chloride content of concrete immediately next to the rebar reaches a critical threshold value. Much interest exists in determining that value and the conditions that affect it, since the threshold is a key parameter in durability prediction and corrosion control. However, corrosion initiation in concrete is a complex phenomenon. Reported values of the threshold in actual concrete systems vary over a wide range, while the factors responsible for that variation are difficult to identify. Consequently, several investigations have attempted to obtain fundamental understanding on the threshold and its determining factors by experiments in solutions simulating concrete pore water (Hausmann 1967, Gouda 1970, Breit 1998, Li and Sagüés 1999a & 1999b).

Fundamental issues examined in the past and of continuing interest include the sensitivity of the threshold to the pH of the pore water, and to the surface condition of the steel. A key question that has received scant attention is whether the threshold is a deterministic function of the exposure conditions, or if it can only be expressed statistically. Related matters, also little investigated, are the possible dependence of the threshold on the type and amount of steel surface area considered, and on the steel potential. This work addresses these concerns.

In Chapter 2 and recent publications (Li and Sagüés 2000b & 2000c) the effect of steel surface condition was investigated by examining the behavior in model solutions of rebar steel in its normal as-produced condition (with a mill scale), as-produced plus surface rusting, and in a white-metal sandblasted condition. Testing was conducted by open circuit immersion (OCI) in naturally aerated alkaline solutions of pH 12.6, 13.3 and 13.6 that simulated the main components of concrete pore water (Constantiner and Diamond 1997). The chloride corrosion threshold for those experiments ($[Cl^-]_T$) was defined as the maximum chloride concentration for which no active corrosion initiation was observed after prolonged (weeks-months) exposure at the open circuit potential, which was typically -100 mV to -200 mV in the Saturated Calomel Electrode (SCE) scale. The value of $[Cl^-]_T$ was found to markedly increase with $[OH^-]$, and to be about twice as much for sandblasted steel than for steel with as-produced or rusted mill scale. The results also showed that once $[Cl^-]_T$ was exceeded, corrosion started on some but not necessarily all of the specimens in a series of replicates. This observation indicates a stochastic component in the corrosion initiation process in these systems (as already recognized in the early work by Haussman (1967), a behavior that needs examination. Furthermore, the OCI results yielded values of $[Cl^-]_T$ that, for the same pH, tended to be higher than thresholds reported elsewhere for steel exposed to potentials as high as the oxygen evolution potential (E_{OE}) (Li and Sagüés, 2000b & 2000c). Such result underscores the threshold sensitivity on electrode potential. Normal exposure conditions in aerated concrete result in steel potentials similar to those encountered in the OCI tests, but other situations (immersed structures, cathodic prevention (Pedeferi, 1996) necessitate information on the behavior over a range of potentials.

The OCI experiments and comparable potentiostatic tests have the advantage of long stabilization times and hence less chance of obscuring artifacts due to excessive test acceleration. However, examination of the stochastic aspects (including surface area effects) and potential dependence of corrosion initiation, in a variety of surface conditions, would be very time consuming if conducted with quasi static methods such as OCI. As an alternative, cyclic polarization (CYP) experiments, which have been widely used to determine pitting and repassivation potentials of many alloys in aggressive environments (Pourbaix et al. 1963, Wilde 1972, Thompson and Syrett 1992), can rapidly provide valuable insight on these issues. Consequently, CYP experiments were conducted to establish the potential-dependent corrosion initiation and repassivation behavior of steel in alkaline solutions with various chloride levels. The experiments used numerous replications to assess the statistical behavior of corrosion initiation, and examined different levels of surface roughness to reveal the effect of surface condition. The findings of those experiments are presented in this chapter, while the results of a subsequent investigation on the effect of area size will be given in Chapter 4.

3.2 Experimental

Specimens ~15cm long were cut from ordinary A-615 reinforcing steel bars (size #4, diameter ~1.2cm) from the same heat used in Chapter 2. The steel chemical composition (in wt%) was: 0.43 C, 0.007 P, 0.038 S, 1.11 Mn, 0.22 Si, 0.03Cr, 0.11 Ni, 0.37 Cu, and Fe (bal.) (see Table 2.1). One end of each specimen was first drilled and tapped, then machined to produce a truncated conical shape. Two types of specimens (I and II) were used. In Type I specimens (sandblasted surface, the base condition used for the majority of the tests), only the conical bevel surface (~1 cm^2) was ground to 600 grit emery paper, while the rest of the bar surface (with diamond-pattern surface deformations) was sandblasted completely removing the mill scale. The nominal exposed surface area of this type of specimen was ~60 cm^2. For Type II (surfaces abraded to several roughness levels, as variations from the base condition), each bar was first machined to a diameter of ~1 cm and then the whole surface (~50 cm^2) was either dry ground to 60 grit or wet ground in one or several steps to a final finish of 120, 320, or 600 grit, respectively. All the specimens were assembled using a custom configuration schematically shown in Figure 3.1(a). To avoid crevice corrosion, the acrylic washer was very tightly pressed against the tip of the specimen by fastening the screw on the top of the assembly. This new specimen arrangement was more convenient than that used Chapter 2 in that the assembly of each specimen could be finished instantly. Some of the specimens were repeatedly used after resurfacing.

A sealed rectangular plastic tank (10 cm $\times$ 22 cm $\times$ 22 cm) containing ~4.6 L testing solution was used in the experiments (Figure 3.1(b)). Four graphite rods (0.6 cm $\times$ 31 cm) (two on each side of the tank) were symmetrically positioned with respect to the specimen, which was in the middle of the tank. A saturated calomel electrode (SCE) was placed with the sensing tip ~1 cm from the specimen. All potentials are given in the SCE scale. The solution inside the tank was continuously deaerated by introducing commercially pure nitrogen through a gas purger. Four base solutions (Table 3.1), a pH12.6 saturated calcium hydroxide solution (SCS) and three types of simulated concrete pore solutions (SPS2 of pH13.6, SPS3 of pH13.1, and SPS4 of pH11.6) were prepared. Reagent grade sodium chloride crystals were used to

adjust the chloride concentration ([Cl^-]) of the base solutions. Table 3.2 shows the chloride concentration for each test condition. The test cell was at ambient room temperature, 21±2ºC.

The CYP tests were performed with a forward (in the noble direction) scan rate (denoted by v_f) of 0.167mV/sec starting at –0.85 V. As will be shown in the Chapter 4, the v_f value used in the present work was below the range where pitting potentials became highly sensitive to the choice of v_f. The polarization direction was reversed with a faster backward scan rate of 0.417 mV/sec once the nominal anodic current density had reached 100 $\mu A/cm^2$ (irrespective of whether the current was due to pitting corrosion or to oxygen evolution). A faster return scan rate was used to lessen the severity of corrosion damage on the steel surface (Berke 1986) and to diminish solution contamination by corrosion products. Before applying the CYP schedule, all the specimens were conditioned at –1 V for 2000 seconds to achieve a reproducible initial surface condition. The CYP tests were repeated at least 12 times at most of the chloride contents, and 50 times for one special test case. A newly surfaced specimen was used each time.

CYP tests were also performed on some specimens that had been previously prepassivated. Those specimens were first immersed in a naturally aerated, chloride-free SCS or SPS2 for a specified period of up to 82 days (called the prepassivation time, t_{pp}) to allow the development of a given extent of passivity. The open-circuit potential of each specimen at the end of prepassivation, E_{oc}', was recorded. Each specimen was then carefully transferred (avoiding any contact of the steel surface solids that may mechanically disrupt passivity) into another cell containing the same type of solution but with a specified [Cl^-]. Prior to the CYP testing, the transferred specimen was usually conditioned at E_{oc}' for 1000 seconds. After that, the specimen was tested using the same CYP schedule as described earlier but starting at E_{oc}' (instead of –0.85V) so as not to reduce the pre-existing passive film. The test conditions for this series of tests are listed in Table 3.3.

The CYP tests yielded the pitting potential (denoted by E_p; the average of a series of repeated experiments will be denoted by $\underline{E_p}$) and the repassivation potential (E_r; average denoted by $\underline{E_r}$). Figure 3.2 shows schematic CYP curves of experiments in which steel experiences either pitting/repassivation (a) or no pitting (b). In case (a), E_p was defined as the potential at which the nominal anodic corrosion current density (denoted by i) first reached 10 $\mu A/cm^2$, and E_r was defined as the potential where the backward scan on the cyclic polarization curve intersected the forward scan. Besides E_p and E_r, two other parameters related to the anodic current density were also recorded. One was the plateau passive current density (i_p) and the other was the maximum anodic corrosion current density (i_{max}). In case (b), corrosion did not initiate and the anodic current surge near ~0.6V (depending on solution pH) was due to the oxygen evolution reaction. The value E_{OE} was defined as the potential corresponding to an oxygen evolution current density of 10 $\mu A/cm^2$. In such case, neither E_r nor i_{max} applied, and E_p was nominally assigned a value equal to E_{OE}. The actual E_p (if polarization to that extent could be achieved) would presumably be nobler than the assigned value.

Active corrosion on all cases examined was initially visually manifested by well defined, small pits. However, further corrosion propagation at an initial pit site was usually lateral, in

the form of a dark surface stain often many mm^2 in size. Upon removal of corrosion products, metal loss was observed over much of the discolored region. The terminology “pit” and “pitting” will be applied in the following to the corroded spots and associated initiation/repassivation potentials respectively, but only for convenience and recognizing that the corrosion morphology can differ substantially from that of a high aspect ratio pit.

3.3 Results

3.3.1 Types of Cyclic Polarization Behavior

Figure 3.3 shows typical cyclic polarization curves of sandblasted steel obtained in SCS with 0.01M NaCl. The i_p value was ~4 $\mu A/cm^2$ and generally reproducible. From EIS measurements that will be presented in Chapter 5 , the apparent interfacial capacitance (C_F) of sandblasted steel in SCS was <200 $\mu F/cm^2$ in the time domain range of these experiments. Based on the values of C_F and v_f, the charging current density due to the interfacial capacitance during the forward scan was estimated to be on the order of 0.03 $\mu A/cm^2$ and hence negligible compared with the current densities over much of the scan. Because of the high solution conductivity, the results were not corrected for IR drop. The surge in current density at ~0.6V was as expected from the H_2O electrochemical stability diagram (Pourbaix 1966) for the oxygen evolution process.

The behavior shown in Fig. 3.3 can be categorized into three modes designated by A, B, and C. In mode A (run #3) pitting did not initiate up to E_{OE}. In mode B (run #1) pitting initiated at a high potential (near E_{OE}); this initiation normally took place during the forward scan but in some instances during the reverse scan instead. In mode C (runs #2 and #4) pitting initiated easily at potentials as low as ~0V. Whenever pitting initiated, a large hysteresis loop could be observed. For $[Cl^-] \leq 0.004M$, all the specimens behaved as in mode A. For $[Cl^-] > 0.04$ M, the behavior was usually as in mode C, although E_p varied significantly from test to test. For intermediate concentrations (e.g. $[Cl^-] = 0.01$ M, Fig. 3.3,), all three modes could be observed, varying at random from test to test.

Figure 3.4 shows several typical cyclic polarization curves obtained for sandblasted steel in SPS2 with 0.6 M $[Cl^-]$. All three CYP modes observed in SCS were encountered also in SPS2. Mode A was only observed when $[Cl^-] \leq 0.4$ M whereas mode C was manifested when $[Cl^-] \geq 1.0$ M. Mode B was observed only when $[Cl^-] = 0.6$ M and 0.8 M.

3.3.2 Effect of $[Cl^-]$ on E_p and E_r

Figure 3.5 shows E_p and E_r for sandblasted steel as a function of $[Cl^-]$ in SCS. When $[Cl^-] = 0.001$ M and 0.004 M, pitting did not initiate in any of the repeated tests and E_p was assigned a nominal value equal to E_{OE}. Even when $[Cl^-] = 0.008$ M and 0.01M, fewer than 50% of the specimens pitted during the CYP test. For higher $[Cl^-]$, pitting usually initiated at potentials distinctly below E_{OE}. For $0.01M \leq [Cl^-] \leq 1.0$ M, $\underline{E}_p$ decreased roughly linearly with increasing $[Cl^-]$ but at most concentrations E_p showed large variability. In contrast, E_r showed much less variability and $\underline{E}_r$ appeared to be nearly independent of $[Cl^-]$.

Figure 3.6 shows E_p and E_r for sandblasted steel as a function of $[Cl^-]$ in SPS2. The overall behavior resembles that shown in Fig. 3.5 for SCS. When $[Cl^-]$ = 0.4M, no pitting corrosion occurred up to E_{OE}. When $[Cl^-]$ = 0.6 M, only about half of the specimens pitted during the CYP test. When $[Cl^-] \geq 0.8$ M, pitting initiated in each test. $\underline{E}_p$ decreased markedly when $[Cl^-]$ increased from 0.6M to 0.8 M but remained almost unaffected by further increases. As in SCS, $\underline{E}_r$ appeared to be nearly independent of $[Cl^-]$.

3.3.3 Effect of Surface Finish on E_p and E_r

Figure 3.7 compares E_p values of sandblasted and 600 grit finished steel in SCS and SPS2. With the exception of SCS at high chloride contents, $\underline{E}_p$ in both solutions was significantly higher (e.g., by ~0.7V in SPS2 at 0.1 M $[Cl^-]$) for steel with the finer 600 grit finish than for the sandblasted steel. Otherwise, the overall trends of E_p and $\underline{E}_p$ with varying $[Cl^-]$ and $[OH^-]$ observed for sandblasted steel were also encountered for the 600 grit finish.

Figure 3.8 compares E_p and E_r obtained in the series of tests in SPS2 with 1M $[Cl^-]$ for which the entire range of surface finishes was examined. The sandblasted finish was assigned the nominal grit number 50, corresponding to the maximum diameter of the impacting particles used (~250 μm). There was a substantial decrease in $\underline{E}_p$ as the roughness of the steel surface decreased. In contrast, E_r showed little dependence on surface finish except for the higher value observed at 600 grit.

3.3.4 Effect of $[OH^-]$ on E_p

Comparison of the E_p values shown in Figs. 3.5-3.7 indicates that a change of $[OH^-]$ from 0.04M (pH12.6 SCS) to 0.56M (pH13.6 SPS2) significantly increased $\underline{E}_p$ for a fixed $[Cl^-]$. In Figure 3.9, the effect of $[OH^-]$ on E_p over a wide pH range (from pH 11.6 to 13.6) is shown for 600 grit steel in SPS4, SCS, SPS3, and SPS2 with 1.0M NaCl. $\underline{E}_p$ increased by ~0.15V/pH unit from pH11.6 to pH 12.6. A much steeper increase of $\underline{E}_p$ (> 0.8 V/pH unit) was observed from pH 12.6 to pH 13.6, suggesting the inhibiting effectiveness of OH^- ions. From Fig. 3.9 it is also seen that E_p obtained in SPS4 or SCS with 1.0M NaCl was nearly reproducible (the apparent reproducible E_p obtained in SPS2 with 1.0M NaCl will be explained later). On those occasions (corresponding to very high $[Cl^-]/[OH^-]$ ratios, denoted by CR hereafter), visual observation of the steel surface shortly after the surge in anodic current revealed that pits tended to be small and numerous. However, pitting initiation was usually limited to very limited number of spots whenever CR was not significantly high.

3.3.5 Effect of Prepassivation on E_p

Figure 3.10 shows the effect of prepassivation in SPS2 on E_p of rebar steel in SPS2+2M NaCl. It can be seen that $\underline{E}_p$ of the sandblasted steel increased gradually from t_{pp}=0 day to 6 days. For both sandblasted steel and 600 grit steel, $\underline{E}_p$ increased by ~0.2V when $t_{pp} \geq 6$ days. No further significant increase in $\underline{E}_p$ was observed after more prepassivation time greater than 6 days.

Figure 3.11 shows the effect of prepassivation in SCS on E_p of sandblasted steel in SCS with 0.04M and 1.0M NaCl. In SCS+0.04M NaCl, $\underline{E}_p$ appeared to be higher after prepassivation (t_{pp}= 6 and 30 days) than that without prepassivation (t_{pp}= 0 day). In SCS+1.0M NaCl, the effect of prepassivation on $\underline{E}_p$ actually has not been determined because all the specimens corroded while the prepassivated specimen was potentiostatically polarized at E_{oc}' (prior to the application of CYP). In this case, the time elapsed (denoted by τ, called induction time) before pitting initiation was recorded. It was found that τ scattered significantly and log(τ) was approximately normally distributed (Fig. 3.12).

3.4 Discussion

3.4.1 Distribution of E_p

For most of the test conditions examined, E_p obtained in multiple replicate tests was far from a unique value. This observed non-deterministic nature of E_p has also been found in other systems (Shibata and Takeyama 1977) and prompted a statistical examination of the present results. To that effect, a large population of replicate tests in any given test condition can be considered. The cumulative pitting probability for a given potential E may then be defined as the fraction of tests that result in pitting at or below that potential. For a limited population of N replicate tests, the cumulative pitting probability can be approximated by the fraction PP(E) defined as follows:

$$PP(E) = \frac{n(E)}{1+N} \qquad (3.1)$$

where E is the electrode potential, n(E) is the number of specimens which actually experienced pitting and for which $E_p \leq E$, and N is the total number of replicate tests.

Figures 3.13 to 3.16 shows PP of sandblasted and 600-grit finish steel in both SCS and SPS2 media, as a function of potential and using the solution $[Cl^-]$ as a parameter. The results show S-shape distributions, shifting to the right as the chloride concentration decreased. The PP distributions tended to be quite narrow at very high chloride concentrations and broader as the chloride content decreased.

At low enough chloride concentrations some of the distributions were either truncated, or approached a nearly vertical line, when potentials near E_{OE} were reached. The truncated distributions corresponded to instances where at least some of the specimens failed to exhibit pitting up to E_{OE}, in which cases E_p was assigned a nominal value equal to E_{OE}. The approach to a nearly vertical line (e.g. 1.0 M $[Cl^-]$ in Fig. 3.15) denotes cases where several specimens actually pitted at or very near E_{OE}. As explained in Chapter 2, this latter occurrence may reflect the effect of local OH^- depletion during O_2 evolution with consequent facilitation of pitting. Thus, the nearly vertical portion by E_{OE} will be considered as an artifact and these distributions will also be considered as truncated.

The large variability of E_p has been reported for many systems. Shibata and Takeyama (1977) found that E_p of 304 stainless steel in 3.5% NaCl solution followed a Gaussian distribution. However, Salvago and Fumagalli (1995) reported that the distribution of

breakdown potential of 304 stainless steel in 0.1M HCl solution may or may not be Gaussian. In the present work, the test populations are in most cases sparse (about 12 replicates), which obscures their statistical character. A longer series of 50 replicates was tested for the case of sandblasted steel in SCS with 0.04 M [Cl^-] (for which there is little truncation at E_{OE}) in an attempt to obtain additional information. For that series, the ratio of the interquartile range (E_p (PP=0.75) - E_p (PP=0.25)) to the standard deviation of the sample was ~0.6 compared to 1.3 in an ideal normal distribution (Sincich, 1996). A value of 0.6 or less has a very low chance (<1:300) of occurring for a random 50-sample from an ideal normal distribution, so at least in this case the behavior significantly deviated from that of a normal distribution. As will be discussed in Section 3.4.3, knowledge of the functional form of the pitting potential distribution curve would be very desirable. For that purpose, future investigations should be conducted with large specimen populations.

3.4.2 Distribution of E_r

The values of E_r showed also significant variability in replicate tests and a statistical analysis was attempted. Similarly to the pitting case, a cumulative repassivation probability for an ideal large population was approximated by the fraction RP(E) defined as follows:

$$RP(E) = \frac{m(E)}{1+M} \qquad (3.2)$$

where m(E) is the number of specimens for which $E_r \geq E$, and M is the total number of specimens that actually experienced pitting in a series of repeated tests.

E_r measurements were conducted extensively for sandblasted steel in SPS2 and SCS. The corresponding RP distributions are shown in the same graphs as the PP distributions in Figs. 3.13 and 3.14. Single series available for 600 grit finish in SPS2 and SCS are shown in Figs. 3.15 and 3.16. In each of Figs. 3.13-3.16 the RP distributions tended to start at potentials below the lowest E_p values recorded in the same figure, and to span a narrower potential range (from ~-0.8 V to ~-0.4 V) than that of E_p. Unlike E_p, E_r showed little systematic variation with [Cl^-] or [OH^-]. As it was noted in Fig. 3.8, E_r was also little affected by the degree of surface roughness. Instead, E_r was sensitive to the maximum corrosion current density (i_{max}) recorded during each CYP test, as shown in Fig. 3.17, which is a composite of data from all the CYP tests performed in SPS2 and SCS. Clearly E_r was a strong function of the severity of corrosion attack (indicated by i_{max}) that had occurred before repassivation.

The plot in Figs. 3.17 suggests also that the decreasing trend of E_r with i_{max} encounters a lower limit (shared by the various surface conditions and solution compositions) at ~-0.8 V. This value is close to the potential range required for iron immunity within a localized acidic environment (Pourbaix,1966), and would not seem related to true repassivation. As only one return scan rate (0.417 mV/s) was used in this investigation, it is not known whether nobler E_r values would have resulted from slower return scans, as proposed by Dunn et al. (2000) for the case of high performance alloys. However, the long term corrosion potential of steel when it experiences stable pitting in alkaline solutions (see Chapter 2) (and also in concrete) with chlorides often reaches values as negative as -0.4 V to -0.6 V (Rasheeduzzafar et al. 1992),

clearly without causing repassivation. Thus, it does not appear likely that E_r would become much nobler if the return scan rates were lowered even to values small enough to represent near steady state regimes. This observation, and the near lack of solution composition or surface roughness effects on E_r, severely limits its usefulness to assess conditions leading to pitting in the present system. Consequently, the rest of the discussion will focus on the insight that the E_p behavior may give on the initiation of localized corrosion.

3.4.3 Implications to the Chloride Corrosion Threshold

Localized corrosion initiation may be viewed as the outcome of a competitive process between the inhibiting properties of hydroxyl ions and the breakdown-inducing effect of chloride ions. As indicated in Chapter 2, corrosion initiation in this type of system has long been thought to be a function of the chloride to hydroxide ion ratio, CR =$[Cl^-]/[OH^-]$. This parameter may be conveniently examined first with the extensive set of E_p results for sandblasted steel in SCS and SPS2 (no prepassivation), plotted together in Figure 3.18 as function of CR. The results for the two solutions follow roughly a general trend of decreasing $\underline{E}_p$ with increasing CR, from a nominal E_{OE} value for CR< ~0.2 (SCS) or CR<0.7 (SPS2) to a common trendline when CR >~1. Figure 3.18 also shows E_r, underscoring the low sensitivity of that parameter to test variables. The values of $\underline{E}_p$ and the standard deviation, σ, of distributions of E_p for which all values were less than E_{OE} (that is, without truncation artifacts) are shown in Figures 3.19 and 3.20. Those figures include also results from non-truncated distributions obtained from the 600 grit tests (no prepassivation) performed in both solutions as well as in SPS3 and SPS4. Approximately simple, common trends were revealed when plotting the $\underline{E}_p$ results as function of the inverse of CR; parameters for each trend are shown with each graph. $\underline{E}_p$ showed a roughly linear increase with CR^{-1} for both surface finishes. The trendline for 600 grit was steeper, resulting in higher $\underline{E}_p$ values as CR^{-1} increased, thus indicating higher corrosion resistance of the smoother surface finish when CR is low. However, the trendlines converged toward an E_p range of ~-0.4 V to -0.2 V at small values of CR^{-1} (high $[Cl^-]/[OH^-]$), indicating less differentiation in corrosion resistance under those conditions. The value of σ also increased with CR^{-1} and followed a trend roughly shared by all the surface conditions and solution compositions examined (Fig. 3.20). At the smallest values of CR^{-1}, σ was only about 10-20 mV but it became about one order of magnitude higher as CR^{-1} increased. Examination of Figs. 3.13-3.16 reveals that σ increased as $\underline{E}_p$ increased. This feature has also been observed for other systems (Ilevbare et al. 2000).

At smaller values of CR than those considered in Figs. 3.19-3.20 the E_p distributions are truncated at E_{OE} so both E_p and σ become less meaningful. A truncated distribution may be viewed as the portion below E_{OE} of a fictitious distribution having a pitting potential $\underline{E}_p$* and standard deviation σ* beyond those recorded in Figs. 3.19-3.20. However, extrapolation to higher CR^{-1} values is not always warranted. This is evident when comparing the behavior of sandblasted steel in SCS and SPS2 solutions (Figure 3.18) for CR < ~1. The value of $\underline{E}_p$ for the high pH SPS2 increases abruptly to near E_{OE} when CR decreases from 1.5 to 1, while the transition is much more gradual in the lower pH SCS so that $\underline{E}_p$ did not closely approach E_{OE} until CR<~0.2. Although there are fewer data, a similar relative difference in behavior at low values of CR (but over a different CR range) can be discerned when comparing the E_p trends for the 600 grit surface condition in SCS and SPS2.

The decrease of σ with CR (Fig. 3.20) agrees with the observed corrosion morphology trends. Whenever CR was high, pits tended to be numerous on both sandblasted and 600 grit specimens. This behavior suggests that the nucleation of pits may have occurred at numerous microscopically distributed features (e.g. MnS precipitates (Szklarska-Smialowska 1972, Stewart and Williams 1992) that are present regardless of surface condition). Such hypothesis would also agree with the approach toward a common range of E_p values at high CR (Fig. 3.19) for the sandblasted and 600 grit surface trends. The large number of pits on any given specimen would then result in little variability from sample to sample and consequently small σ values. As CR decreased fewer pits were apparent, so the specimen-to-specimen variability in E_p and thus σ would be expected to increase as observed.

For moderate values of CR, $\underline{E}_p$ was sensitive to surface roughness, decreasing with it. This behavior may reflect in part the presence of a larger effective surface area on the rougher surface specimens, thus multiplying the number of active pit nucleation sites (which should be fewer per unit area than when CR is high). Moreover, at least in the sandblasted surfaces the erosion process may have created numerous occluded spots under deformation platelets (Levy 1991), which could act as microcrevices favoring localized corrosion initiation compared to a smooth surface.

The above discussion did not consider the effect of prepassivation , which increased the resistance to localized corrosion (Figs. 3.10 and 3.11). The PP distribution curves shifted to the right as t_{pp} increased, with much of the effect taking place during the first week or so (Figs. 3.21 and 3.22). This observation suggests that pitting initiation is strongly affected by the maturity of the passive film and that the build-up of that film is a gradual process. It should be noted that although $\underline{E}_p$ increased with t_{pp}, prepassivation did not change σ significantly when truncation did not take place (Fig. 3.23).

In many field applications passive steel in concrete develops an open-circuit potential, E_{oc}, of ~ -0.1 V (Sagüés 1994), which remains near that level for a long time until chloride ion contamination of the pore water causes the onset of active corrosion. If the process of corrosion development in the laboratory CYP tests was representative of that in the field, a chloride corrosion threshold CR_T could be postulated as the value of CR that would cause E_p to be equal to -0.1 V. Since E_p is not unique, CR_T could be redefined instead as the highest value of CR that results in a pitting probability of zero at -0.1 V. That definition presupposes a termination of the pitting probability cumulative distribution at a finite limiting potential E_{pl} that depends on CR. Faced with only a limited set of replicate experiments with a given CR and surface condition/base solution combination, the value of E_{pl} could be approximated by the lowest value of E_p determined in the set. In the present case series of experiments for a given surface condition/base solution combination were performed at discrete values of CR. CR_T would then be a value somewhere between the lowest CR that yielded $E_{pl} < -0.1V$, and the highest CR that yielded $E_{pl} > -0.1V$.

The above definition was applied to the measurements and yielded the values listed in Table 3.4, which lists also for comparison the values of CR_T obtained by the OCI method and reported Chapter 2. As discussed in Chapter 2, the CR_T values obtained by OCI were roughly

in agreement with those reported for steel in concrete, after accounting for the partition between total chloride in concrete and that in the pore water.

The results indicate that CR_T as defined above is a function of the base test solution, with the pH13.6 SPS2 yielding a significantly higher threshold value (as was expected by examination of Fig. 3.18) in all cases. The higher pitting resistance of the smoother 600 grit finish is also evident. These trends had been observed also in the OCI experiments in Chapter 2, although the estimated threshold values reported there were different from those of the regular CYP tests. The limited data available (Figs 3.10 and 3.11) reveal that prepassivation increased CR_T values, comparable to those obtained with the OCI method. This is not surprising, since the OCI technique effectively allows for an extended prepassivation period before and during the early chloride additions to the base solution. These results suggest that even though operating in an apparently scan-rate independent regime, conditions in the regular CYP tests fail to yield a passive layer with the maturity present in slowly evolving systems. Thus, regular CYP tests in conjunction with the assumptions used above do not seem to be suitable for a quantitative estimate of chloride threshold in concrete.

The CYP experiments revealed however a marked stochastic character of the localized corrosion of steel in alkaline solutions. This character is expected to be present to some extent also under the quasistatic conditions encountered for steel after long exposures to concrete pore water, as suggested by the little change in σ after prepassivation (Fig. 3.23) and by the variability in induction times for pitting initiation on prepassivated steel in SCS+1.0M NaCl potentiostatically polarized at –0.15V (Fig. 3.12). An important consequence of stochastic behavior is that the assumption of a limiting potential E_{pl} may be unwarranted. Thus, a small but finite corrosion initiation probability may exist at potentials significantly below that assigned to E_{pl} from a series of tests with a limited number of small specimens, either tested in liquid solutions or in concrete. That would also mean that the estimated value of CR_T would allow for a small but finite chance of corrosion initiation at lower CR levels. Field structures have steel areas that can be several orders of magnitude greater than those of laboratory specimens. As pitting probability increases with area (Shibata 1982, Burstein and Ilevbare, 1996) in many systems, even a very small probability of corrosion unresolved in small scale laboratory tests could mean high likelihood of corrosion in the field. The area dependence of PP will be addressed in Chapter 4.

Knowledge of the functional form of the pitting probability distribution could provide a powerful means of using limited laboratory data to forecast extreme events such as those that may be important for large structures. In the absence of other information, a working assumption (for example, of Gaussian behavior) could be made to apply the present results to that effect. Unfortunately, the only large data set available (PP for sandblasted steel in SCS with 0.04 M [Cl^-]) suggests that the behavior is more complex. Resolution of this important issue is needed.

3.5 Conclusions

1) The pitting potential (E_p) was not a unique function of solution composition or steel surface condition; the behavior of E_p should be considered statistically. The variability of E_p tended to decrease at high values of the ratio CR (= $[Cl^-]/[OH^-]$).

2) The average value of E_p ($\underline{E}_p$) for a series of replicate tests decreased with $[Cl^-]$ and increased with $[OH^-]$. For a given solution composition $\underline{E}_p$ decreased as the roughness of the steel surface increased. However, E_p was less sensitive to surface roughness when CR was high.

3) The repassivation potential E_r was nearly independent of solution composition and steel surface finish. Instead, E_r was influenced by the severity of corrosion that took place during the return scan of the polarization cycle. A lower limit for E_r of ~-0.8 V (SCE) is consistent with the condition for steel immunity.

4) The functional form of the distribution of pitting potentials for a given solution and steel surface condition was not identified. Results from a large series of repeat tests deviated significantly from a simple Gaussian distribution.

5) Increasing the maturity of the passive film by prepassivation increased $\underline{E}_p$ significantly, but did not change much the spread of the pitting probability distribution.

6) Estimation of a chloride corrosion threshold CR_T was made by assuming for simplicity that the pitting probability is zero at the open circuit potential when $CR<CR_T$. Agreement of the CR_T values thus obtained was poor when comparing values from regular cyclic polarization (CYP) tests and long term open circuit immersion tests. The agreement improved when the specimens were prepassivated before CYP.

7) The statistical behavior of E_p may allow small but finite probabilities of corrosion at values below the CR_T obtained with the above definition. Those probabilities can become high if a large steel area (as in a field structure) is considered.

Table 3.1 Base chemical composition (g/L) and pH values of test solutions

Solution type	NaOH	KOH †	$Ca(OH)_2$*	pH
SCS	0	0	2	12.6
SPS2	8.33	23.3	2	13.6
SPS3	2.64	7.37	2	13.1
SPS4	0.0833	0.233	0	11.6

† Reagent grade KOH had only a purity of 85.3%.
* Most of the $Ca(OH)_2$ was not dissolved.

Table 3.2 Chloride concentration for each test condition (M)

Solution type	Sandblasted	600 grit*	320 grit*	120 grit*	60 grit*
SCS	0.001~1	0.04~1	—	—	—
SPS2	0.1~3	1~3	1	1	1
SPS3	—	1	—	—	—
SPS4	—	1	—	—	—

* Repassivation potentials were determined on selected specimens only.

Table 3.3 Test conditions for prepassivated specimens

Specimen type	Prepassivating solution	t_{pp} (days)	CYP solution
Sandblasted/60cm^2	SCS	6, 30	SCS+0.04M [Cl^-]
Sandblasted/60cm^2	SCS	6, 30	SCS +1.0M [Cl^-]
Sandblasted/60cm^2	SPS2	1, 3, 6, 30, 82	SPS2+2.0M [Cl^-]
600grit/50cm^2	SPS2	6, 30	SPS2+2.0M [Cl^-]

Table 3.4 CR_T values obtained by assuming existence of E_{pl} for CYP method

Test method	OCI	CYP		
		Regular		Prepassivated
Surface finish	Sandblasted	Sandblasted	600 grit	Sandblasted
SPS2	$3.6< CR_T <4.5$	$1.1< CR_T <1.4$	$3.6< CR_T <5.4$	$3.6<CR_T$
SCS	$0.5< CR_T <1$	$0.5< CR_T <1$	$2.5< CR_T <5$	$1<CR_T$

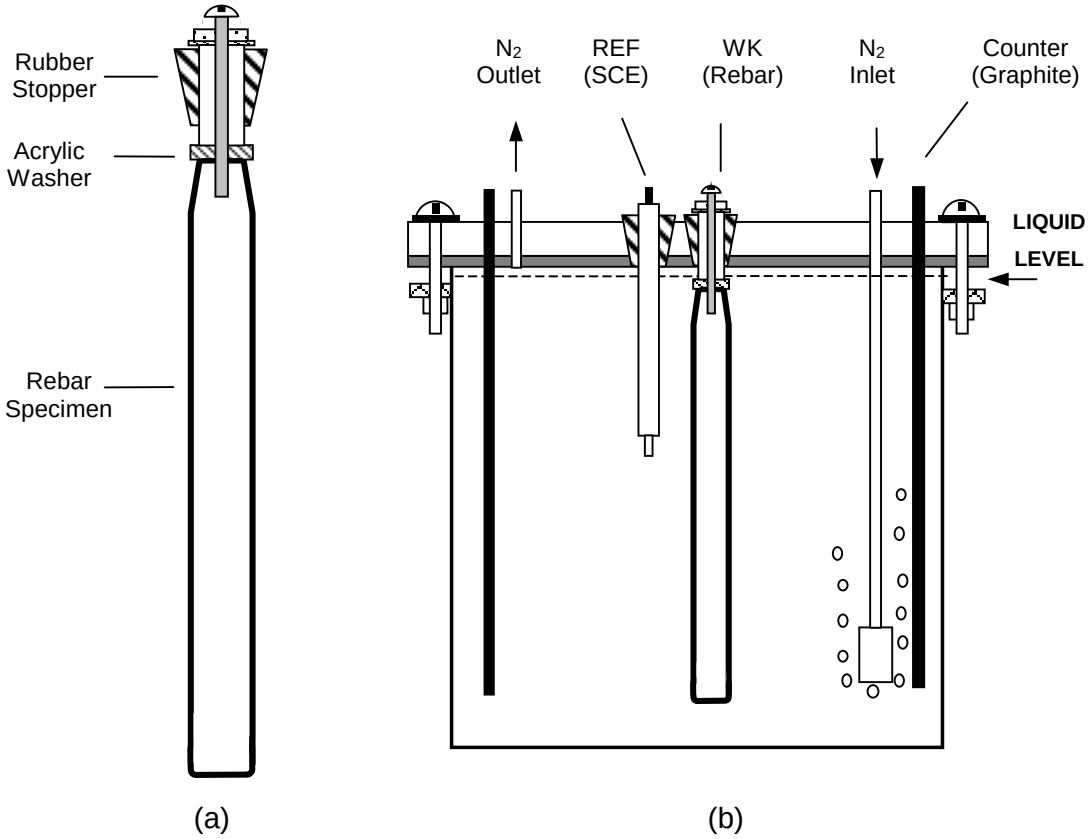

Figure 3.1 Schematic graph showing the assembly of the specimen (a) and the cell (b) used in the experiments

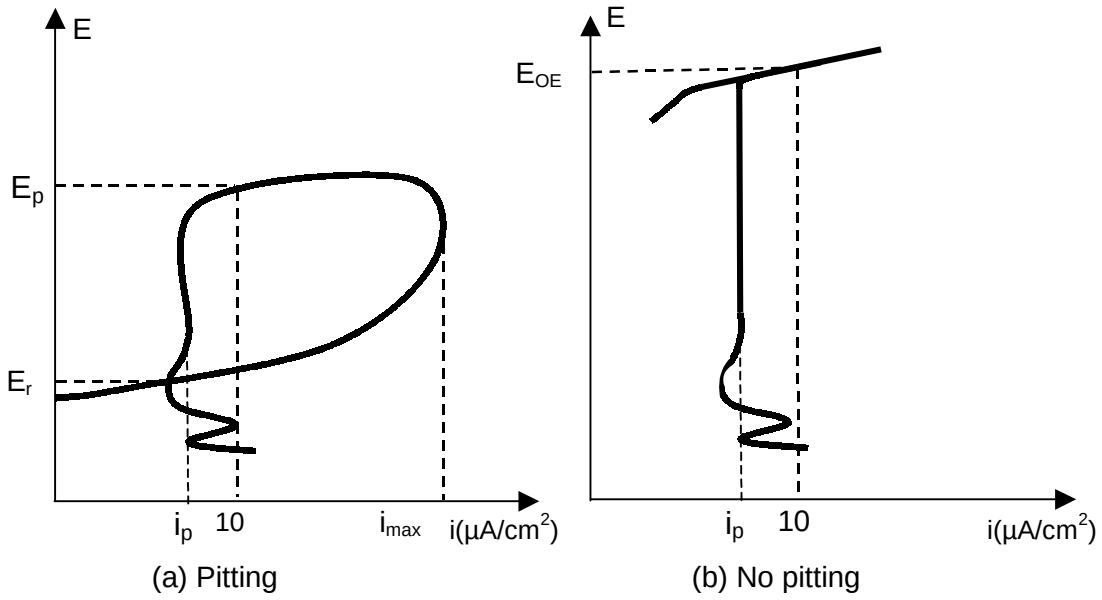

Figure 3.2 Schematic graph showing the determination of electrochemical parameters (E_p, E_r, i_p, and i_{max}) from CYP curves for the case of pitting (a) and no pitting (b)

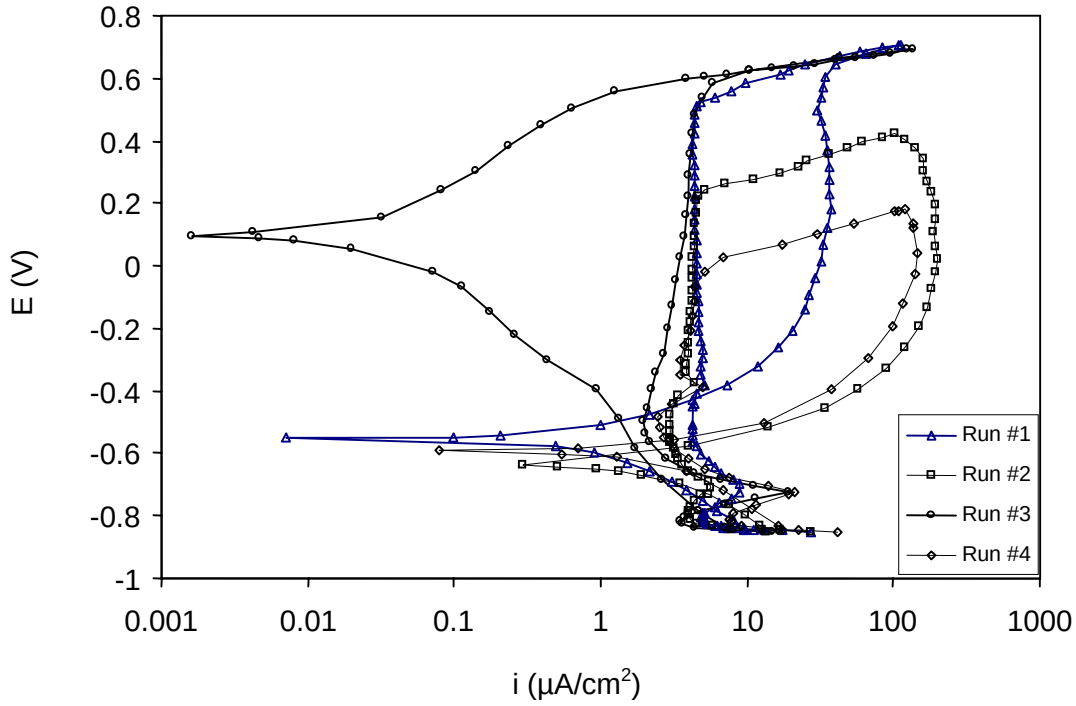

Figure 3.3 Typical CYP curves of sandblasted rebar specimens in SCS with 0.01M NaCl

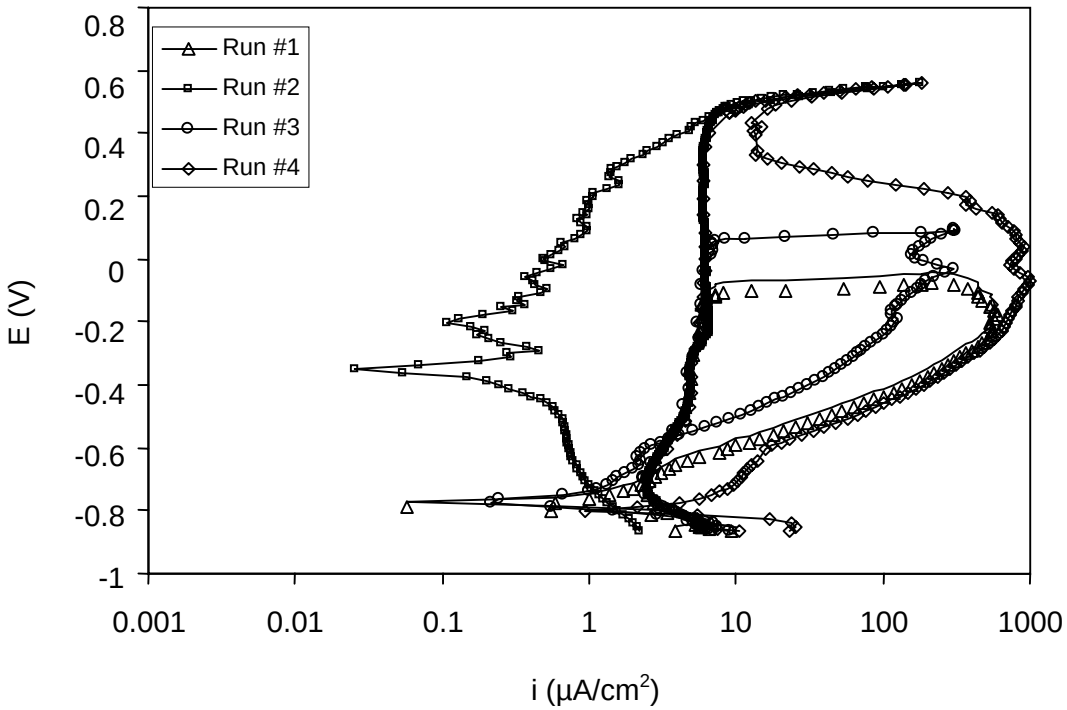

Figure 3.4 Typical CYP curves of sandblasted rebar specimens in SPS2 with 0.6M NaCl

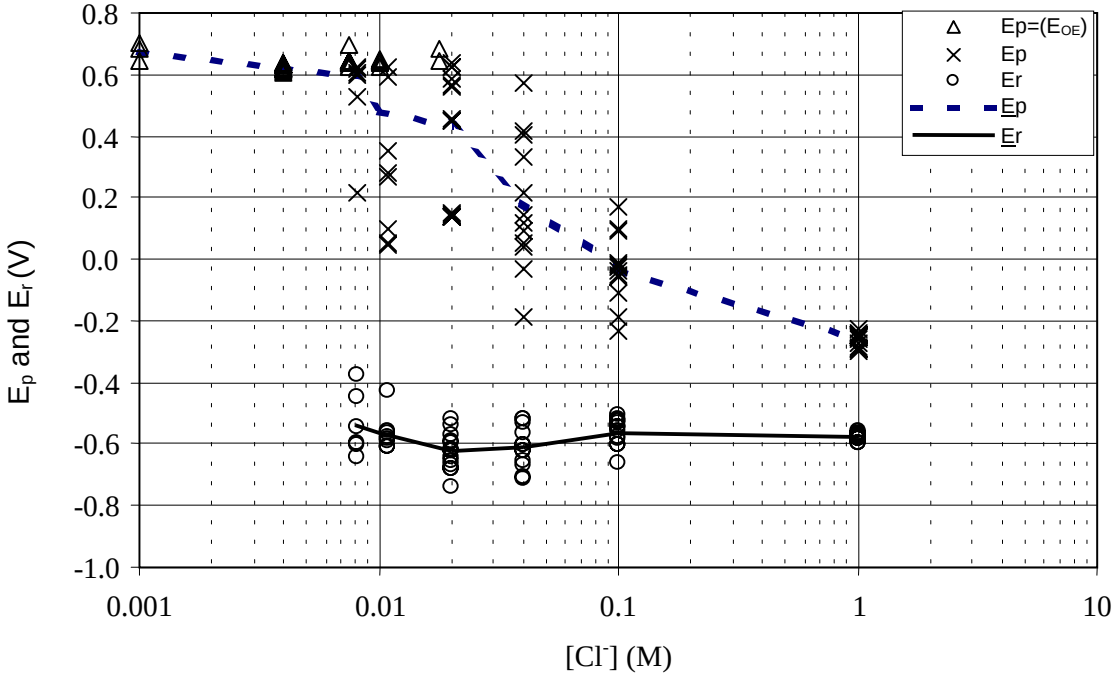

Figure 3.5 E_p and E_r of sandblasted steel as a function of $[Cl^-]$ in SCS. (The Δ symbols indicate pitting was not observed and E_p was assigned a nominal value equal to E_{OE}. Some symbols shifted for clarity)

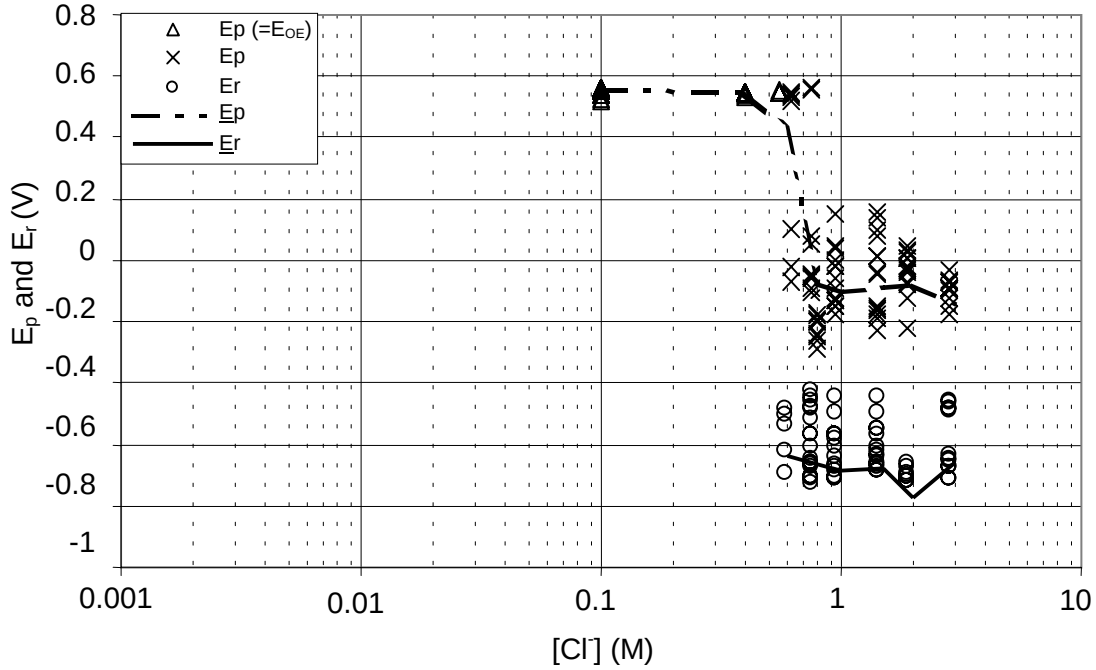

Figure 3.6 E_p and E_r of sandblasted steel as a function of $[Cl^-]$ in SPS2 (The Δ symbols indicate pitting was not observed and E_p was assigned a nominal value equal to E_{OE}. Some symbols shifted for clarity)

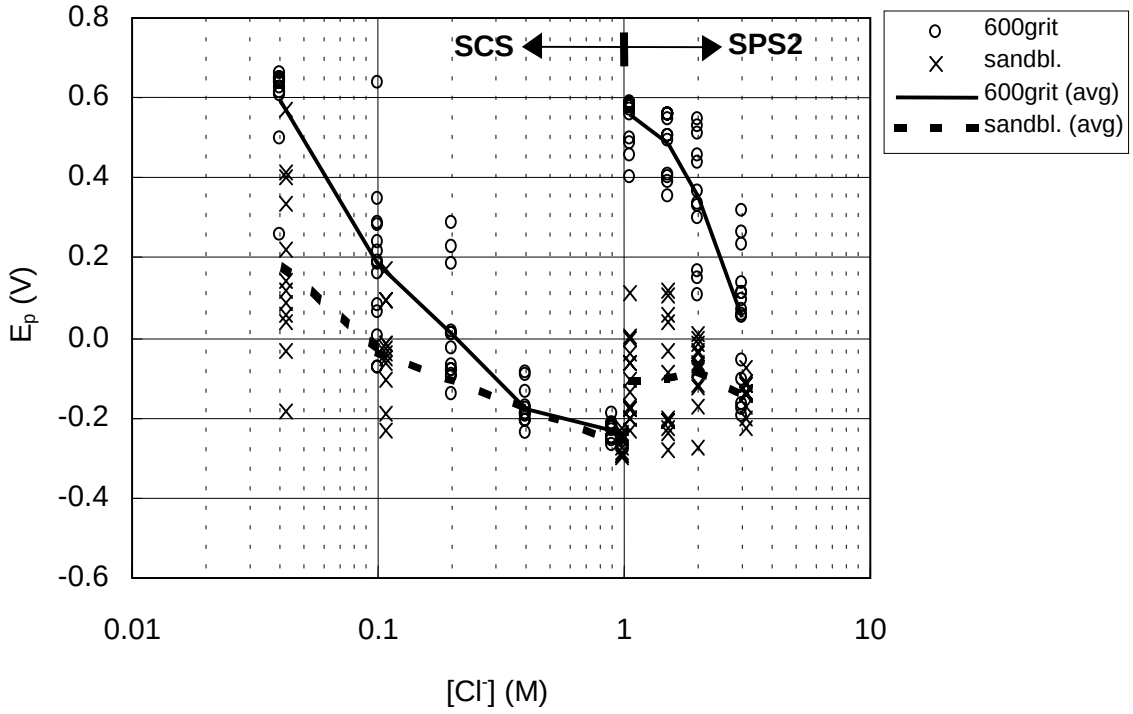

Figure 3.7 Effect of surface finish (sandblasted vs. 600 grit) on E_p in SCS and SPS2 with various NaCl additions (some symbols shifted for clarity)

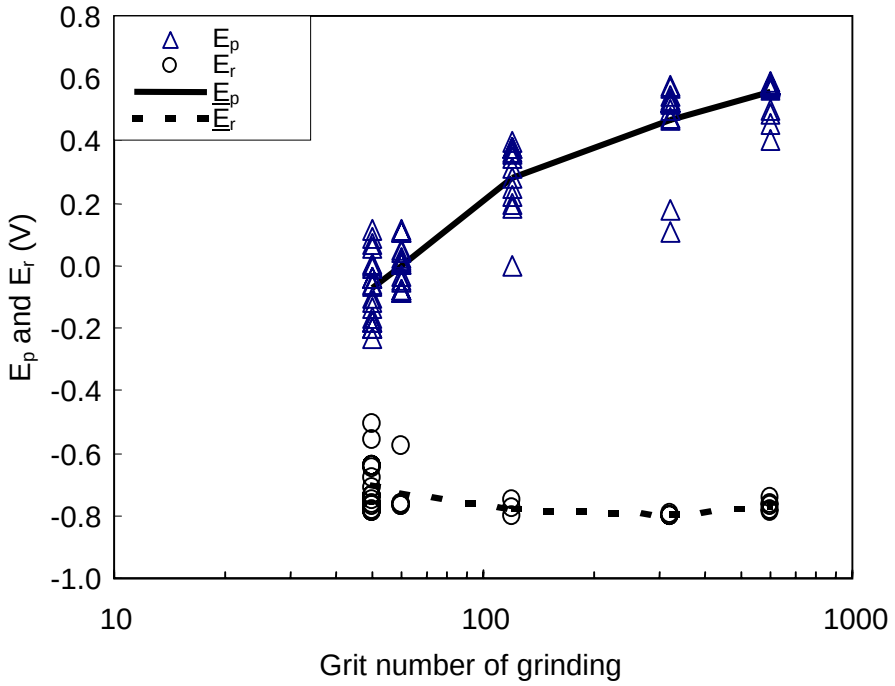

Figure 3.8 Effect of various surface finishes on E_p and E_r in SPS2 with 1.0M NaCl

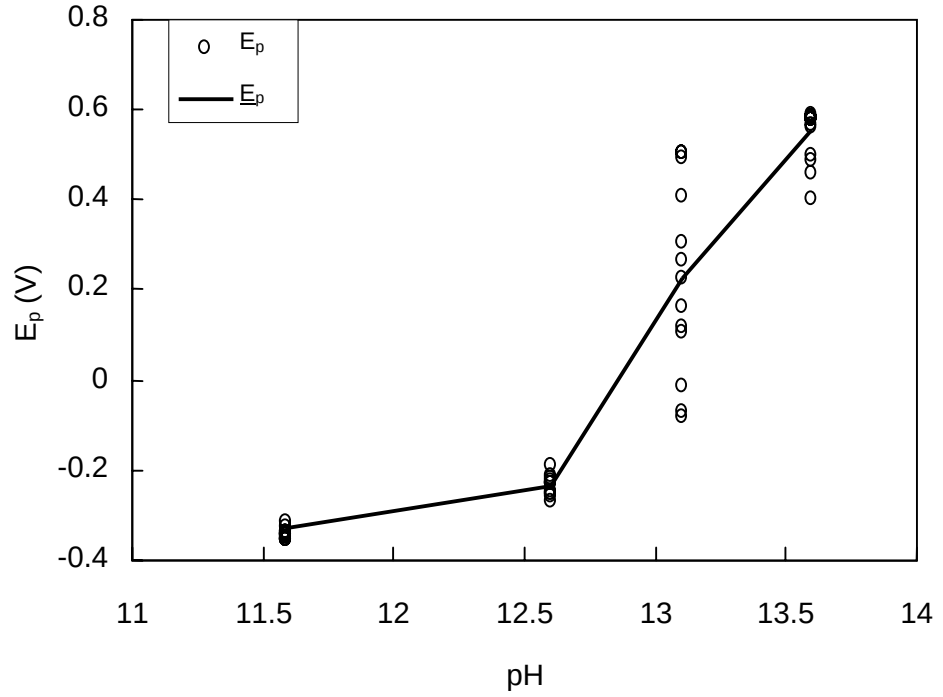

Figure 3.9 Effect of solution pH on E_p of 600 grit steel in alkaline solutions (SPS4, SCS, SPS3, SPS2) with 1.0M NaCl

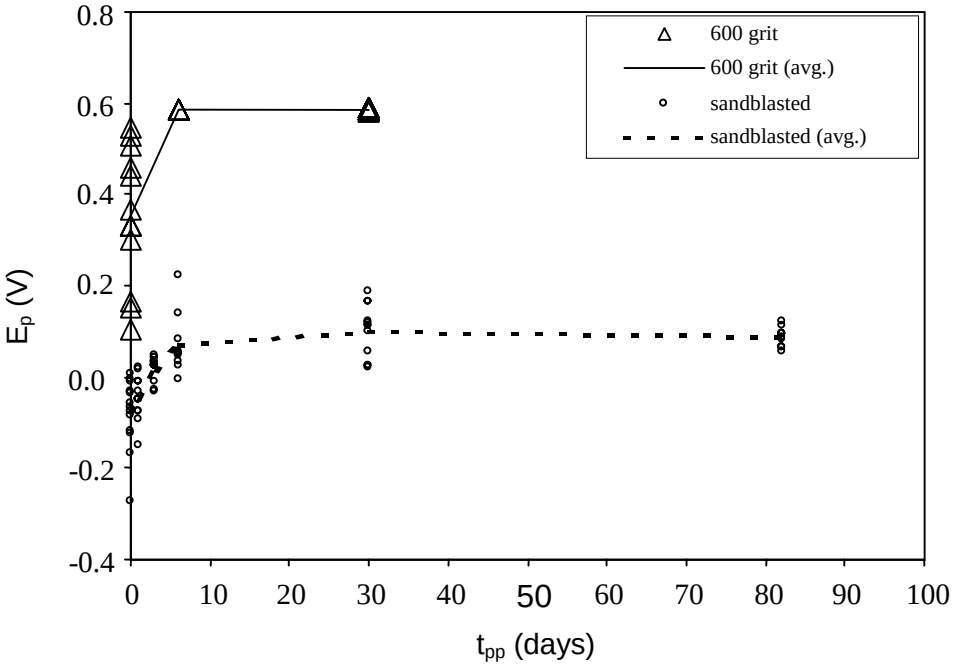

Figure 3.10 Effect of t_{pp} (in SPS2) on E_p of rebar steel (600girt /50cm^2 or sandblasted/ 60cm^2) in SPS2 with 2.0M NaCl

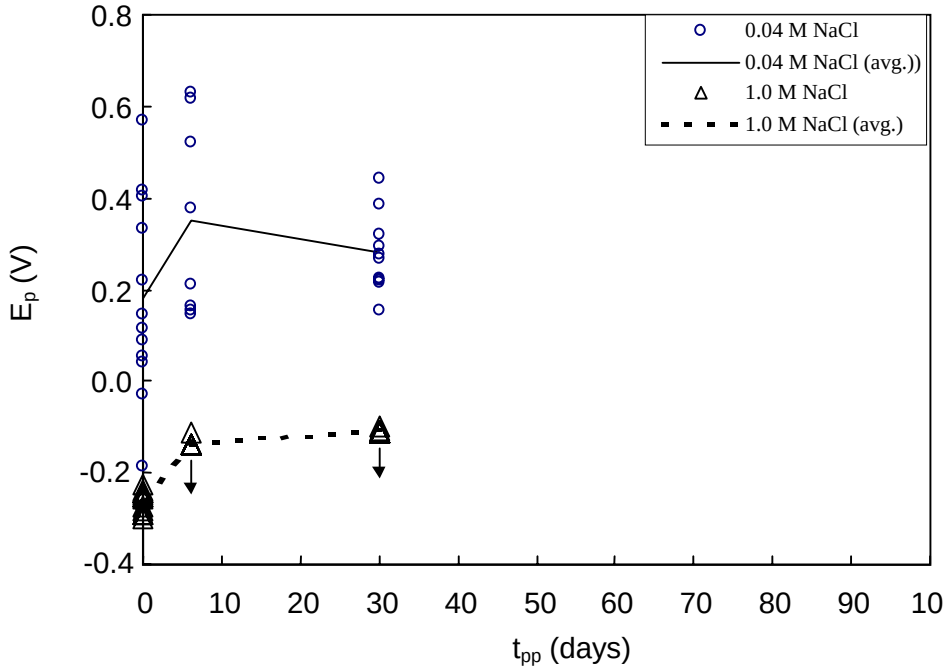

Figure 3.11 Effect of pre-passivation (in SCS) on E_p of sandblasted rebar steel in SCS with 0.04M and 1.0M NaCl

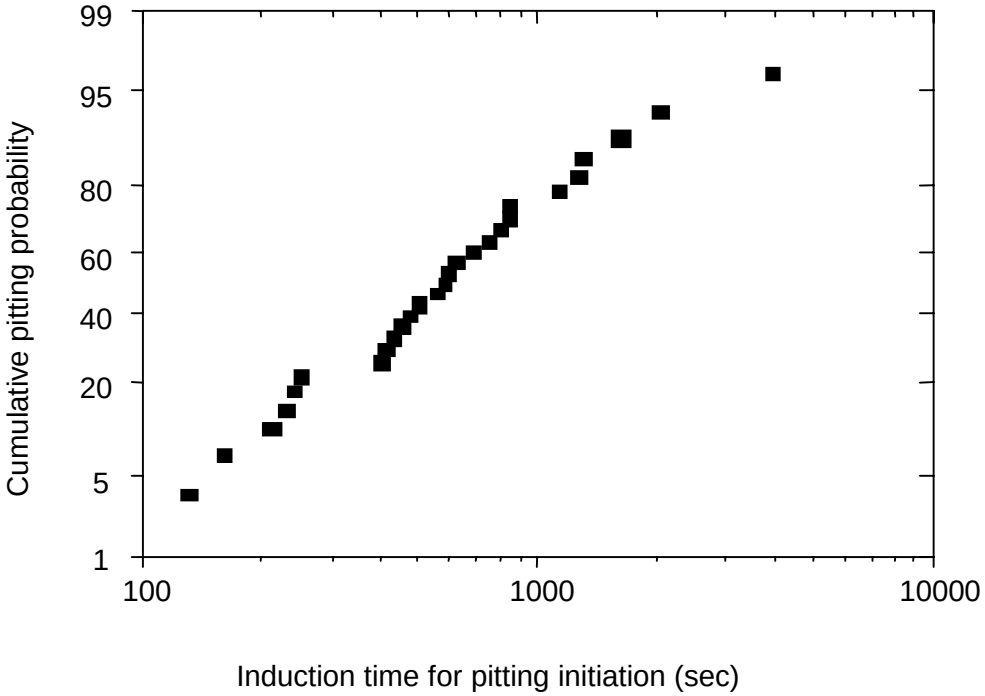

Figure 3.12 Distribution of cumulative pitting probability as a function of pitting induction time obtained on prepassivated (t_{pp}=6 days) sandblasted steel in SCS with 1.0M NaCl (steel was potentiostatically polarized at -0.15V.)

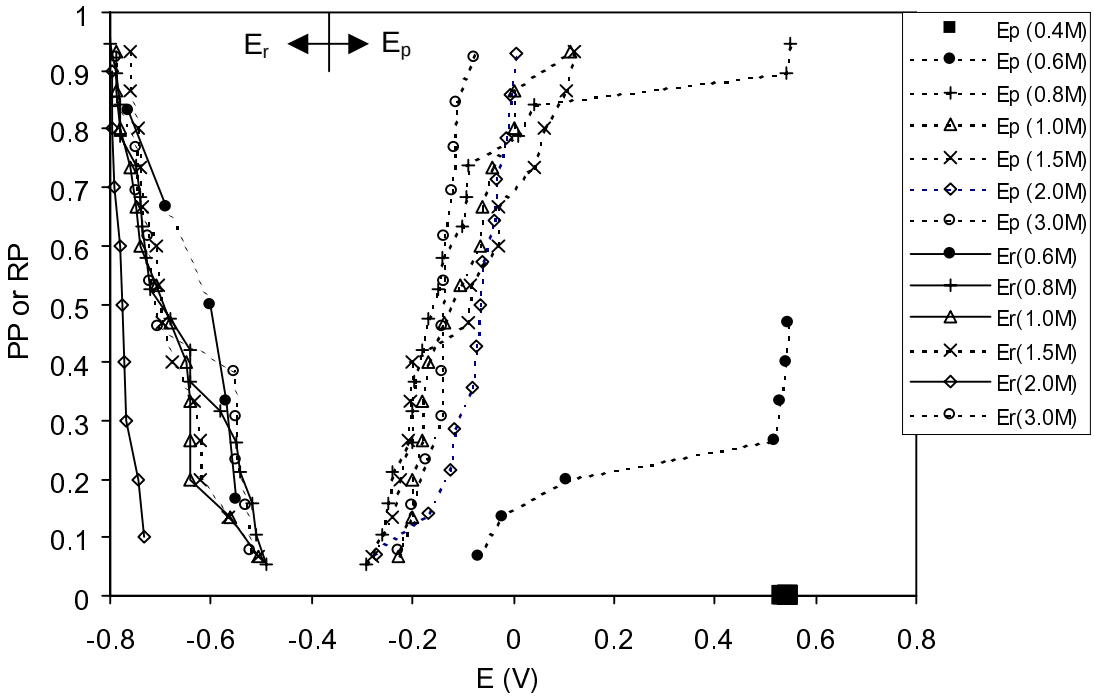

Figure 3.13 Distribution of PP and RP for sandblasted specimens in SPS2 with various NaCl additions

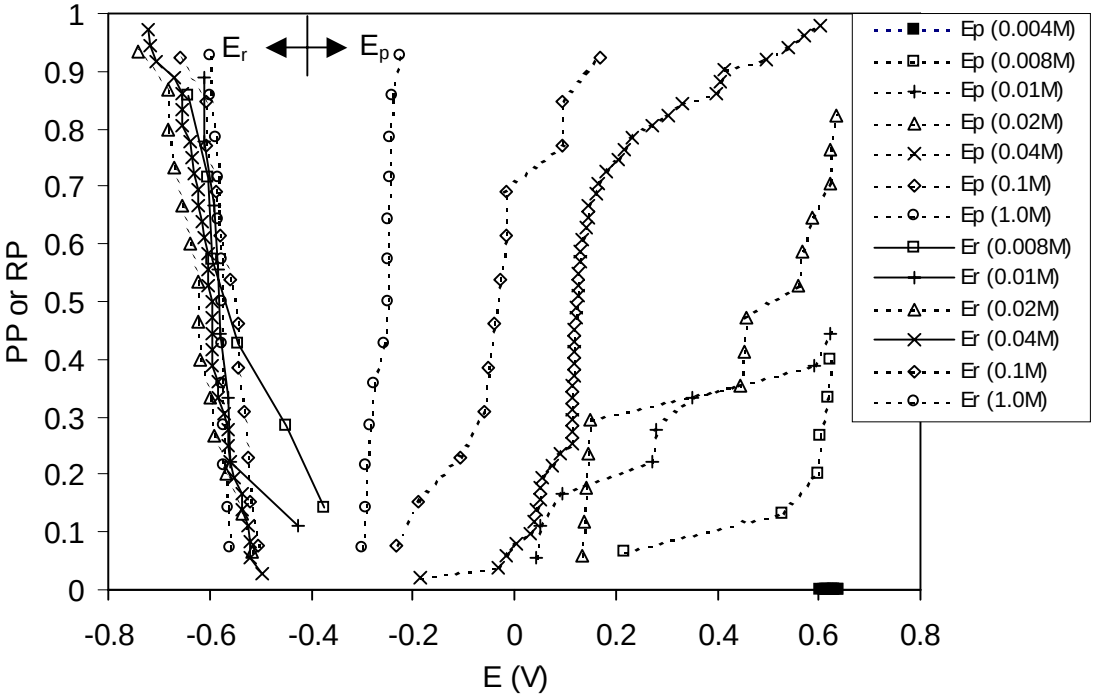

Figure 3.14 Distribution of PP and RP for sandblasted specimens in SCS with various NaCl additions

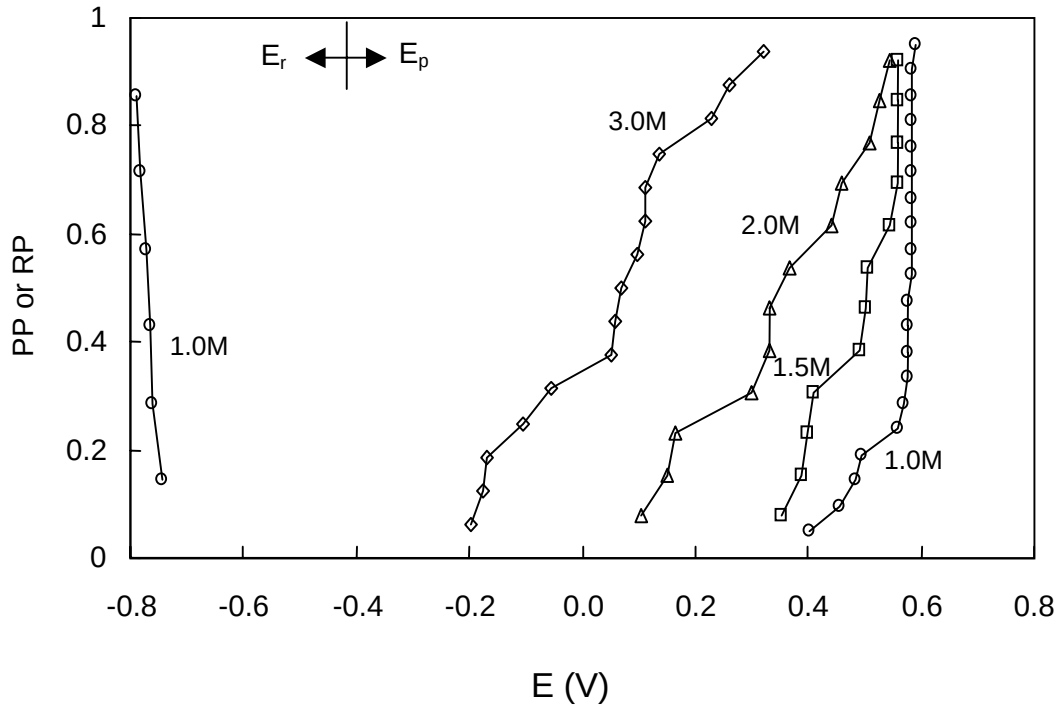

Figure 3.15 Distribution of PP and RP for 600 grit specimens in SPS2 with 1.0 to 3.0M NaCl (E_r was only measured on selected specimens for 1.0M NaCl)

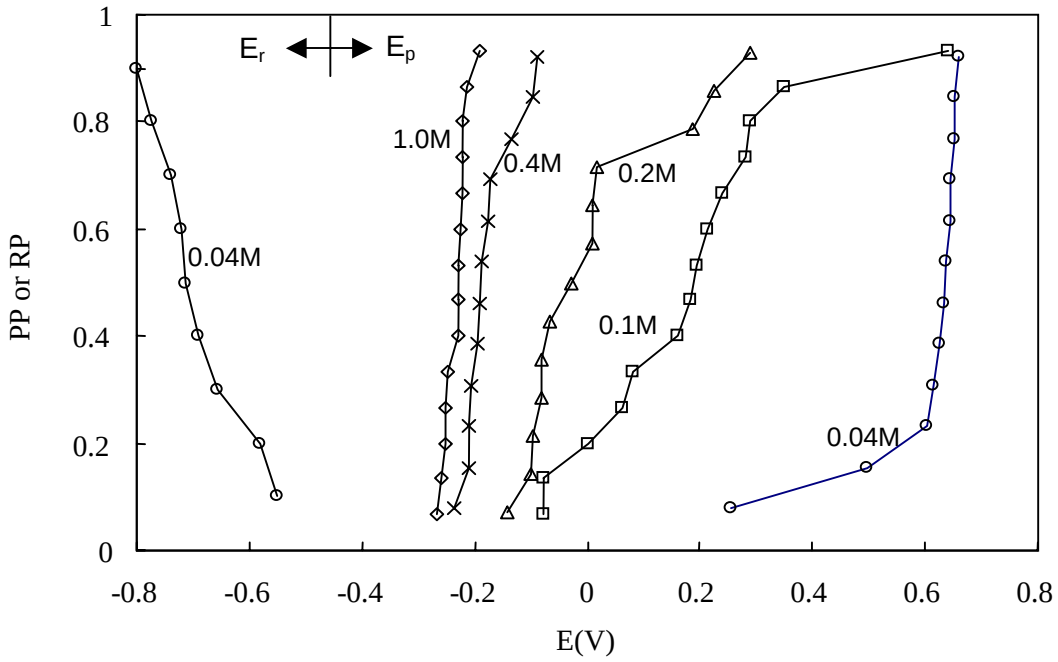

Figure 3.16 Distribution of PP and RP for 600 grit specimens in SCS with various NaCl additions (E_r was only measured on selected specimens for 0.04M NaCl)

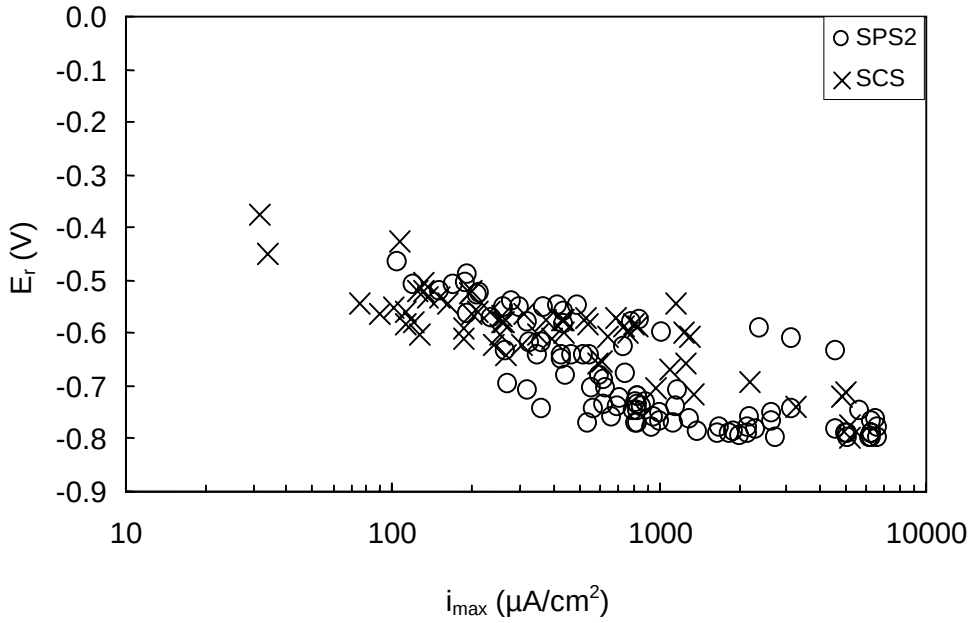

Figure 3.17 Relationship between E_r and i_{max} obtained in SPS2 and SCS with [Cl^-] ranging from 0.008M to 3.0M on rebar specimens with different surface finishes

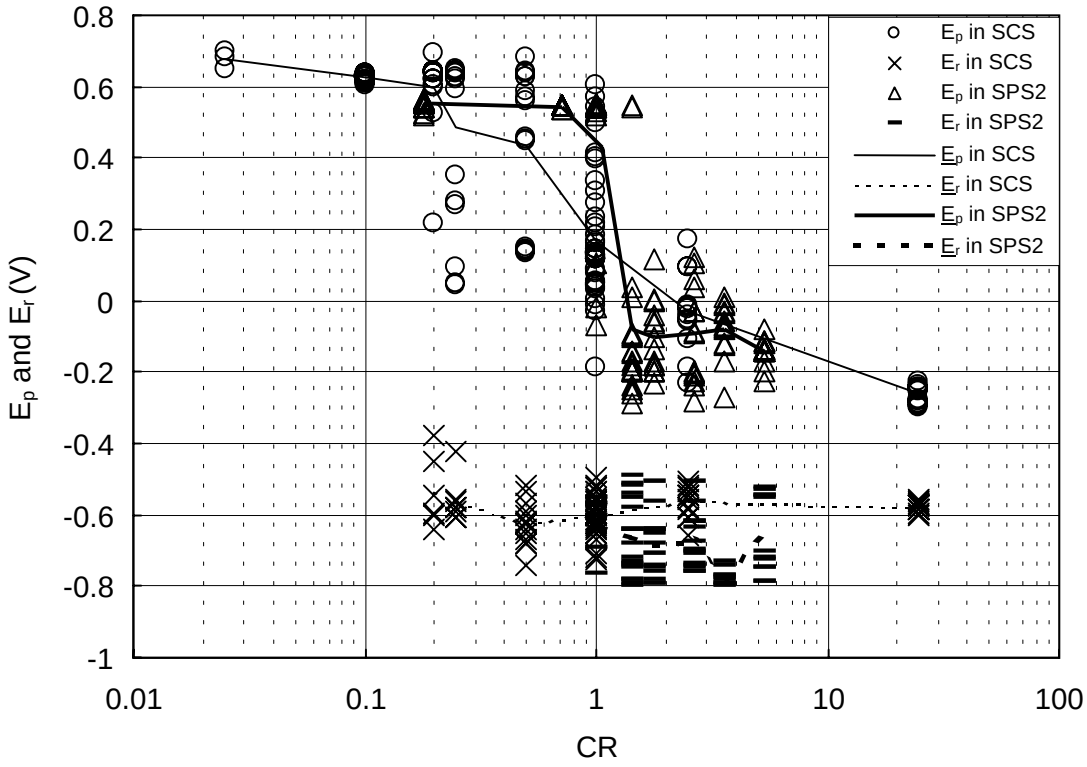

Figure 3.18 Dependence of E_p and E_r on CR for sandblasted steel in SCS and SPS2

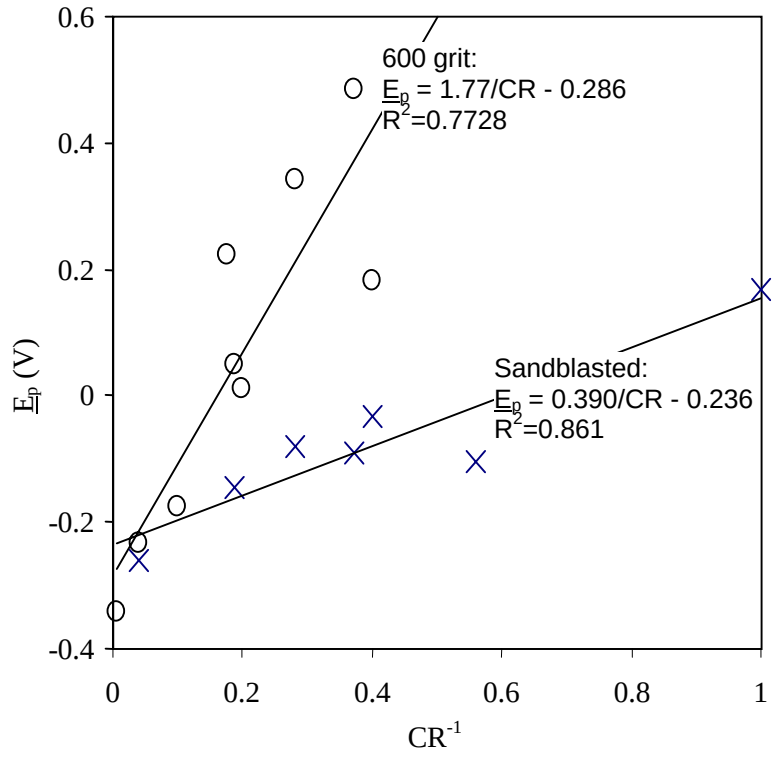

Figure 3.19 Dependence of $\underline{E}_p$ on CR^{-1} at various test conditions

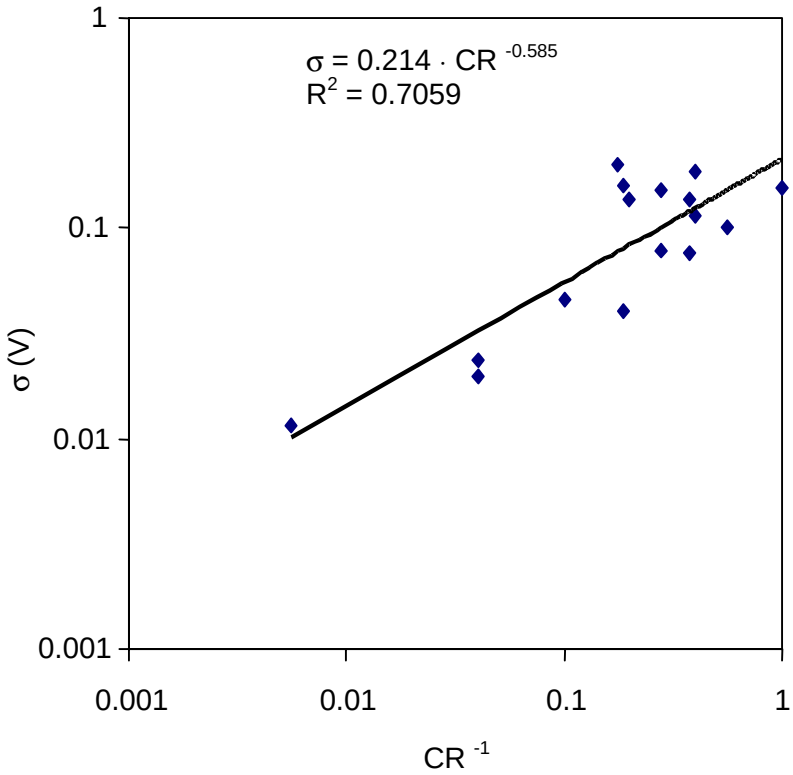

Figure 3.20 Dependence of σ on CR^{-1} for all the test conditions

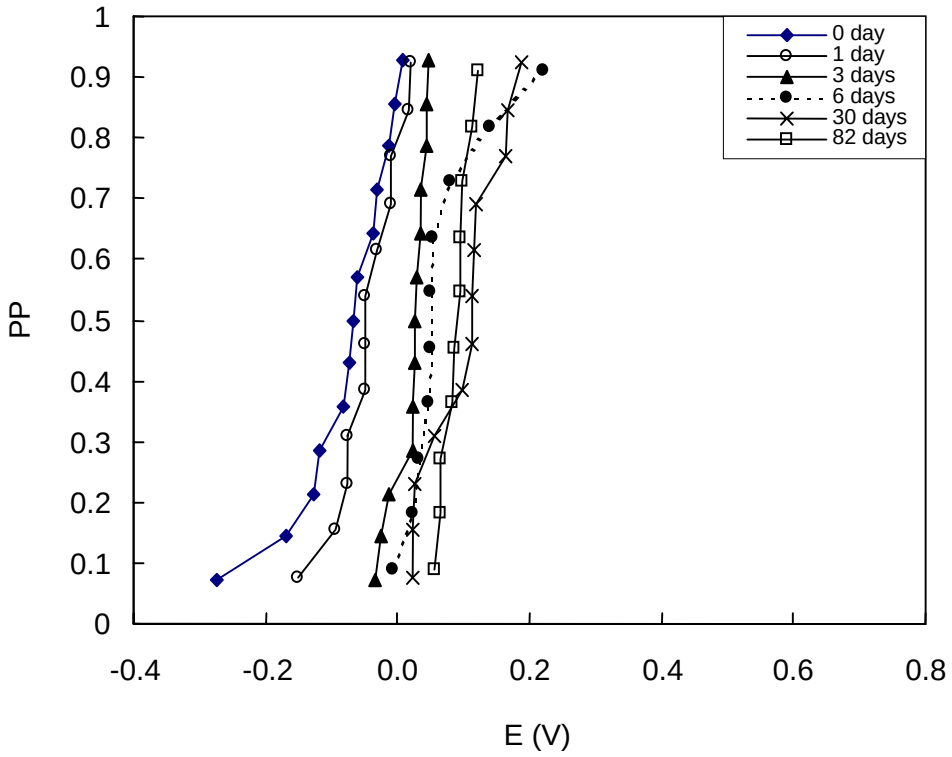

Figure 3.21 Effect of prepassivation in SPS2 on PP distribution of sandblasted steel in SPS2+2.0M NaCl

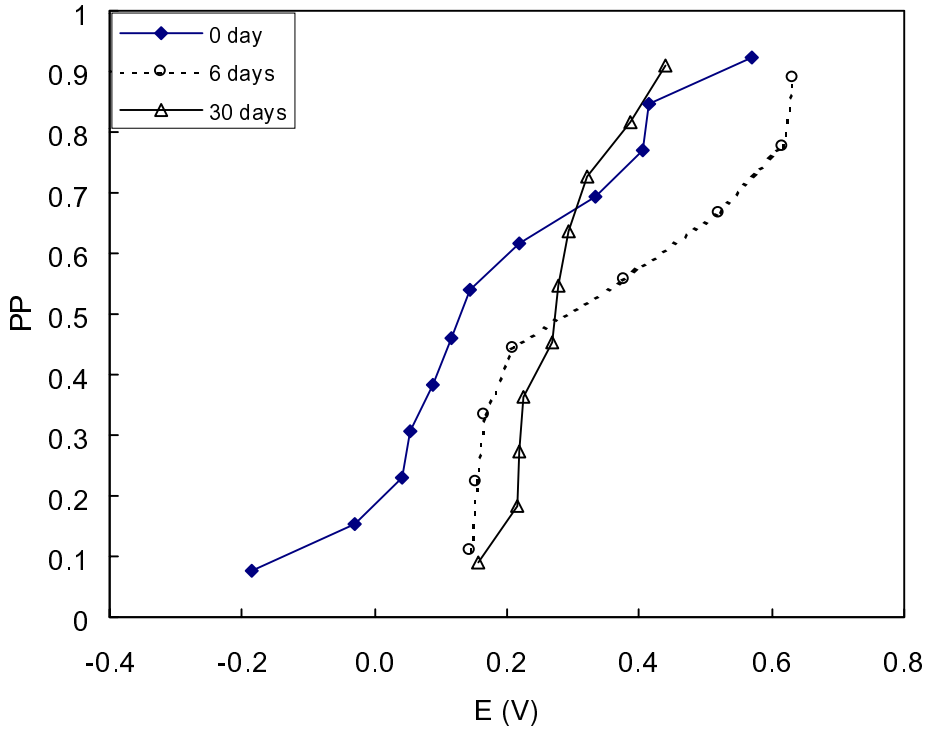

Figure 3.22 Effect of prepassivation in SCS on PP distribution of sandblasted steel in SCS+0.04M NaCl

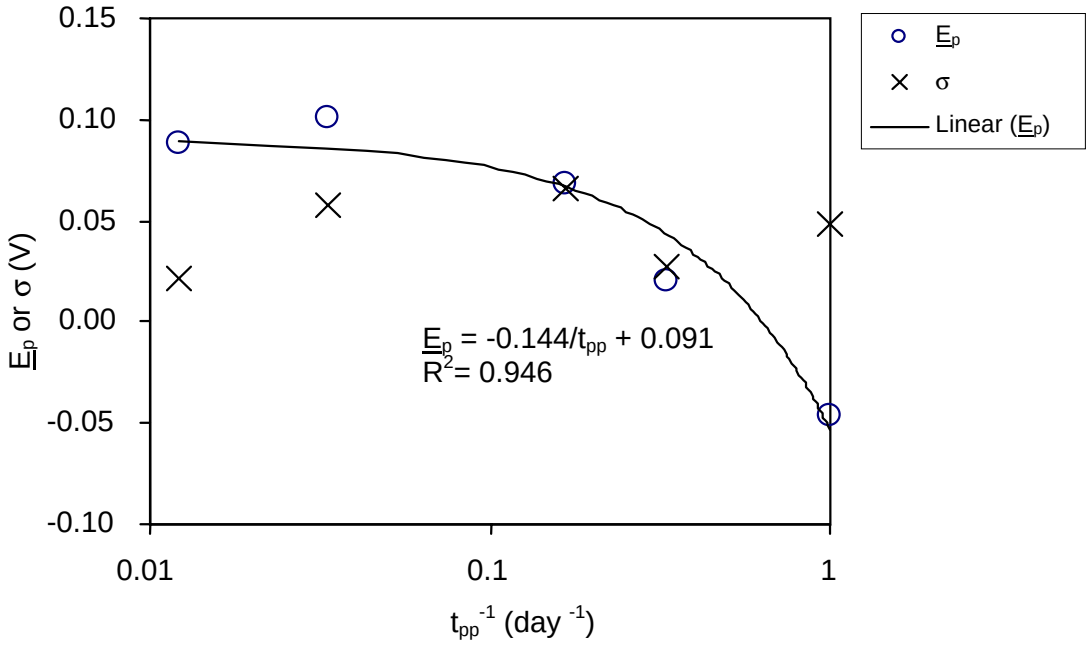

Figure 3.23 E_p, σ of rebar steel (sandblasted/60cm^2) in SPS2+2.0M NaCl as a function of the prepassivation time (t_{pp}) in SPS2

CHAPTER 4: EFFECT OF SPECIMEN SIZE ON PITTING AND REPASSIVATION POTENTIALS

4.1 Introduction

In Chapters 2 and 3, the chloride-induced corrosion of reinforcing steel in alkaline solutions has been investigated with the open circuit immersion (OCI) and cyclic polarization (CYP) methods. The specimens used in those experiments had a nominal surface area of ~50 to 60 cm^2. Laboratory experiments to determine pitting potential (E_p) often use specimens of comparable or even much smaller size (typically $\leq 5cm^2$). For example, the exposed surface area of the specimen specified by ASTMG5-94 for making potentiostatic and potentiodynamic anodic polarization measurements is ~$5cm^2$. As has been observed in Chapter 3, the pitting potential displayed very large variability if the chloride-to-hydroxide ratio (CR) was not very high. Pitting initiation is often related with the "weak points" on metal surface, such as sulfide inclusions, grain boundary defects, etc (Szklarska-Smialowska 1986). The number of such types of defects on a specimen surface is expected to be proportional to its total surface area. Therefore, the chance for pitting initiation on a larger specimen is likely to be higher than on a smaller one. Since the actual surface area of steel in a structure can be several orders of magnitude larger than that of a specimen normally used in a laboratory test, uncertainty exists when laboratory results are directly applied to larger structures without taking the specimen area effect into consideration.

The life span of a large structure experiencing pitting corrosion is often related to the maximum pit depth, which tends out to be a function of the sample size (Fontana 1986). Progress has been made in the application of extreme-value statistics to the analysis of maximum pit depth (Aziz 1956, Eldredge 1957, Shibata 1996). However, studies on the effect of specimen size on pitting initiation (especially E_p) are very limited. Mears and Brown (1937) found that an increase in the area of aluminum specimens immersed in NaCl increased the corrosion probability but decreased the number of breakdown sites per unit area due to "mutual protection" (Evans 1981). Nevertheless, the frequency of pitting occurrence roughly obeys a Poisson distribution. Using the potentiodynamic polarization (PDP) technique, Shibata (1982) studied the surface area dependence of pitting potential for 304L stainless steel in 3.5% NaCl at 35ºC. The surface area of the specimens used in those tests ranged from $0.157cm^2$ to $3.95cm^2$. E_p was found to be lower for specimens with smaller surface area when PDP was performed at a fast scan rate (8mV/sec), but E_p was nearly independent of specimen surface area when a slow scan rate (0.333mV/sec) was used. Nevertheless, Shibata predicted that in other cases for different materials or environments, the effect of surface area on E_p could not be neglected. In a recent work by Burstein and Ilevbare (1996), E_p of SS316 was found to be significantly dependent on the specimen size. However, the maximum specimen size used in those tests was only 0.5 cm^2 and the PDP scan rate was also high (1mV/sec). The corrosion system in the present investigation (reinforcing steel in highly alkaline solutions containing NaCl) is significantly different from those has been studied (mainly stainless in neutral or acidic chloride-containing solutions). Therefore, it is important to study whether E_p of rebar steel is subject to the influence of the specimen surface area, especially when E_p is used to estimate the chloride corrosion threshold in real concrete structures. To that purpose, the effect of surface area (denoted by S, and varied over three orders of magnitude) of rebar steel

specimens with two types of surface finish (sandblasted or ground to 600 grit) on E_p was investigated using the CYP method. In addition, since E_p has also been reported to be a function of anodic polarization scan rate (Manning, 1980) (denoted as v_f hereafter), CYP was also performed on 60 cm^2 sandblasted specimens in SPS2 with 1.5M NaCl at various scan rates (denoted by v_f) to establish how dependent was E_p on the choice of v_f.

4.2 Experimental

All specimens were cut from ordinary A-615 reinforcing steel bars (size #4, diameter ~12mm) from the same batch used previously. The steel chemical composition (in wt%) was: 0.43 C, 0.007 P, 0.038 S, 1.11 Mn, 0.22 Si, 0.03Cr, 0.11 Ni, 0.37 Cu, and Fe (bal.). Due to the difference in size and shape, specimens can be categorized into the following six types:

1) Type I: This was the same Type I specimen described in Chapter 3. Each bar was ~15cm long with the diamond-pattern surface deformations. The bar was sandblasted to remove the mill scale and its nominal exposed surface area was ~60cm^2.

2) Type II: This was also the same Type II specimen described in Chapter 3. Each bar (~15cm long) was first machined to a diameter of ~1cm and then the whole surface (~50cm^2) was ground in several steps to 600 grit finish. Its nominal exposed surface area was ~50cm^2.

3) Type III: The specimen had the same size and shape as Type II. However, it had combined surface finishes. The specimen was first fully ground to a 600 grit finish, then after proper covering, only a very small portion (a band of ~1.4mm wide around the bar) in the middle of each specimen was sandblasted. The protective cover was removed after sandblasting. Consequently, each bar had a sandblasted zone of ~0.5cm^2 and a 600 grit finish zone of ~50cm^2.

4) Type IV: The specimen was similar to type II but much shorter (~1.5 cm length). It was either sandblasted or ground to a 600 grit finish. Its nominal surface area was ~5cm^2.

5) Type V: The specimen had a base portion (~ϕ0.8 cm $\times$ 2 cm) for electrical connection and a protruding portion (~ϕ0.2 cm $\times$ 4 cm). The protruding portion was either sandblasted or ground to a 600 grit finish. For testing, only part of the protruding portion (~0.8 mm from the tip) was immersed in the solution so that the nominal surface area in contact with solution was ~0.5 cm^2.

6) Type VI: A very small thin rod (1 cm $\times$ ϕ0.25 cm) was machined from the rebar and electrical connection was made at one end of that rod. The steel (except the other ϕ0.25cm cross-section) was then cast into metallographic epoxy in the shape of a lollipop. The exposed end was perpendicular to the rebar rolling direction and was either sandblasted or wet ground to a 600 grit finish. The nominal surface area was ~0.05cm^2.

For clarity, each specimen (except type III) was named in terms of “surface finish/surface area”. For example, Type I specimens were designated as “sandblasted/60cm^2”.

The configuration and assembly of each type of specimen is shown in Figure 4.1. The results for Type I and Type II specimens were mainly from Chapter 3.

The test cell was exactly the same as used previously (Fig. 3.1(b)) .The base test solutions (SCS and SPS2) were also the same as used previously (Table 3.1). Reagent grade NaCl was used to adjust chloride content in each solution. A cyclic polarization (CYP) technique as described in Chapter 3 was employed. In SPS2 with 1.5M NaCl, anodic polarization was also conducted at various scan rates (0.00334mV/s, 0.0167mV/s, 0.167mV/s, 1.67mV/s, and 10mV/s) on sandblasted/60cm^2 specimens. However, most of the CYP tests were performed with v_f =0.167mV/sec. On each CYP curve, the anodic current density normally reached a plateau before a sudden current surge due to pitting initiation, as has been shown in Fig. 3.2. This nearly constant anodic current density on each CYP curve is called the plateau passive current density (i_p). Because i_p was scan rate dependent (as will be shown), the pitting potential (E_p) is defined as the electrode potential at which the anodic corrosion density has reached three times of i_p immediately after stable pitting initiation. Using the same criterion as in Chapter 3, the repassivation potential (E_r) was defined as the potential on the CYP curve where the backward scan intersected the forward scan. All the reported E_p values came from specimens experiencing actual pitting initiation. In cases when crevice corrosion took place at the edge of a specimen bordering the plexiglas washer (Type I to IV), at the liquid line (Type V), or at the epoxy mounting (Type VI) in a test, that CYP test result was discarded. Considering reports from previous studies that E_p had a very large variability, tests at each condition were usually repeated for ~12 times, using a freshly finished specimen each time. All the reported potential values are in the SCE scale and all the tests were conducted at ambient room temperature, 21±2ºC.

4.3 Results

4.3.1 Effect of Scan Rate on E_p

Figure 4.2 presents the distribution of E_p as a function of v_f (from 0.00334 mV/sec to 10 mV/sec) for sandblasted/60cm^2 steel in SPS2 with 1.5M NaCl. It is clear that E_p experienced much scatter at any given scan rate. The average E_p values (denoted by $\underline{E_p}$) at a given scan rate were much higher for $v_f \geq$ 1.67mV/sec than for $v_f \leq$ 0.167 mV/sec. Therefore, using a v_f of 1.67 mV/sec or faster is likely to overestimate E_p significantly. However, $\underline{E_p}$ became relatively v_f independent when $v_f \leq$ 0.167 mV/sec. Therefore, a v_f of 0.167mV/sec was thus chosen for the rest of experiments as a reasonable compromise to keep test times short (e.g. less than a few hours) while avoiding excessive scan rate dependence. This result was applied also to select the scan rate used for the experiments described in Section 4.2.

Figure 4.3 shows i_p as a function of v_f for sandblasted/60cm^2 in SPS2 without and with 1.5M NaCl. It can be observed that log(i_p) increased linearly with log(v_f) in the v_f range investigated (from 0.00334 mV/sec to 10 mV/sec), so that an empirical relationship may be proposed:

$$i_p = i_{p1}(v_f)^n \qquad (4.1)$$

where v_f is the anodic scan rate in mV/sec, i_{p1} is the projected value of i_p (in $\mu A/cm^2$) when v_f=1mV/sec, and *n* is the slope of the line in Figure 4.3. A simple regression yields i_{p1}=26.9; *n*=0.79 and i_{p1}=21.7; *n*=0.76 for SPS2 and SPS2+1.5M NaCl, respectively. These results also indicate that i_p was nearly unaffected by the presence of chloride ions in the solution.

4.3.2 Effect of Surface Area on E_p and E_r

Figure 4.4 shows that there was a strong dependence of E_p on the nominal surface area (S) of sandblasted specimens in SCS with 0.1M and 1.0M NaCl, respectively. The average E_p (denoted by $\underline{E}_p$ hereafter) decreased nearly linearly with log(S). The slope (denoted by k, = $\partial(\underline{E}_p)/\partial(\log(S))$) was between 0.1V/decade to 0.3V/decade, depending on the value of S.

A similar dependence of E_p on specimen surface area was also observed for 600 grit specimens (Figure 4.5) in SCS with 0.1M and 1.0M NaCl. For $0.5cm^2 \leq S \leq 50cm^2$, k was ~0.3 V/decade.

Figure 4.6 shows the area dependence of E_p for sandblasted specimens in SPS2 with 1M, 2M, and 3M NaCl, respectively. Again, E_p was strongly affected by the specimen surface area. For $0.05\ cm^2 \leq S \leq 0.5\ cm^2$, k was ~0.3V/decade. However, for $0.5\ cm^2 \leq S \leq 60\ cm^2$, k was ~0.2V/decade when $[Cl^-]$=1.0M and ~0.1V/decade when $[Cl^-]$=2.0 M or 3.0 M.

The area dependence of E_p for 600 grit finish specimens in SPS2 with 1.0 M, 2.0M, and 3.0M NaCl is presented in Figure 4.7. When $[Cl^-]$=1.0M, most of the E_p values were very close to the oxygen evolution potential (E_{OE}), and $\underline{E}_p$ appeared to be independent of surface area. When $[Cl^-]$=2.0M and 3.0M, no systematic dependence of $\underline{E}_p$ on S was observed. For example, for $[Cl^-]$=2.0M, $\underline{E}_p$ first decreased by ~0.2V from $0.5cm^2$ to $5cm^2$, then increased by ~0.1V from $5\ cm^2$ to $50cm^2$.

Figure 4.8 shows E_r as a function of the surface area of sandblasted specimens obtained in SPS2 with 1.0M and 2.0 M NaCl. Similarly to E_p, E_r also showed some variability. Nevertheless, from Fig. 4.8 it is seen that E_r was insensitive to the specimen surface area and a lower limit of ~-0.8 V was manifested for all the area conditions.

4.4 Discussion

4.4.1 Effect of Anodic Polarization Scan Rate on E_p

The E_p distribution of sandblasted steel in SPS with 1.5M NaCl (Fig. 4.2) clearly indicated E_p was v_f dependent. $\underline{E}_p$ slightly increased from 0.00334mV/sec to 0.167mV/sec but significantly increased (by ~0.2V) when v_f was 1.67mV/sec or higher. This observation is in good agreement with those reported by Leckie (1965) and by Szauer and Jakobs (1976) (Figure 4.9), although those results were obtained for other systems. At slow v_f (between 10mV/h and ~600 mV/h), $\underline{E}_p$ slightly shifted in the noble direction with increasing v_f. At faster v_f (> ~600 mV/h), $\underline{E}_p$ shifted appreciably to more noble values. That observation can be explained by the dependence of pitting initiation time on potential. It has been found that, the nobler the potential, the shorter the time required for pit initiation.(Broli and Holton 1977, Schwenk 1964). Consequently, when v_f is high, a rapid increase in current density (due to

corrosion) can only be observed at potentials corresponding to a sufficiently short induction time. This means that at high v_f, E_p is more positive than at slow v_f (Szklarska-Smialowska 1986). To better understand this phenomenon, a qualitative explanation is given as follows:

First, the following assumptions are made:

1) Whenever electrode potential is above a critical value (E_{crit}), pitting initiation is expected to occur.

2) When steel is potentiostatically polarized at E> E_{crit}, the pitting initiation time is only a function of E.

3) The pit initiation time increased exponentially with decreasing E (Broli and Holton 1977, Schwenk 1964).

The relationship between potential and pitting initiation time can be schematically represented by curve I in Figure 4.10. This curve can also be derived by the point defect model (Haruna and Macdonald 1997). The straight lines v_{f1} to v_{f9} represent the time evolution of electrode potential corresponding to scan rates in the order of increasing. According to the above assumptions, if steel is potentiostatically held at E_1 for time t_1, pitting corrosion starts. However, if the potential E_1 is reached from potentiodynamic polarization starting from E_0 with the scan rate for v_{f7} in a time period of t_1, pitting will not happen because insufficient time was allowed at potential E_1. Under the most conservative estimation, steel will corrode only after it is continuously polarized up to time t_2 (with $t_2=2t_1$), when E reaches E_2 ($E_2=E1+t2\cdot v_{f7}$). However, the most probable E_p at a scan rate of v_{f7} is expected to be somewhere between E_1 and E_2 since the pitting initiation time at $E>E_1$ is expected to be much less than t_1, as indicated by curve I. If the E_p corresponding to each scan rate is obtained in the same way as for v_{f7}, the highest possible E_p values under potentiodynamic polarization of different scan rates will be represented by curve II, which illustrates that E_p is a function of v_f.

The above model gives a reasonable explanation about the functional relationship between E_p and v_f shown in Figs. 4.2 and 4.10. However, other relationships between E_p and v_f have been noted in the literature. Lizlovs and Bond (1975) reported that the E_p values of several types of ferritic stainless steel in 1M NaCl were comparable when tests were performed either with a fast scan rate of 50V/hr or a slow scan rate of 260mV/hr. Ginsberg and Huppatz (1972) also found that the E_p values of pure Al and Al-5Zn alloy specimens in artificial seawater were nearly independent of v_f for 100 mV/hr $\leq v_f \leq$ 10 V/hr. Based on a more comprehensive investigation of the scan rate effect on the E_p for various types of materials (austenitic stainless steel, duplex stainless steel, 20-type stainless steel, and nickel-based alloys) in 4% NaCl with 0.01M HCl at 70ºC, Manning (1980) concluded that the functional relationship of Ep versus scan rate is dependent on the material studied (varying passivation/depassivation kinetics). Those observations indicate that the assumptions that have been made in the previous section may not be satisfied in some situations. For example, the induction time is usually not a unique function of potential, as has been shown in Chapter 3 (Fig. 3.12).

Nevertheless, it has been commonly observed, e.g. by Manning(1980), that E_p either shifted slightly in the noble direction or was nearly unaffected with increasing v_f, when v_f was below a certain level (~0.36V/h to 0.6V/h, depending on the corrosion system). E_p determined at slow scan rates was also found to be close to that determined by the stationary potentiostatic method (Manning 1980). Therefore, E_p obtained with slow scan rates is more useful than that obtained with fast scan rates. In the present investigation, E_p determined with a v_f of 0.167mV/sec appeared to be out of the domain where E_p had strong dependence on v_f.

The observation that $\underline{E}_p$ increases with v_f appears to contradict some of our previous results. As noted in Chapter 3, $\underline{E}_p$ of prepassivated steel was found to be much higher than that without prepassivation (regular CYP). If $\underline{E}_p$ was raised due to an improvement reflecting increased passive film maturity from prepassivation, a similar effect should also have been observed when a slower scan rate was used, since at a slower scan rate steel is polarized for much longer time in the passive condition before it finally reaching E_p. However, $\underline{E}_p$ was found to decrease with decreasing v_f. One possible explanation for this observed disagreement may be attributed to the difference in how the passivity was achieved in each case. In the prepassivation tests, the passive film was produced in a chloride-free solution. However, in a regular CYP test, the passive film was created directly in a chloride-containing medium. As a result, the maturity and the structure of the passive film built in this two different media could be significantly different, hence causing E_p to depend differently on behavior with respect to passivation time. Further study on this issue is needed.

4.4.2 Distribution of E_p

In Chapter 3, E_p of rebar steel with either sandblasted (S= ~60cm^2) or 600 grit surface finish (S= ~50cm^2) in alkaline solutions of various [OH^-] and [Cl^-] combinations was found to be not a unique function of the test condition. As a result, the pitting of steel was evaluated using a statistical approach. The cumulative pitting probability for a given potential E was defined as the fraction of tests that result in pitting at or below that potential. It was also found that the cumulative pitting probability curve shifted in the noble direction as the chloride to hydroxide ratio (denoted by CR= [Cl^-] /[OH^-]) decreased. Using the same definition, the cumulative pitting probability curves of sandblasted steel and 600 grit finish steel in SCS with 1.0M NaCl are plotted as a function of potential in Figs. 4.11 and 4.12, respectively, using specimens surface area as a parameter. It can be seen that the S-curves shifted in the noble direction as steel surface area decreased. Therefore, decreasing the steel surface area had a similar effect on the E_p distribution as reducing CR (Chapter 3). Ideally, pitting initiation is related to the presence of “weak” points on the steel surface. The total number of those “weak” points on a specimen surface is expected to be proportional to its surface area. Therefore, it is reasonable to expect that $\underline{E}_p$ decreases with increasing S, as observed.

For many of the cases studied, the standard deviation of E_p (denoted by σ) did not strongly depend on S (Fig. 4.13). Instead, σ was strongly correlated with $\underline{E}_p$; σ decreased significantly as $\underline{E}_p$ decreased (Fig.4.14), regardless of the specimen size. This trend has also been observed for steel with various surface finishes and tested in solutions of various CR values (Chapter 3).

4.4.3 Area Effect and Stochastic Theory of Pitting Corrosion

The large variability of E_p documented in this and the previous chapter strongly indicates that the pitting initiation of rebar steel in chloride-containing alkaline solutions is a random phenomenon. Therefore, the stochastic theory which has been successfully applied to the explanation of the statistical variation of E_p and induction time related with the pitting corrosion of stainless steel by Shibata and Takeyama (1977), Baroux (1988) , among others, may also be applicable to the pitting corrosion of rebar steel. The stochastic theory can be applied to the pitting initiation process as follows:

First, the following assumptions and definitions are made:

1) There are N identical specimens experiencing polarization at a potential E.

2) Each specimen is passive at the beginning of the polarization and it will either remain passive or pit (to be active) after a certain time t.

3) Each specimen can only change from the passive state to the active state, i.e., once pitting initiates, steel can not be repassivated at the same potential. (This assumption assumes that only the birth process of the stochastic theory takes place.)

4) At a controlled potential E, the pits already present on a specimen do not interfere with the generation of new pits.

5) The future probability of pitting generation does not depend on what has happened in the past, but is completely specified once the probability of pit generation at present is known.

If the number of specimens that has pitted at time t is n(t), then the pitting probability of a specimen at time t will be:

$$p(t)=n(t)/N \qquad (4.2)$$

If we now introduce the pitting generation rate g(t) (= $d\omega(t)/dt$, where $\omega(t)$ is the elementary pitting probability per unit area) as defined by Baroux (1988), the total number of specimens that will pit at time $t+\triangle t$ will be:

$$n(t+\triangle t)= n(t)+[N-n(t)]\, g(t)S\triangle t \qquad (4.3)$$

Dividing by N both sides of Eq.(4.3) and applying Eq.(4.2), we have

$$p(t+\triangle t)= p(t)+[1-p(t)]\, g(t)S\triangle t \qquad (4.4)$$

Eq.(4.4) can be rewritten as:

$$\frac{p(t+\Delta t)-p(t)}{\Delta t} = g(t)S[1-p(t)] \qquad (4.5)$$

For a very small time increment $\triangle$t, Eq.(4) becomes:

$$dp(t)/dt = -g(t)\, S[1-p(t)] \qquad (4.6)$$

It we define the probability that a specimen will be passive at time t as P(t), (often called the survival probability), then

$$P(t)=1-p(t) \qquad (4.7)$$

By substituting Eq.(4.7) into Eq.(4.6), we have

$$\frac{dP(t)}{dt} = -g(t)SP(t) \qquad (4.8)$$

Eq.(4.8) is the basic equation describing the stochastic pitting process when only the pure birth process is taken into account. It can also be derived from other approaches (Shibata 1996). Eq.(4.8) can also be reorganized as:

$$\frac{d\ln P(t)}{dt} = -Sg(t) \qquad (4.9)$$

As a result, when plotting ln(P(t)) against time t, the slope obtained on the curve corresponds the pitting generation rate of each specimen.

Now, the effect of specimen surface area on the pitting probability will be examined. Consider two specimens which have the same condition (made of the same material and having the same surface finish) except for their surface area, being S_1 and S_2, respectively. From Eq.(4.9), we have:

$$d\ln P_1(t) = -S_1 g_1(t)dt \qquad (4.10)$$

$$d\ln P_2(t) = -S_2 g_2(t)dt \qquad (4.11)$$

Since both types of specimens are identical except for size, $g_1(t)$ should be equal to $g_2(t)$. Therefore, by dividing Eq.(4.10) by Eq.(4.11), we have

$$\frac{d\ln P_1(t)}{d\ln P_2(t)} = \frac{S_1}{S_2} \qquad (4.12)$$

or

$$d\ln P_1(t) = \frac{S_1}{S_2} d\ln P_2(t) \qquad (4.13)$$

Since Eq.(4.12) and Eq.(4.13) are directly derived from Eq.(4.9), they are valid as long as the pure birth stochastic theory applies to the pitting initiation process. These equations are independent of how g(t) behaves with respect to time t and potential E. By integrating both sides of Eq.(4.13) for the time interval between 0 and t, we have:

$$\ln P_1(t) - \ln P_1(0) = \frac{S_1}{S_2}[\ln P_2(t) - \ln P_2(0)] \quad (4.14)$$

since $P_1(0)=P_2(0)=1$, Eq.(13) becomes

$$P_1(t) = P_2(t)^{(\frac{S_1}{S_2})} \quad (4.15)$$

For potentiodynamic polarization, t is a linear function of potential E, hence Eq.(4.15) can also be expressed as

$$P_1(E) = P_2(E)^{(\frac{S_1}{S_2})} \quad (4.16)$$

or

$$p_1(E) = 1 - [1 - p_2(E)]^{\frac{S_1}{S_2}} \quad (4.17)$$

Eqs. (4.16) and (4.17) can also be directly obtained from a mathematical approach. Consider again the above case of two specimens with area S_1 and S_2 (with $S_1>S_2$). Now conceptually divide specimen S_1 into k ($k= S_1/S_2$) identical sections so that each section has the size of S_2. If it is assumed that the pitting initiation processes on k identical sections of S_2 are independent of each other and the survival probability of specimen S_2 at potential E is known and equal to $P_2(E)$, then the survival probability of specimen S_1 at E will simply be:

$$P_1(E) = P_2(E)^k = P_2(E)^{(\frac{S_1}{S_2})} \quad (4.18)$$

which is the same as Eq.(4.16).

According to Eq. (4.17), the pitting probability in a population of specimens each having surface area S_1 can be predicted from the pitting probability of another population having surface area S_2, if the other parameters of each specimen population are the same. If at a certain potential E, $p_2(E)$ is very small, then employing Taylor series expansion, Eq.(4.17) can be approximately reduced to the following simpler form:

$$p_1(E) = (\frac{S_1}{S_2}) \cdot p_2(E) \quad (4.19)$$

Eq.(4.19) predicts that the change of pitting probability is linearly proportional to the change of the steel surface area, as has been usually expected (Evans 1981). However, Eq. (4.19) is no longer valid if $p_2(E)$ is not very small. In that case Eq.(4.17) has to be employed for the prediction of $p_1(E)$ from $p_2(E)$. The validity of Eq.(4.17) may be examined by comparing its prediction with experimentally determined p(E) values. Figures 4.15 and 4.16 show experimentally determined p(E) distribution as a function of E for 600 grit finish steel specimens ($0.5cm^2$, $5cm^2$, and $50cm^2$) in SCS with 1.0M NaCl and 0.1M NaCl, respectively. The theoretical p(E) were calculated with Eq.(4.17) using the experimental p(E) of specimens which were either 10 times larger or 10 times smaller than those for which the prediction was made. As can be seen, the calculated p(E) distributions for the three groups of specimens are

in reasonable agreement with the experimental values. Moreover, the theoretical calculations extend to E_p values for the $0.5cm^2$ and $5cm^2$ specimens where $p(E)<0.01$. If such prediction were correct, much experiment time would be saved and a higher confidence about the limiting value of the most critical pitting potentials could be gained.

Results from Chapter 3 indicated that E_p increased as the roughness of steel surface decreased. In the present section, it can also been seen (from Figs. 4.4 - 4.7) that, for steel of same nominal surface area, $\underline{E}_p$ of 600 grit finish was significantly higher than $\underline{E}_p$ of sandblasted finish. Due to the area effect and the increase of actual area with roughness, however, the $\underline{E}_p$ of a smaller, coarser specimen may still be nobler than that of a larger, smoother specimen. For example, in SCS with 1.0M NaCl, the $\underline{E}_p$ value of 600grit/$0.5cm^2$ specimens was ~0.6V higher than that of the sandblasted/$0.5cm^2$ specimens. However the latter was ~0.2V higher than that of the 600grit/ $50cm^2$ specimens in the same solution. A direct comparison of the p(E) distribution for these three types of specimens was presented in Fig. 4.17. It strongly demonstrates that beside surface finish, the specimen surface area played a very significant role in affecting pitting susceptibility. This conclusion was further verified using type III specimens in CYP tests carried out in SCS with 1.0M NaCl. Whenever a sudden large anodic corrosion current (>~50μA/cm^2) was detected, the specimen was checked visually in-situ to determine the location of the first pit. As soon as the pit was visually detected, the CYP test was terminated. Only on two of 15 repeated tests the pit was formed in the $0.5cm^2$ sandblasted zone — pits were formed in the 600 grit zone on 13 out of 15 specimens tested. The p(E) values as a function of E from these tests were also calculated and plotted in Fig. 4.17. It can be seen that the distribution of the pitting probability with respect to E obtained on specimens with combined surface finish/surface area features almost reproduced those obtained from specimens with only one distinctive surface finish. Therefore, the present investigation strongly indicates that the pitting susceptibility of steel is directly related to its surface area, and that observation is partially supported by the stochastic theory of the pitting initiation process. Therefore, one needs to be very careful when comparing experimental results from different laboratories where specimens with different surface areas were used, even if the chemical compositions of the material and the test method were exactly the same. When specimens of different surface finishes are involved, inference from direct comparison can be further misleading.

However, it has to be pointed out that the agreement between theoretical predictions with Eq.(4.17) and experimental measurements was poorer for other test conditions (e.g., sandblasted steel in SCS with 0.1M and 1.0M NaCl, and sandblasted or 600 grit finish steel in SPS2 with 1.0M, 2.0M, or 3.0M NaCl). There exist a few possible reasons. First, the assumed pure birth process (pitting generation only) of the stochastic theory may not be accurate to describe the pitting corrosion of steel in alkaline solution. Repassivation of a metastable pit is very likely to happen on certain occasions. For example, in Chapter 2, it was shown that the E_{oc} of rebar specimens immersed in SPS+3.0M NaCl fluctuated between the active and passive states (Fig. 2.3). Another major concern is that the E_p distribution curve obtained from measurements of a limited number of replicates for each specific test condition may not be representative of the actual E_p distribution curve of a large population. However, Eq.(4.16) is only expected to be valid for the relationship between the corresponding p(E) of two large

populations. Consequently, deviation of experimental data from theoretical predictions made using Eq.(4.17) is inevitable.

In the above discussion the value of S was only referred to the nominal specimen surface area. For specimens with the same S value, the smoother the surface, the nobler was the $\underline{E}_p$. On the other hand, $\underline{E}_p$ was also related to S — for specimens of the same type of surface finish, the smaller S, the nobler $\underline{E}_p$. Considering that the actual surface area of a specimen (with a fixed S) decreases with increasing surface smoothness, it may be reasonably deduced that the improvement in pitting resistance in that case may be partially attributed to the reduction in the actual surface area. Nevertheless, the area effect by itself can not explain the experimentally observed $\underline{E}_p$ difference between specimens of the same S but different surface finishes. Electrochemical impedance spectroscopy (EIS) measurements (as will be presented in Chapter 5) showed that the nominal interfacial capacitance of sandblasted rebar steel was about four times as large as that of the 600 grit steel in SPS2 at open circuit conditions. Therefore, it may be roughly estimated that, for a fixed S, the actual surface area of a sandblasted surface was about four times that of a 600 grit surface. Under that estimation, the nominal surface area of sandblasted specimens can be normalized to the equivalent area of 600 grit finish (denoted as S′) by multiplying by a factor of four, and then the E_p values of two types of finishes could be directly compared. Figure 4.18 presents the E_p of sandblasted finish and 600 grit finish specimens obtained in SPS2+1.0M NaCl as a function of S′. It can be seen that even after correcting for roughness $\underline{E}_p$ for 600 grit finish was distinctly nobler than that for sandblasted finish in most of the ranges. Therefore, it may be concluded that the improvement in pitting resistance due to surface finish is inherent to the surface treatment, independent of the surface area change effects.

4.4.4 Chloride Corrosion Threshold

In previous chapters, the chloride corrosion thresholds were calculated based on experimental results using specimens with a nominal surface area of ~60 cm^2. According to the findings in this chapter, there exists a trend whereby $\underline{E}_p$ decreased as the surface area of the tested specimens increased. Therefore, the chloride corrosion thresholds proposed in the previous chapters may be less conservative if they are to be applied to large structures. In that sense, the actual chloride corrosion threshold of reinforcing steel in concrete could only be obtained from observations in normal size structures. Direct application of laboratory results of steel pitting susceptibility, obtained with very small (surface area on the order of $1cm^2$) and highly surface finished (smoother than 600 grit finish) specimens, to field structures could be severely misleading. The present findings nevertheless suggest the feasibility of predicting the pitting probability of large steel surfaces by applying Eq.(4.17) to the pitting distribution curve for small-sized steel specimens. However, for proper prediction the distribution of the pitting probability of small-sized steel specimens should be more accurately characterized using large populations.

4.5 Conclusions

1) $\underline{E_p}$ decreased significantly with increasing specimen size; a slope as high as ~0.3V per area decade was observed for 600 grit steel in SCS with 0.1M and 1.0M NaCl.

2) The surface finish of steel also strongly affected $\underline{E_p}$; the smoother was the surface finish, the higher was the $\underline{E_p}$ value.

3) The variability of E_p was not strongly affected by the specimen size. However, it increased with $\underline{E_p}$.

4) E_r was independent of specimen surface area. A low limit of ~-0.8V was observed for all the cases tested.

5) The dependence of E_p on specimen size was explained with the stochastic pitting initiation theory. In some cases, the E_p distribution predicted with equations derived from that theory matches the experimental observation reasonably.

6) E_p could be overestimated when measured with fast scan rates. However, E_p was less anodic polarization scan rate dependent if v_f was low enough.

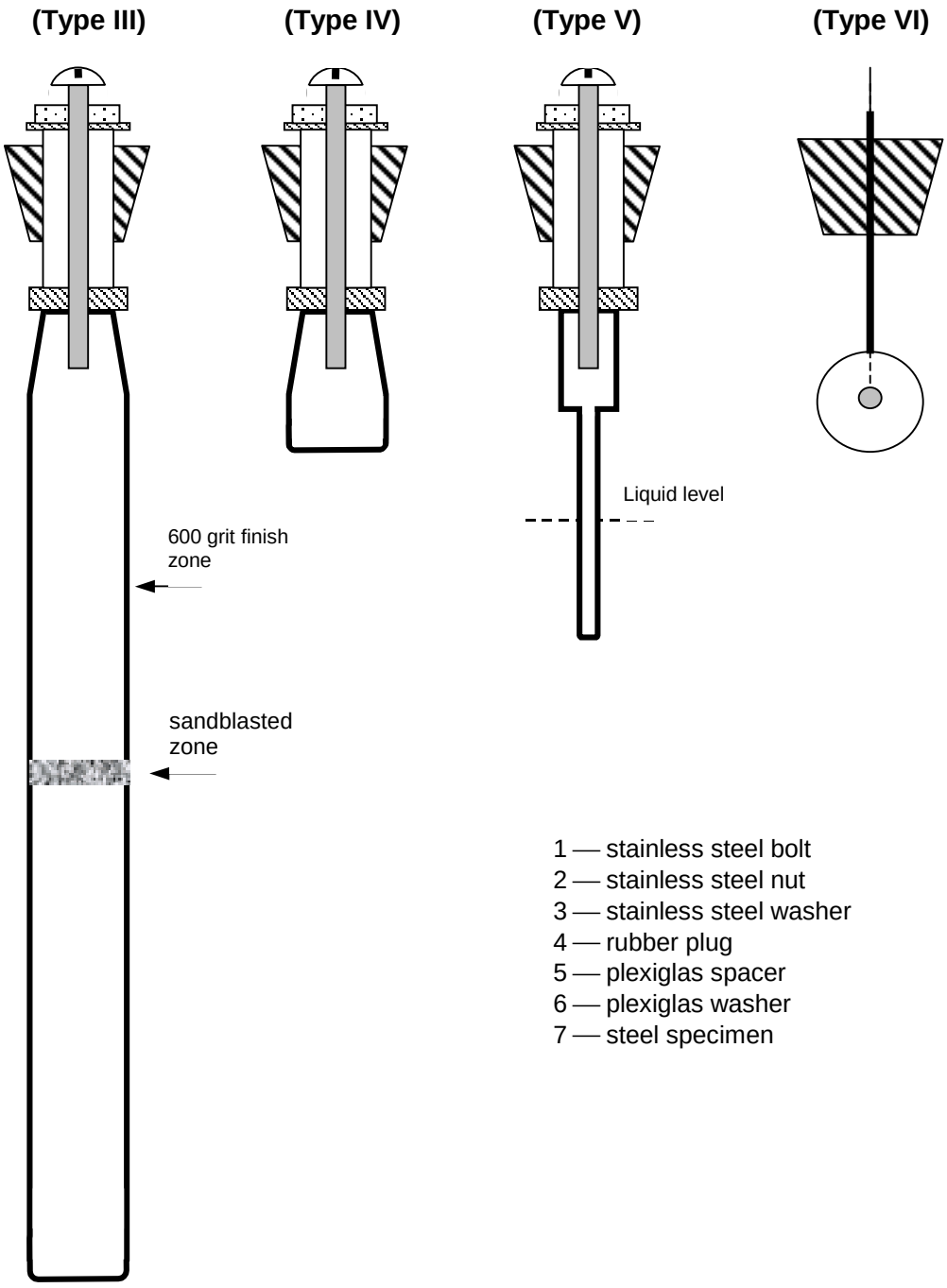

Figure 4.1 Schematic graph (not to scale) showing the assembly of each type of specimens (except Type I and Type II). All the specimens were fully immersed in test solutions except Type V.

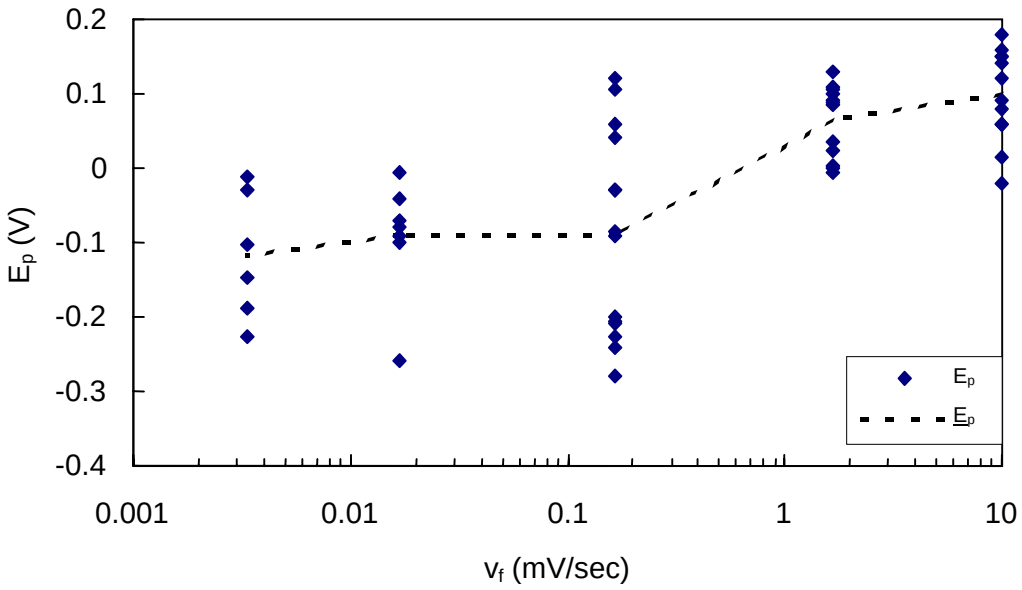

Figure 4.2 Distribution of E_p as function of v_f for sandblasted/60cm^2 steel in SPS2 with 1.5M NaCl

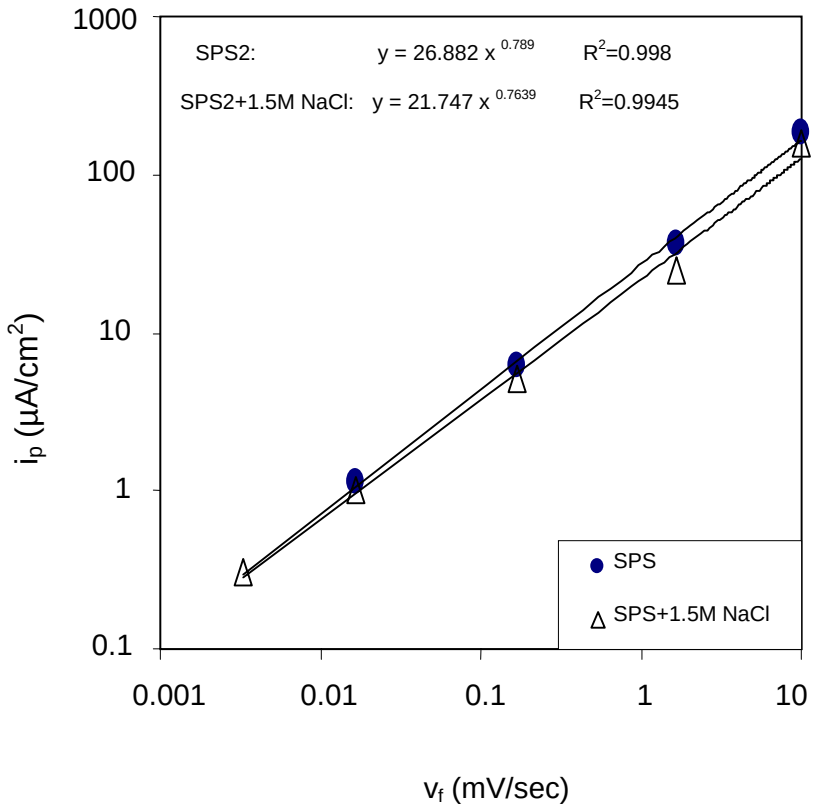

Figure 4.3 Dependence of i_p on v_f for sandblasted/60cm^2 specimens in SPS2 without and with 1.5M NaCl

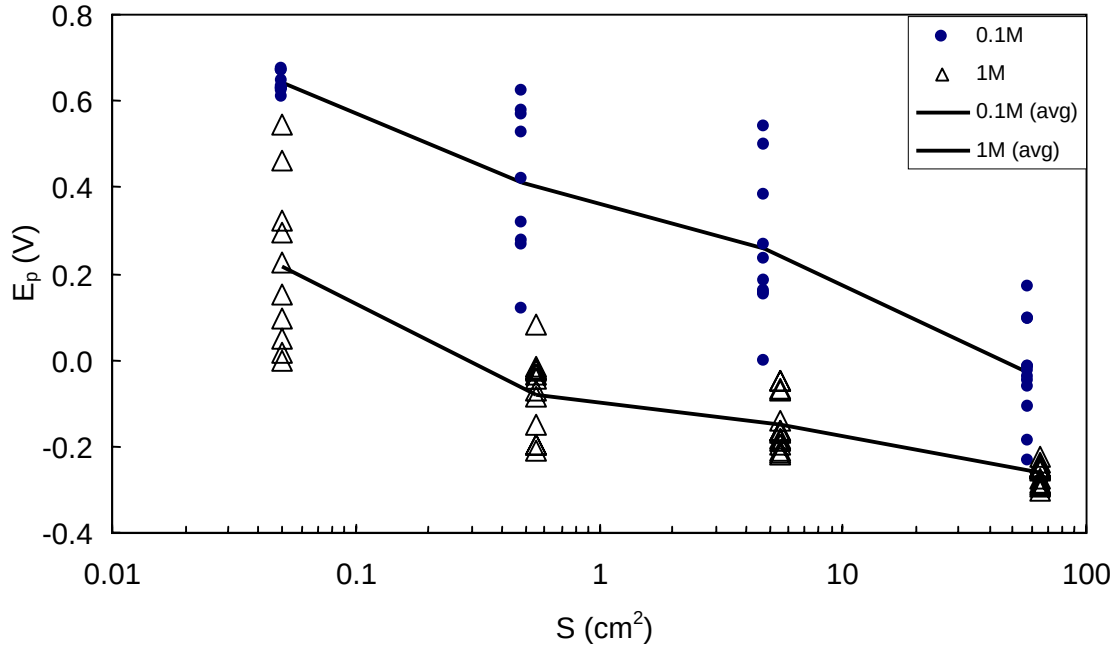

Figure 4.4 Effect of steel surface area on E_p of sandblasted steel in SCS with 0.1M and 1.0M NaCl (some symbols slightly shifted for clarity)

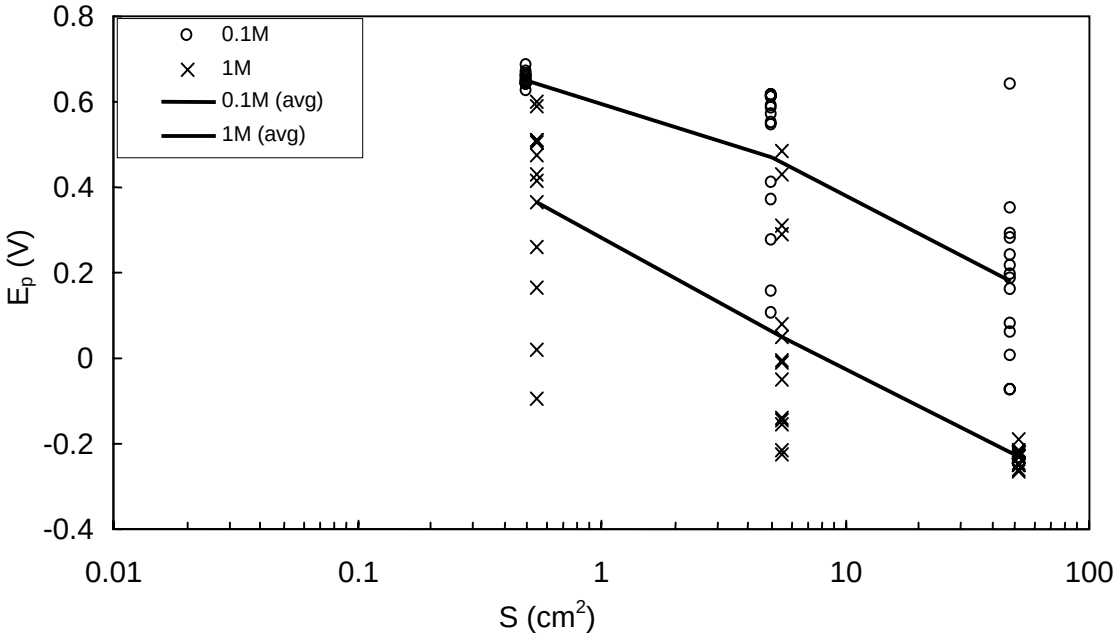

Figure 4.5 Effect of surface area on E_p of 600 grit finish steel in SCS with 0.1M and 1.0M NaCl (some symbols slightly shifted for clarity)

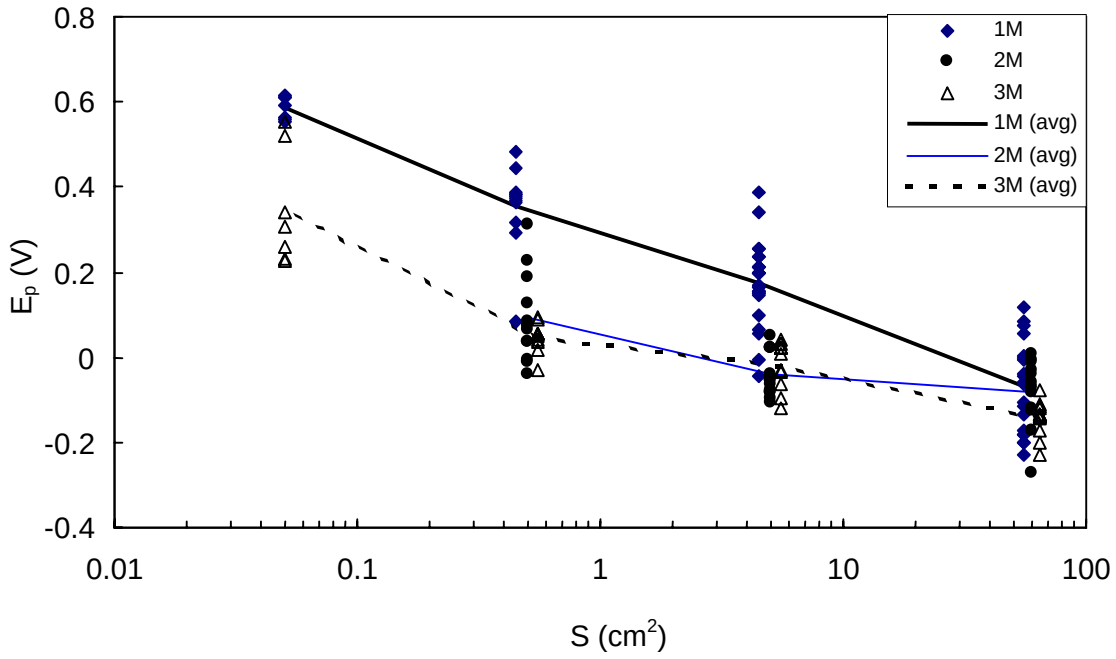

Figure 4.6 Effect of surface area on E_p of sandblasted specimens in SPS2 with 1M, 2M, and 3M NaCl (some symbols slightly shifted for clarity)

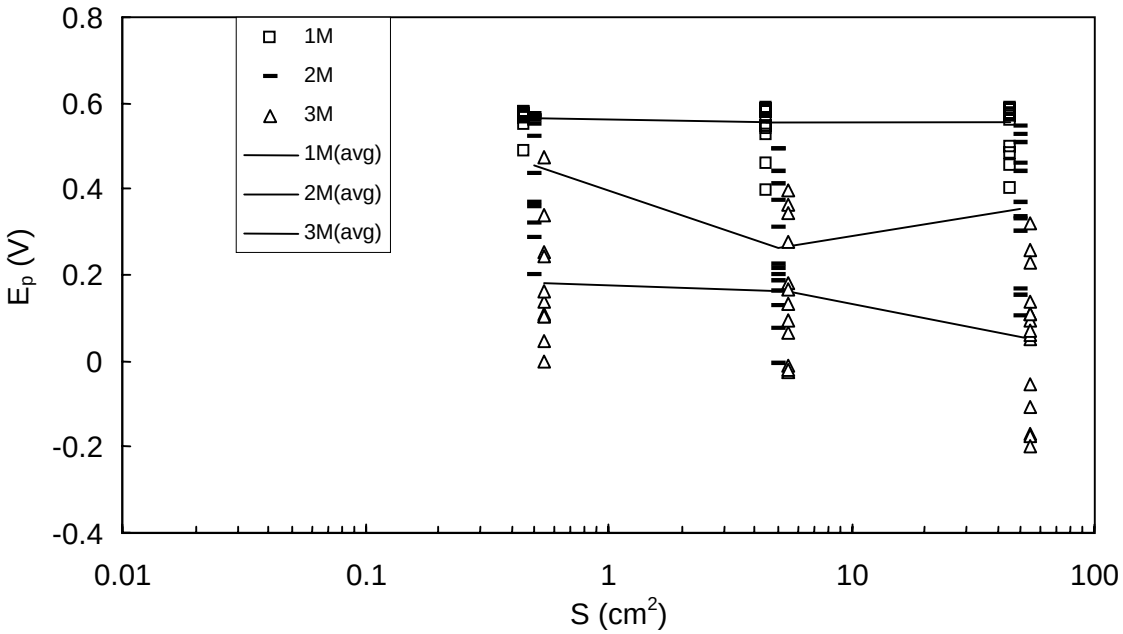

Figure 4.7 Effect of surface area on E_p of 600 grit finish specimens in SPS2 with 1M, 2M, and 3M NaCl (some symbols slightly shifted for clarity)

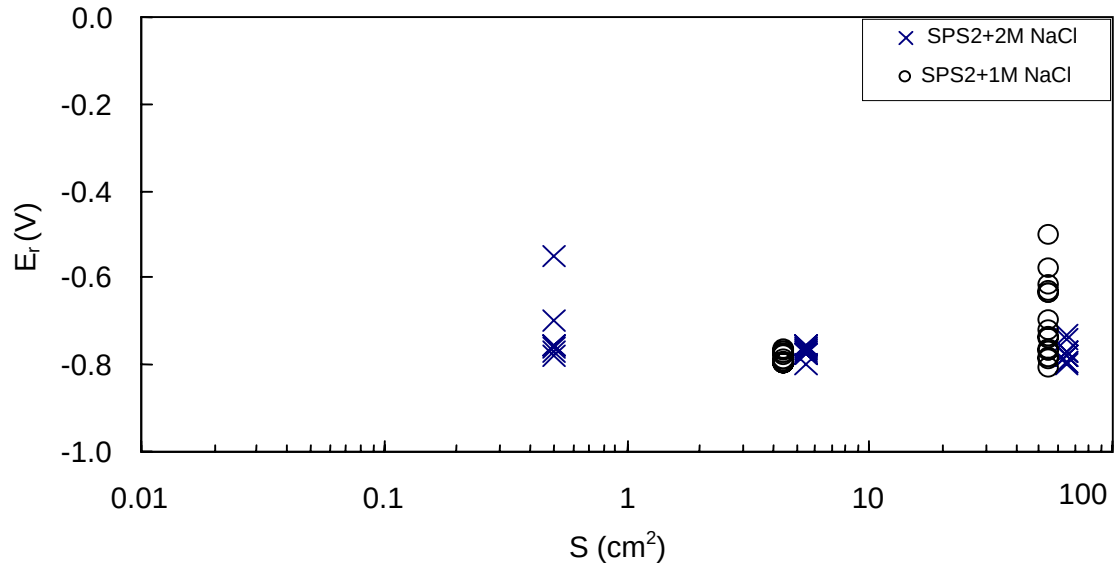

Figure 4.8 E_r as a function of sandblasted specimen surface area in SPS2 with 1M and 2M NaCl (some symbols slightly shifted for clarity)

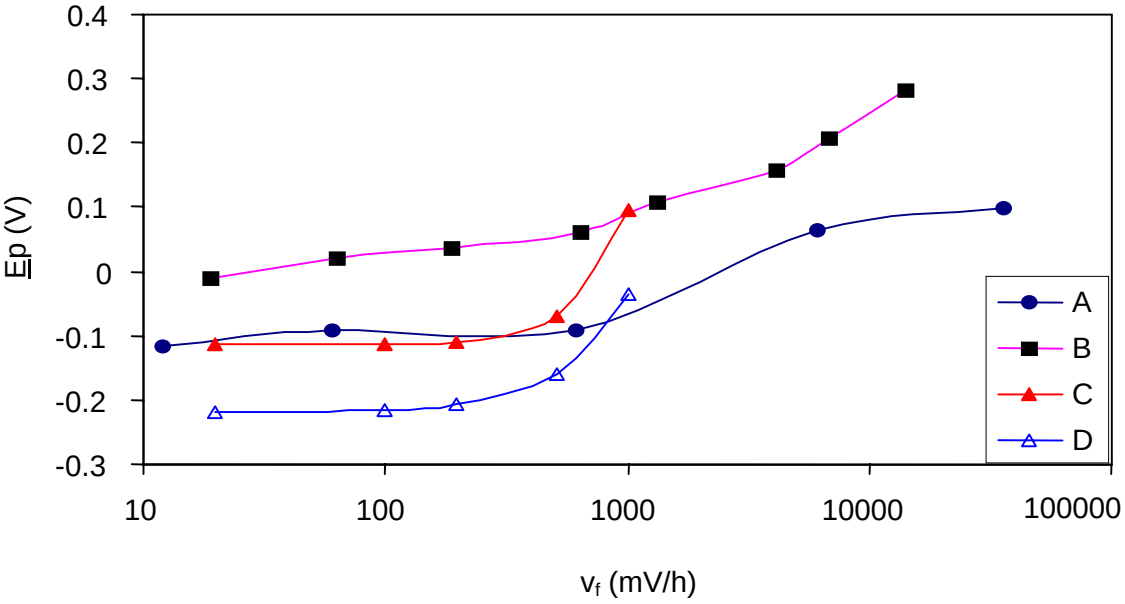

Figure 4.9 $\underline{E}_p$ as a function of scan rate (A-Rebar steel in SPS with1.5M NaCl by Li in this investigation, B-304 stainless steel in 0.1M NaCl by Leckie (1965), C-Carbon steel (M) in borate buffer solution (pH8.4) with 0.05M KCl by Szauer and Jacobs (1976), D-Low alloy steel (LO1) in borate buffer solution (pH8.4) with 0.05M KCl by Szauer and Jacobs (1976))

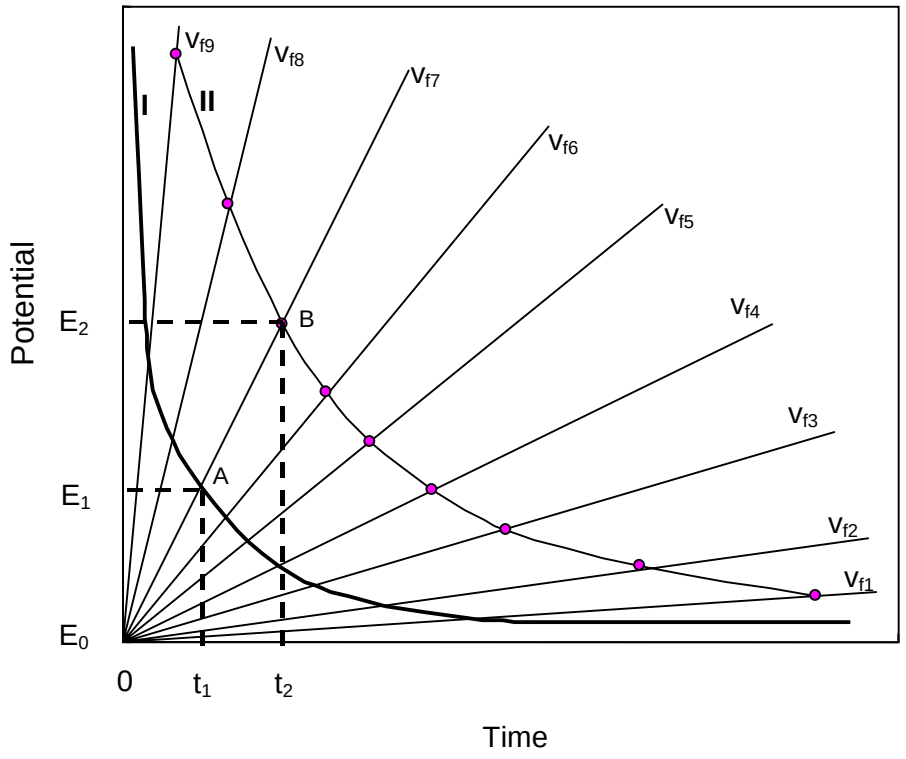

Figure 4.10 Schematic graph showing the dependence of E_p on anodic polarization scan rates

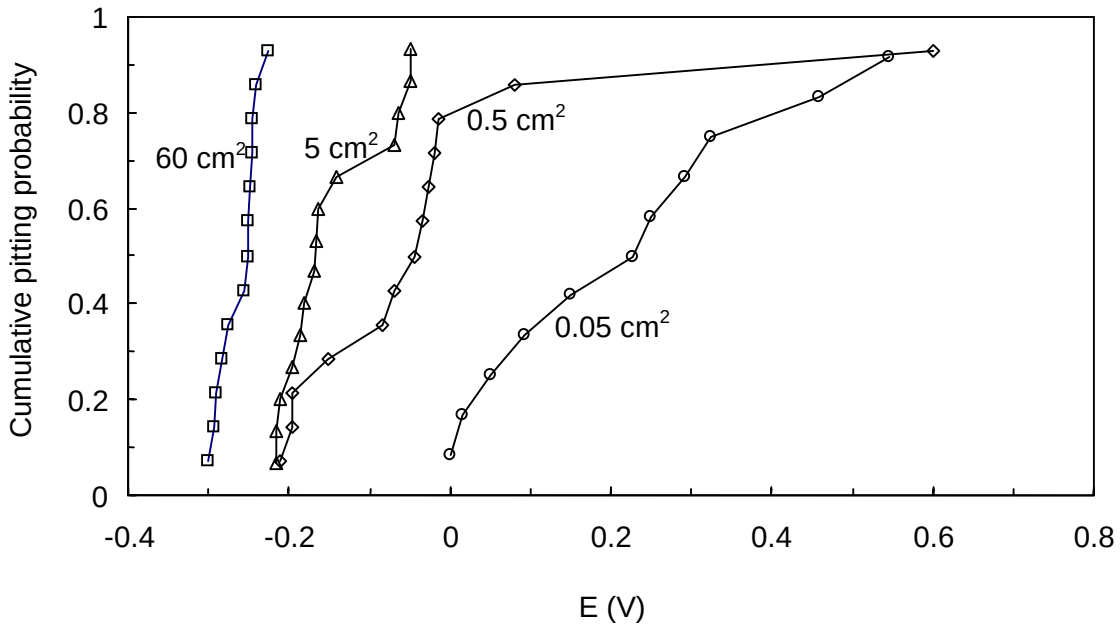

Figure 4.11 E_p distribution of sandblasted steel in SCS with 1.0 M NaCl

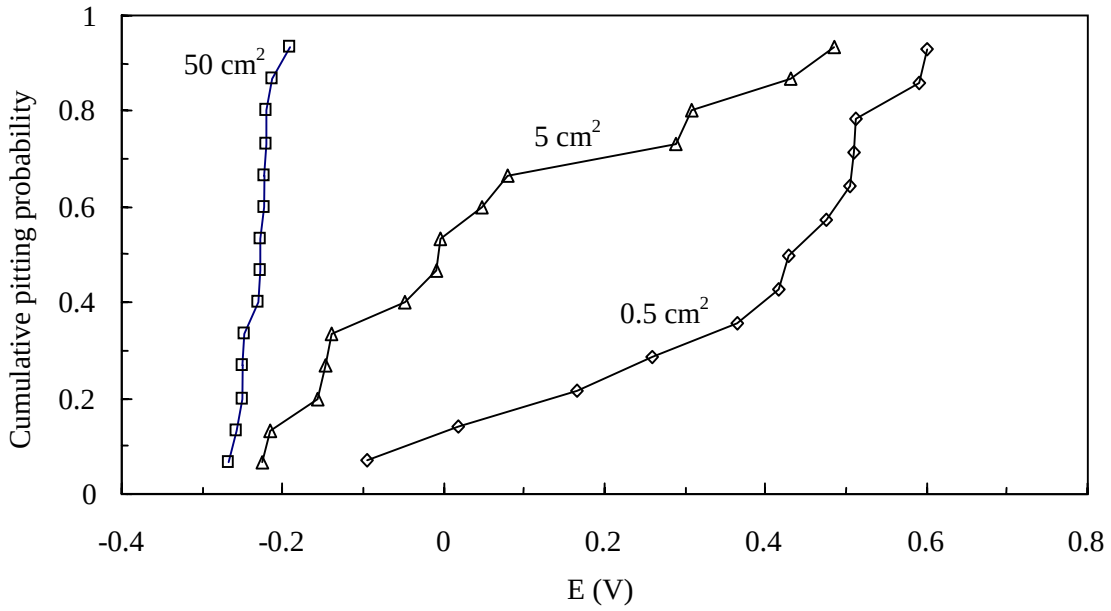

Figure 4.12 E_p distribution of 600 grit finish steel in SCS with 1.0 M NaCl

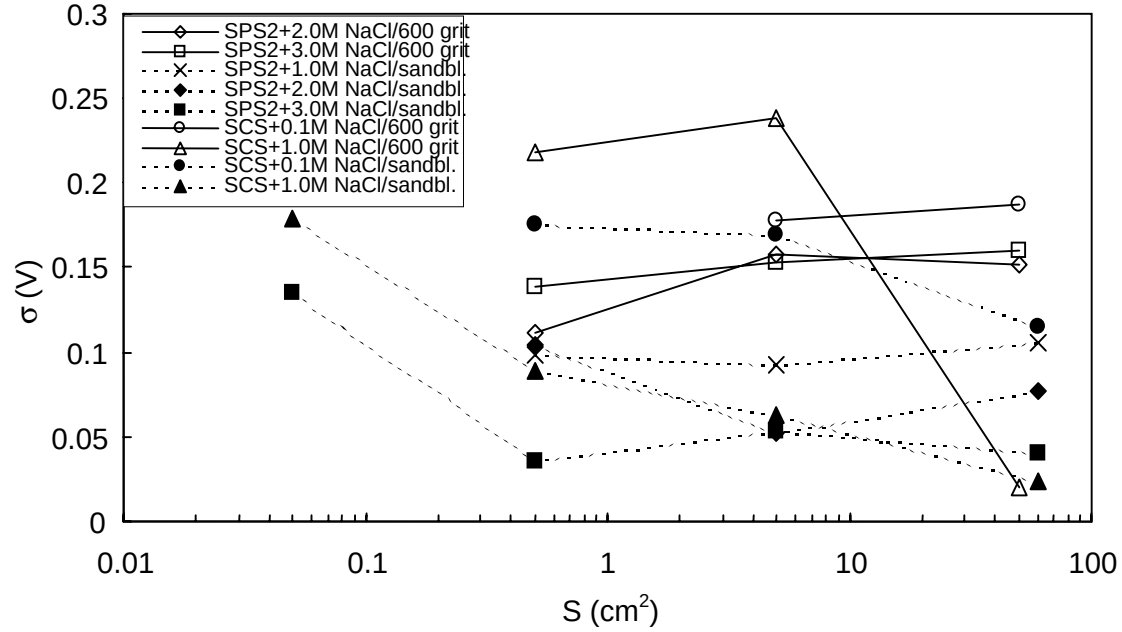

Figure 4.13 Distribution of σ as a function of steel surface area for various test conditions

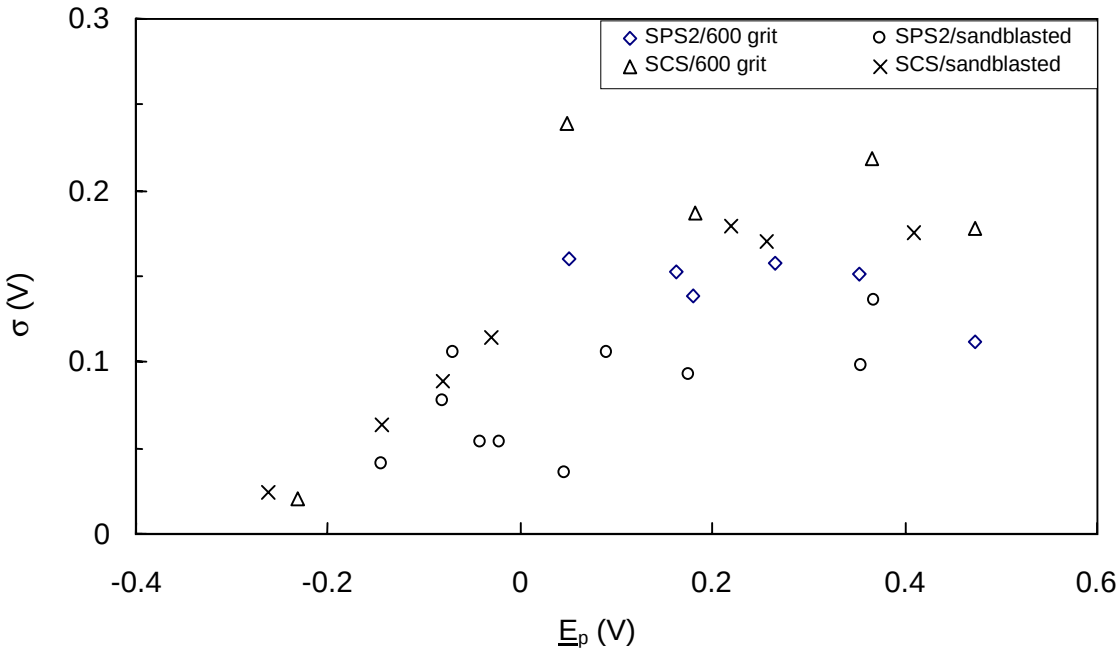

Figure 4.14 Correlation between σ and $\underline{E}_p$ for various test conditions

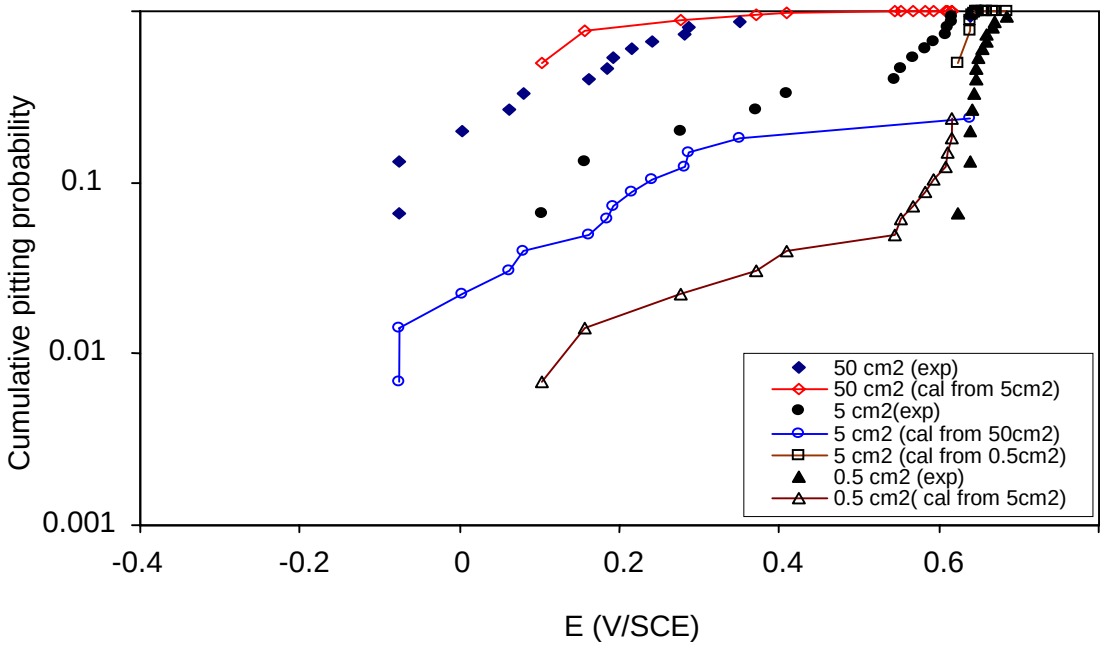

Figure 4.15 Comparison of E_p distribution between experimental and theoretical for rebar steel (600 grit) in SCS with 0.1 M NaCl

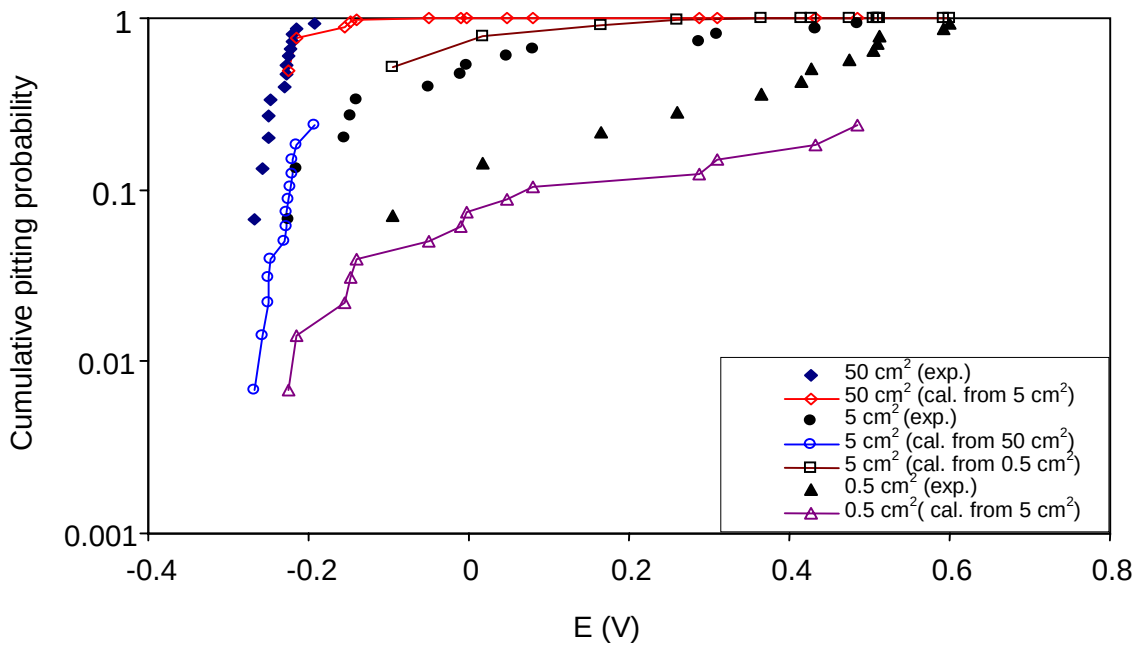

Figure 4.16 Comparison of E_p distribution between experimental and theoretical for rebar steel (600 grit) in SCS with 1.0 M NaCl

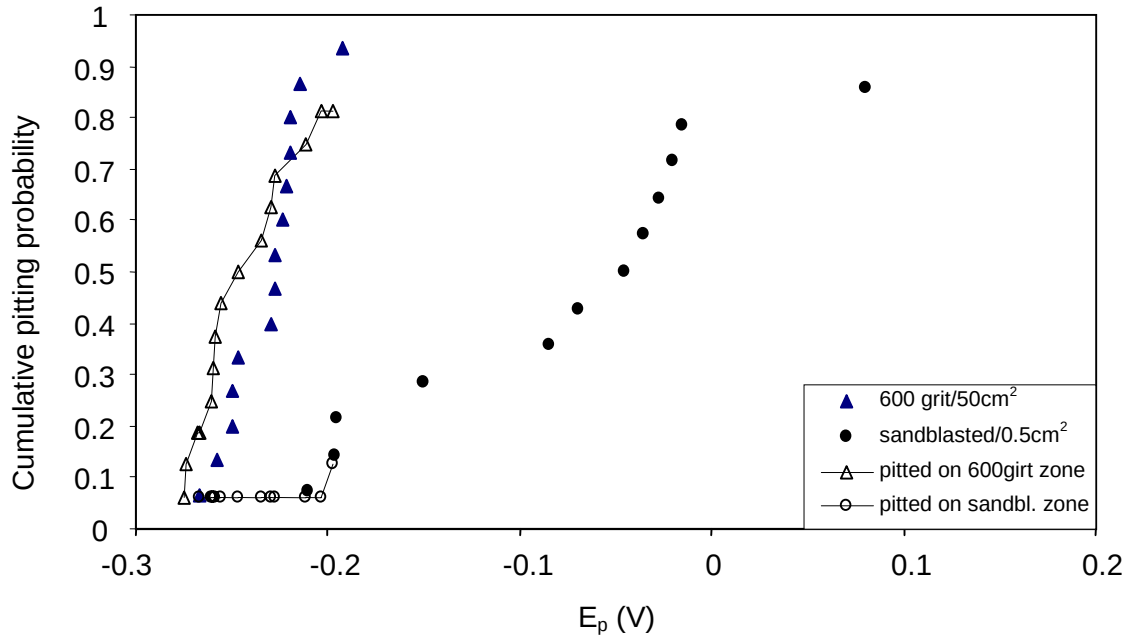

Figure 4.17 Effect of rebar steel surface area and finish on pitting probability in SCS with 1M NaCl (tests were performed on three types of specimens: 1--600 grit/50cm^2; 2--sandblasted/0.5cm^2; 3---combined 600grit/50cm^2+sandblasted/0.5cm^2)

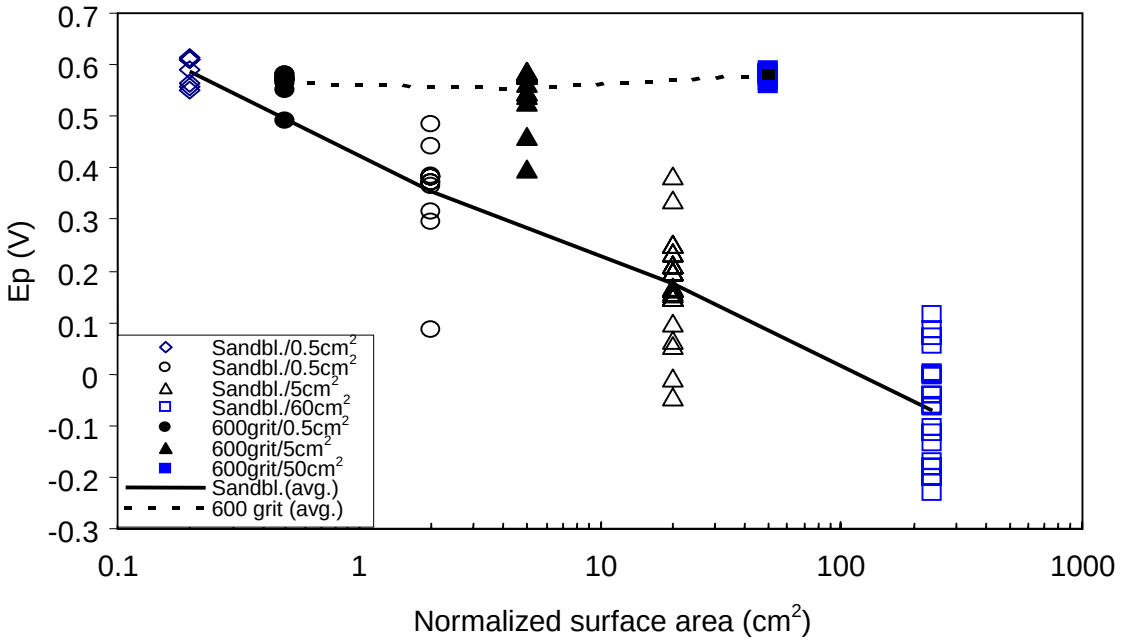

Figure 4.18 Comparison of surface finish (sandblasted vs. 600 grit finish) effect on E_p in SPS2+1.0M NaCl after the specimen surface area was normalized to the 600 grit condition

Chapter 5: Passivity of Steel in Alkaline Solutions

5.1 Introduction

The passivation of iron and carbon steel in both borate buffer solutions and alkaline solutions has been widely documented (Szklarska-Smialowska 1986, Büchleret al. 1997, Larramona and Gutisrrez 1989, Huang and Ord 1985, Videm 1999, Foley 1967). However, investigations on steel passivity have often been focused on the structure and composition of passive films which were usually formed over a very short passivation period. The electrochemistry of the passive film on a steel surface in alkaline solutions after long-term passivation has rarely been reported. Reinforcing steel in concrete is often subjected to many years of passivation before the accumulation of chloride ions on its surface is enough to breakdown the passive layer. Therefore, it is important to understand what determines the steady-state corrosion current density of steel in concrete and whether the maturity of the passive film affects the pitting susceptibility of steel in the presence of chlorides.

The passivity of rebar steel has been preliminarily considered in the previous chapters. In this chapter, the passivity behavior of steel in alkaline solutions (with pH ranging between 8.2 and 13.6) was investigated for cases where the material was either at the open circuit condition or under potentiostatic or potentiodynamic polarization. The purpose of this section of investigation was to quantitatively determine the corrosion current density of steel in alkaline environments after a long-term passivation. The effect of a pre-existing passive film on the pitting potential in chloride-containing solutions was also studied.

5.2 Experimental

Rebar specimens of Type I (sandblasted/ 60cm^2) or type II (600grit/50cm^2) (Figure 3.1a) and the electrochemical cell (Fig.3.1b) described in Chapter 3 were used throughout these experiments. Tests were conducted in one of the following four types of solutions: SPS2 (pH 13.6), SCS (pH 12.6), NCS (0.1 M Na_2CO_3, pH 11.4), and NHS (0.2 M $NaHCO_3$, pH 8.2). All the solutions were prepared with reagent chemicals and distilled water. All the measurements were performed at room temperature, 21 $\pm$ 2 ºC. For each test condition in the following, measurements were performed on duplicate specimens. Electrode potentials are reported on the saturated calomel electrode (SCE) scale.

5.2.1 Open-circuit Immersion (OCI) Tests

Freshly sandblasted or ground rebar specimens were fully immersed in naturally aerated SPS2, SCS, NCS, and NHS. The open circuit potential (E_{oc}) was monitored over a testing period of more than 100 days. During the first few hours of immersion, EIS was only performed in the frequency range from 10 Hz to 0.01 Hz. Each EIS test in that frequency range was finished within ~3 minutes so that the influence of the current perturbation during each EIS measurement on future passivation process was minimized. After longer immersion times, EIS was normally performed in the frequency range from 100 kHz to 1 mHz. In some tests, the lowest frequency was extended to 50μHz. Unless otherwise specified, only a portion of the EIS spectrum (corresponding to frequencies lower than 0.1Hz) was analyzed with the equivalent

circuit shown in Fig. 2.2 to obtain the values of R_p, R_s, Y_o and n. The R_p values were used to calculate the nominal corrosion current density (i_{corr}) by employing Eq.(2.1). The Stern-Geary constant B was assigned a value of 40mV, which will be justified later.

For comparison, commercial 304 stainless steel (denoted as 304SS) specimens were also used in SCS. Each specimen had the same size (~50 cm^2 surface area) and surface condition (600 grit finish) as the Type II specimens.

5.2.2 Potentiostatic Polarization (PSP) Tests

Rebar specimens freshly ground to a 600 grit finish were potentiostatically polarized at 0V immediately after contact with the test solution. The solutions were either free of NaCl or containing a small amount of NaCl (0.1 M in SPS2, 0.004 M in SCS, 0.004 M in NCS, and 0.002M in NHS). Before and during each test, the test solution was deaerated with nitrogen. For most of the tests, polarization was applied for one day and the anodic polarization current (i_a) was recorded.

5.2.3 Potentiodynamic Polarization (PDP) Tests

Potentiodynamic polarization (PDP) was performed on rebar specimens (either sandblasted or with 600 grit finish) in each of the four types of solutions. Each specimen was first conditioned at –1 V for 2000 seconds and then PDP was performed with various anodic polarization scan rates (v_f = 0.0167, 0.167, 1.67, and 10 mV/sec). The preparation procedure of the test specimens and solutions was the same as described in Section 3.2. Test solutions were constantly deaerated with nitrogen before and during each PDP test. The plateau passive current density (i_p, nominally the polarization current density at 0V) for each test was recorded.

5.3 Results
5.3.1 Passivation under Open-circuit Conditions

Fig. 5.1 shows the time evolution of E_{oc} of sandblasted specimens in four types of alkaline solutions. The features of these curves were similar to those shown earlier in Figs. 2.3, 2.5, and 2.7 (before the introduction of NaCl). E_{oc} moved in the anodic direction markedly during the first few days after immersion, and appeared to reach stable values after ~ 20 days. The steady-state E_{oc} was ~-0.1V in SPS2, SCS, and NHS. The steady-state E_{oc} in NCS was ~0.1V higher than in the other solutions.

The time evolution of the Nyquist plots of the EIS response of all the specimens can be exemplified by Figure 5.2, which was obtained from one of the duplicate sandblasted/60cm^2 specimens in SCS. Clearly the low frequency impedance magnitude increased significantly with immersion time.

Figure 5.3 presents the time evolution of the nominal i_{corr} for sandblasted specimens in each type of solution. In all cases i_{corr} decreased with immersion time, t, with no indication that a steady-state i_{corr} had been reached even after 100 days immersion. For $0.1 \leq t \leq 100$ days, the relationship between i_{corr} and t can be empirically expressed as:

$$i_{corr}(t) = i_{corr1} \cdot \left(\frac{t}{day}\right)^{-k_1} \qquad (5.1)$$

where t is the immersion time (in days), $i_{corr}(t)$ is the nominal corrosion current density (in $\mu A/cm^2$) at t, i_{corr1} is the projected corrosion current density (in $\mu A/cm^2$) for t = 1 day , and k_1 is the slope (= - $\partial(\log i_{corr}) / \partial(\log t)$).The values of i_{corr1}, slope k_1 and R^2 obtained for each test condition from numerical regression are listed in Table 5.1. For most of the conditions examined, i_{corr} decreased to ~0.01$\mu A/cm^2$ after ~10 days, irrespective of the solution pH. In NCS, k_1 was the largest and consequently i_{corr} was the lowest after 100 days.

In SCS, the k_1 value of the plain rebar steel was nearly unaffected by the specimen surface finish. However, the steel surface finish strongly affected i_{corr1}; it was about twice as large for the sandblasted finish than for the 600 grit finish (Fig.5.4). On the other hand, k_1 for 600 grit 304SS was much larger and i_{corr1} was much smaller than k_1 of 600 grit rebar specimens in SCS. As a result, i_{corr} of 600 grit 304SS was about one order of magnitude lower than that of 600 grit rebar steel after immersion for 40 days.

In Figure 5.5, the Y_o and n values from EIS measurement for rebar specimens (sandblasted or 600 grit finish) and SS304 specimens (600 grit finish) in SCS are plotted as a function of immersion time. For all three cases, both Y_o and n remained approximately unchanged with time, in significant contrast with the i_{corr}-t behavior. When n~1 (as in the present cases) the CPE behaves approximately as a capacitance of value $Y_o^* = Y_o \cdot s^{1-n}$. The Y_o^* value of 20~30 $\mu F/cm^2$ corresponding to the 600 grit specimens (both plain rebar steel and 304SS) was in agreement with reported double layer capacitance values of smoothly finished steel in liquid solutions (Bard and Faulkner 1980). For a given nominal specimen area, rougher surfaces expose a greater area of metal to the electrolyte, which is reflected in larger measured interfacial capacitance. This behavior was observed here as well. Y_o^* of sandblasted steel (with a rougher surface) was about three times that of the 600 grit rebar (which had a smoother surface). This indication of differences in effective area exposed to the electrolyte agrees with the observed greater values of i_{corr1} (also i_{corr}) for sandblasted finish vs. 600 grit finish specimens.

5.3.2 Passivation under Potentiostatic Polarization

Figure 5.6 demonstrates the time evolution of the anodic current density (i_a) of rebar steel (600 grit finish) under potentiostatic polarization at 0V in SPS, SCS, NCS, and NHS without and with a small amount of NaCl. In all the cases, $\log(i_a)$ decreased nearly linearly with log(t). The trend of those curves indicates that i_a had not reached a steady state after one day. With further polarization time, i_a continued to decrease (Fig.5.7). In SCS, i_a of 600 grit rebar steel in SCS dropped from ~0.04 $\mu A/cm^2$ when t =1 day to ~0.01 $\mu A/cm^2$ when t = 8.5 days. Therefore, further decreasing of i_a upon continual potentiostatic polarization is expected before a steady state develops.

Similarly to Eq.(5.1), i_a can be related to time by:

$$i_a(t) = i_{a1} \cdot \left(\frac{t}{day}\right)^{-k_2} \qquad (5.2)$$

where t is the potentiostatic polarization time (in days), $i_a(t)$ is the anodic current density at t (in $\mu A/cm^2$), i_{a1} is the projected $i_a(t)$ value for t = 1 day (in $\mu A/cm^2$), and k_2 is the slope (= $-\partial(\log i_a) / \partial(\log t)$). The values of i_{a1}, slope k_2 and R^2 obtained by numerical regression for each test condition are listed in Table 5.2.

Table 5.2 compares the i_{a1} and k_2 values measured in the four types of test solutions. In pH13.6 SPS2, k_2 was the smallest and i_{a1} was the largest (0.07 $\mu A/cm^2$). In contrast, in pH 11.4 NCS, k_2 was the largest, and the corresponding i_{a1} was the smallest (0.012 $\mu A/cm^2$). Therefore, i_{a1} and k_2 were solution type dependent.

Figure 5.8 compares the experimentally measured i_{a1} (the average of at least two repeated tests) after one day of potentiostatic polarization for various test conditions. It is clearly seen that i_a was the highest in SPS2 but the lowest in NCS. However, i_a, i_{a1} and k_2 were nearly unaffected by the presence of a small amount of chloride in the solution, as was confirmed by results in Figs. 5.6, Fig.5.8 and Table 5.2.

5.3.3 Passivation under Potentiodynamic Polarization

The PDP curves of rebar steel specimens in the four types of solutions can be exemplified by Figure 5.9, which was obtained from sandblasted/60cm^2 specimens in SPS2. Clearly the PDP curves obtained with different v_f had similar shapes. However, the curves shifted to the left as v_f decreased. The cathodic current tail observed at E < ~-0.95 V for the two slow scan rates was likely due to the hydrogen evolution reaction. Conversely, the large anodic current surge at E > ~0.55V manifested the oxygen evolution reaction as discussed earlier. The anodic current peaks between ~-0.85 V and –0.7 V (depending on v_f) probably corresponded to the beginning of the formation of passive film. Most importantly, the plateau passive current density (i_p), decreased with decreasing v_f, suggesting a slower metal oxidation rate at slower scan rates. According to the measured Y_o values shown in Fig. 5.5, the double layer charging current density is estimated to be at least one order of magnitude lower than the i_p value at each corresponding v_f. Therefore, the contribution of the charging current to the total measured i_p can be neglected. Since the anodic current density did not vary too much when –0.2V < E < 0.4V, the current density value at 0 V was selected in each case as a representative i_p value. It can be seen that $\log(i_p)$ varied linearly with $\log(v_f)$ (Figure 5.10). Therefore, the relationship between i_p on v_f can be expressed as follows:

$$i_p = i_{p1} \cdot \left(\frac{v_f}{mV/sec}\right)^{k_3} \qquad (5.3)$$

where v_f is the anodic polarization scan rate (in mV/sec), i_p is the plateau passive current density (in $\mu A/cm^2$), i_{p1} is the projected i_p for v_f = 1 mV/sec (in $\mu A/cm^2$), and k_3 is the slope (= $\partial(\log i_p) / \partial(\log v_f)$). The values of i_{p1}, slope k_3 and R^2 obtained from numerical regression for each test condition are listed in Table 5.3. In both SPS2 and SCS, k_3 was very close to 1.

The anodic polarization scan rate v_f is related to t by:

$$v_f = \frac{E - Es}{t} = \frac{\Delta E}{t} \qquad (5.4)$$

where E is the electrode potential at time t and E_s is the PDP starting potential. If i_p is the value taken at 0V and PDP started at –1V, Eq.(5.3) can be expressed as:

$$i_p(t) = i_{p1} \cdot \left(\frac{86.4 \cdot t}{day}\right)^{-k_3} \qquad (5.5)$$

Comparison of Eq.(5.1), (5.2) and (5.5) reveals that all three current parameters (i_{corr}, i_a, and i_p) decayed exponentially with time. In Figure 5.11, the current decay slopes (k_1, k_2, and k_3) are plotted as a function of the solution pH. The slopes appeared to be the largest in NCS, and decreased with increasing solution pH above 11.

5.4 Discussion

5.4.1 E_{oc} and i_{corr} at the Open-circuit Condition

Accurate determination of the corrosion current density of rebar steel in alkaline solutions at the open-circuit condition (i_{corr}) is important, since, in principle, it is expected to represent the rate of passive dissolution in concrete. However, direct measurement of i_{corr} of passive rebar steel embedded in concrete is often subject to significant inaccuracies because of the existence of a very large pseudo-capacitance at the steel/concrete interface, especially when the steel surface is very rough and covered with mill scale. As shown in Fig.5.5, for steel free of mill scale and immersed in alkaline solutions, the interfacial capacitance is on the order of 100 μF/cm^2. Consequently, significant information about corrosion reaction rates of steel in liquid solutions may be obtained within an achievable EIS frequency domain range (Sagüés 1993).

E_{oc} and i_{corr} were interrelated. In Figure 5.12, E_{oc} is plotted as a function of i_{corr} for each test condition. Although the time parameter is not shown, generally data points for low E_{oc} and large i_{corr} values correspond to the measurements at the beginning of the immersion test, whereas high E_{oc} and small i_{corr} values correspond to the measurements at the end of the immersion test. Interestingly, the data as a whole suggest that there existed a nearly linear relationship between E_{oc} and log(i_{corr}) when i_{corr}> ~0.03 μA/cm^2, regardless of the experimental conditions (solution type, steel surface condition and chemical composition). Numerical regression yields a slope (= $\partial(E_{oc}) / \partial(\log i_{corr})$) of ~90mV/decade for all the cases. It should be noted that this slope is independent of the value B selected to calculate i_{corr} using Eq.(2.1), as long as B is a constant.

For rebar steel in aerated high pH alkaline solutions, it has been proposed that steel may be oxidized directly to the ferric state (Hausmann, 1998). In such case, the half-cell reaction forming the passive film may be written as :

$$Fe + 3\ OH^- \rightarrow \gamma\text{-}FeOOH + H_2O + 3e^- \qquad (5.6)$$

At the open circuit condition, the most probably cathodic reaction coupled with the iron oxidation reaction was the oxygen reduction process, which may be expressed as follows:

$$\tfrac{1}{2}\, O_2 + 2\, H_2O + 2\, e^- \rightarrow 2\, OH^- \qquad (5.7)$$

Since there is no net electrical current at open circuit, i_{corr} should be equal to the oxygen reduction current per Eq.(5.7) if that is the operating cathodic process. Therefore, the relationship between E_{oc} and i_{corr} as shown in Fig.5.12 can also be interpreted as the cathodic polarization behavior of reaction (5.7). Based on that assumption, the Tafel slope for that cathodic reaction (β_c) was estimated from Fig. 5.12 to be ~90 mV/decade (ignoring the data for 304SS when i_{corr} <0.005μA/cm^2). This value is comparable to cathodic slopes reported by other investigators in similar systems involving oxygen reduction (Zecevic et al. 1987, Gojkovic et al. 1998). The E-log(i) slope for the anodic reaction (β_a, not a Tafel slope) in the passive range can be expected to be extremely large, as manifested by the anodic polarization curves shown in Fig. 5.9. Therefore, the value B in Eq.(2.1) when calculated by the Stern-Geary equation (1957) becomes independent of β_a:

$$B = \frac{\beta_a \cdot \beta_c}{2.303 \cdot (\beta_a + \beta_c)} \cong \frac{\beta_c}{2.303} \cong 40\text{mV} \qquad (5.8)$$

Consequently, the value B of 40 mV was adopted for i_{corr} calculations.

In estimating the durability of rebar in concrete, Andrade and Alonso (1994) proposed that a threshold i_{corr} value of ~0.1 to 0.2 μA/cm^2 could be used to indicate the difference between passive and active states of rebar steel in concrete. However, according to the present investigation, the steady-state i_{corr} of plain rebar steel in the passive condition is expected to be much lower than that proposed threshold. In Fig. 5.12, i_{corr} has been shown to be a function of E_{oc}. The E_{oc} of plain rebar steel in SPS2 and SCS after 100 days of open-circuit immersion appeared to reach a steady-state value of ~-100mV. The E_{oc} of regular (with mill scale) and sandblasted rebar steel in the passive condition after seven years in sound concrete in this laboratory was also measured to be between 0V and –100mV (Sagüés and Li 2000). Therefore, Fig. 5.12 suggests an expected steady-state i_{corr} between 0.001 and 0.01 μA/cm^2 for plain rebar.

In comparison, the i_{corr} of 304SS in SCS was about one order of magnitude less than that of plain rebar steel. This may be attributed to a lower exchange current density of the oxygen reduction reaction on a SS304 surface, as is implied by the E_{oc}-i_{corr} relationship shown in Fig.5.12. Those results also show a lower slope for 304SS, when i_{corr} <~0.005 μA/cm^2, than that obtained at higher i_{corr} values. A similar feature has also been reported for oxygen reduction on platinum electrode in alkaline solutions by Sepa and Vojnovic (1980), who attributed this observation to the intermediate coverage of the electrode surface by the absorbed oxygen species.

5.4.2 EIS Response of Passive Steel at Open-circuit Conditions

As shown in Fig. 5.2, when the lowest frequency for the EIS measurement was 1mHz, the Nyquist plots of the EIS spectra revealed only a very limited portion of the semi-circle expected from the equivalent circuit (Fig.2.2). Therefore, there was concern as to whether the R_p calculated with that limited information reasonably approximated the actual R_p value. For that reason, EIS was performed extending the test frequency range to very low values (50 μHz) on selected tests. The Nyquist and the Bode phase angle plots of the EIS response for a sandblasted rebar specimen (after 136 days of immersion) and a 600 grit SS304 specimen (after 18 days of immersion) in SCS thus obtained are displayed in Figures 5.14 and 5.15, respectively. Clearly, most of the semi-circle expected from the assumed equivalent circuit was actually displayed, and the equivalent circuit simulation result fitted the experimental result quite closely.

To determine the error introduced by truncating the EIS spectrum, values of $R_{s,}$ R_p, Y_o and n were obtained using the same equivalent circuit to simulate the EIS spectrum but choosing data from different frequency ranges. The results are compared in Table 5.4. The results show that the relative difference between the values of each parameter ($R_{s,}$ R_p, Yo, or n) simulated using different ranges of the EIS response was less than 10%. Therefore, it can be confidently concluded that the R_p values obtained from EIS spectra measured only in the 10^5Hz to10^{-3} Hz frequency range (which was the case of most of the EIS measurements) were representative of the actual R_p values that would have been obtained from a much wider measured spectrum. In addition, additional analysis revealed that the relative deviations of the real and the imaginary parts of the measured impedance were less than ~5% when the testing frequency was below ~1kHz, where most information relevant to corrosion rate determination resides (Sagüés 1993). Consequently, the i_{corr} values obtained from the regular EIS measurements are not expected to involve large errors.

5.4.3 Comparison of i_{corr}, i_a ,and i_p

Regardless of the experimental techniques and assumptions used, the decay of the current density parameters (i_{corr}, i_a, or i_p) with time followed a power law. This observation is in agreement with that reported by Macdonald and Roberts (1978) for the current transients of carbon steel in 1M NaOH using a potentiostatic method. In Fig.5.16, i_{corr}, i_a ,and i_p are plotted as a function of time using Eqs. (5.1), (5.2) and (5.5) and the parameters listed in Tables 5.1, 5.2, and 5.3 for 600 grit finish rebar steel in SCS. The i_p values appear to be higher than those of i_{corr} and i_a. This is partially because during the conversion of Eq.(5.3) to Eq. (5.5), i_p is arbitrarily defined as the value taken at 0V instead of at a more negative potential value at which the passive current density plateau was first observed. Nevertheless, all three current density parameters decreased to values less than 0.01 μA/cm^2 for t=100 days. Although those current density parameters are expected to decrease further with continuing polarization, a steady-state value below 0.001 μA/cm^2 is unlikely for rebar steel, as has been indicated when discussing Fig. 5.12. This expectation should be tested in future experiments.

5.5 Conclusions

1) The passivation of reinforcing steel in aerated alkaline solutions (between pH 8.2 and pH 13.6) was a gradual process. A steady-state passive film appears to be formed after more than 100 days of open-circuit immersion. The steady-state i_{corr} of rebar steel was estimated to be 0.01~0.001 μA/cm^2.

2) A strong correlation between i_{corr} and E_{oc} was observed. Regardless of the steel surface condition and solution pH, a slope of ~0.09V/decade was obtained in all cases examined.

3) Regardless of the electrochemical techniques used, the logarithm of anodic current density decreased nearly linearly with log(t). The current decaying rate was the fastest in NCS.

4) After about 40 days of open-circuit immersion in SCS, the i_{corr} of 600 grit 304 stainless steel was less than 10^{-3} μA/cm^2, which was about one order of magnitude lower than that of rebar steel after 100 days of open-circuit immersion.

Table 5.1 i_{corr1}, k_1 and R^2 for rebar and 304SS at open-circuit condition

Surface condition	Solution type	i_{corr1} (μA/cm^2)	k_1	R^2
Sandblasted/rebar	SPS	0.227	0.61	0.9894
	SCS	0.130	0.59	0.9969
	NCS	0.130	0.84	0.9925
	NHS*	0.103	0.73	0.9785
600 grit/rebar	SCS*	0.053	0.57	0.9837
600 grit/304SS	SCS	0.020	0.84	0.9952

* Regression based on results with $t \leq 25$ days.

Table 5.2 i_{a1}, k_2 and R^2 for rebar (600 grit finish) under potentiostatic polarization

Solution type	$[Cl^-]$ (M)	i_{a1} (μA/cm^2)	k_2	R^2
SPS	0	0.074	0.65	0.9973
	0.1	0.076	0.61	0.9973
SCS	0	0.040	0.68	0.9989
	0.004	0.042	0.67	0.9940
NCS	0	0.015	0.91	0.9979
	0.004	0.012	0.94	0.9994
NHS	0	0.024	0.75	0.9964
	0.002	0.026	0.80	0.9964

Table 5.3 i_{p1}, k_3 and R^2 for rebar under potentiodynamic polarization

Solution Type	surface condition	i_{p1} (μA/cm^2)	k_3	R^2
SPS	sandblasted	26.6	0.79	0.9971
	600 grit	9.4	0.75	0.9985
SCS	sandblasted	20.4	0.86	0.9960
	600 grit	7.4	0.79	0.9974

Table 5.4 Comparison of R_s, R_p, Y_o and n values obtained by applying the same equivalent circuit simulation to limited frequency ranges selected from a broader spectrum measured experimentally

Test condition	Total frequency range (Hz)	Selected frequency range (Hz)	R_s (ohm)	R_p (ohm)	Yo ($\Omega^{-1}s^n$)	n
Sandblasted rebar in SCS for 136 days	10^5~5×10^{-5}	10^5~5×10^{-5}	3.3	8.72×10^4	0.00615	0.921
		10^5~10^{-3}	3.3	8.34×10^4	0.00615	0.922
		10^{-3}~5×10^{-5}	3.3*	8.76×10^4	0.00616	0.921
600 grit 304SS in SCS for 18 days	10^5~5×10^{-5}	10^5~5×10^{-5}	3.8	6.00×10^5	0.00102	0.952
		10^5~10^{-3}	3.8	5.55×10^5	0.00102	0.953
		10^{-3}~5×10^{-5}	3.8*	6.07×10^5	0.00101	0.949

* R_s was fixed for that value during simulation.

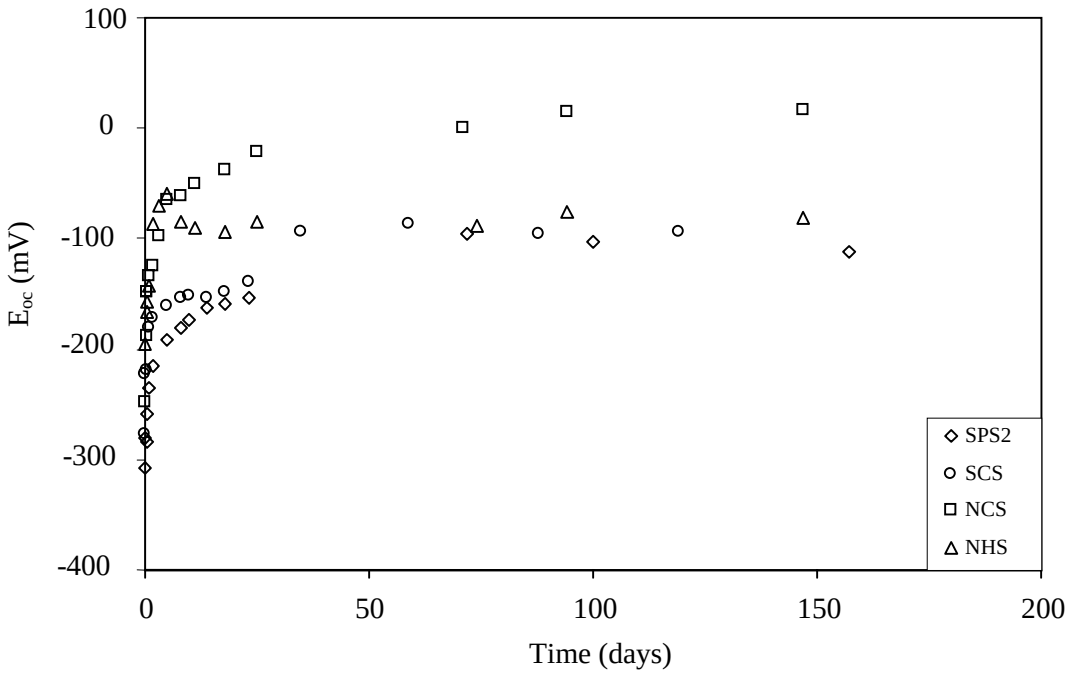

Figure 5.1 Time evolution of E_{oc} of sandblasted rebar specimens in SPS2, SCS, NCS, and NHS

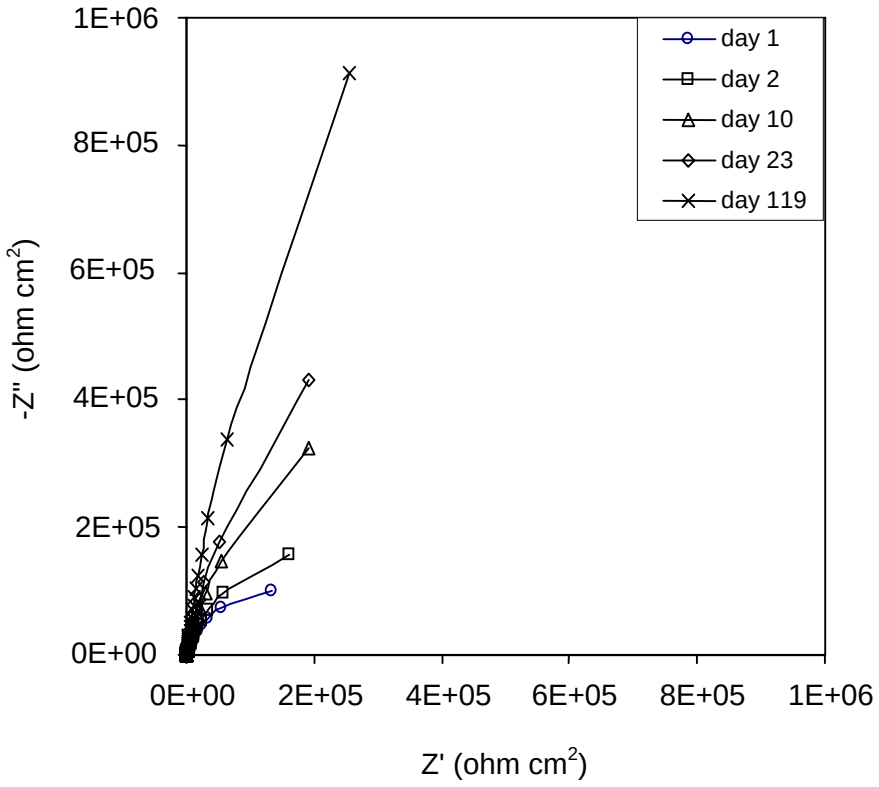

Figure 5.2 Time evolution of Nyquist plots of the EIS response on a sandblasted rebar specimen in SCS (The lowest frequency datum in each plot is for 1 mHz.)

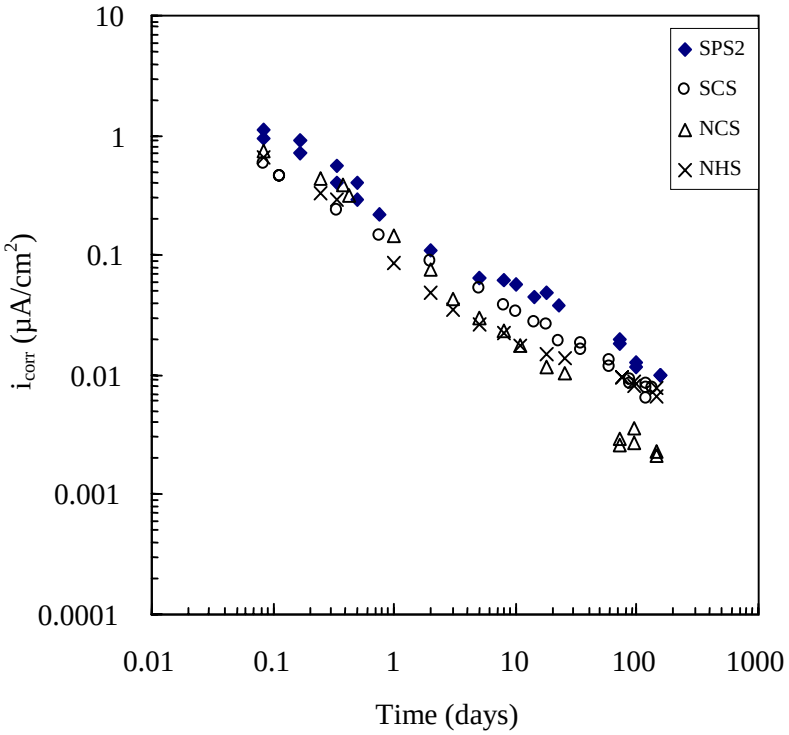

Figure 5.3 Time evolution of i_{corr} of sandblasted rebar specimens in SPS2, SCS, NCS, and NHS

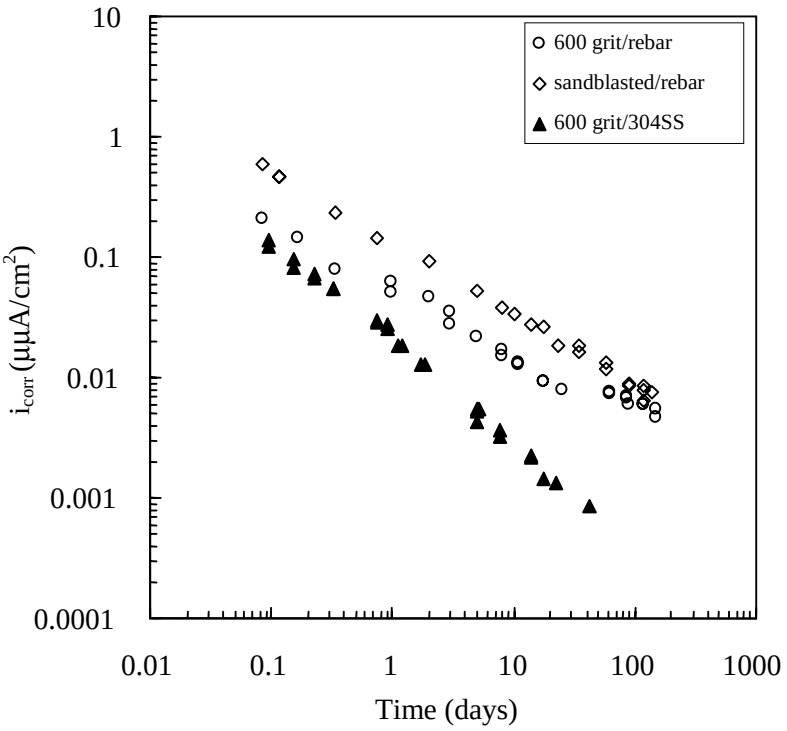

Figure 5.4 Comparison of the time evolution of i_{corr} for rebar steel (sandblasted vs. 600 grit) with i_{corr} for 304SS (600 grit) in SCS

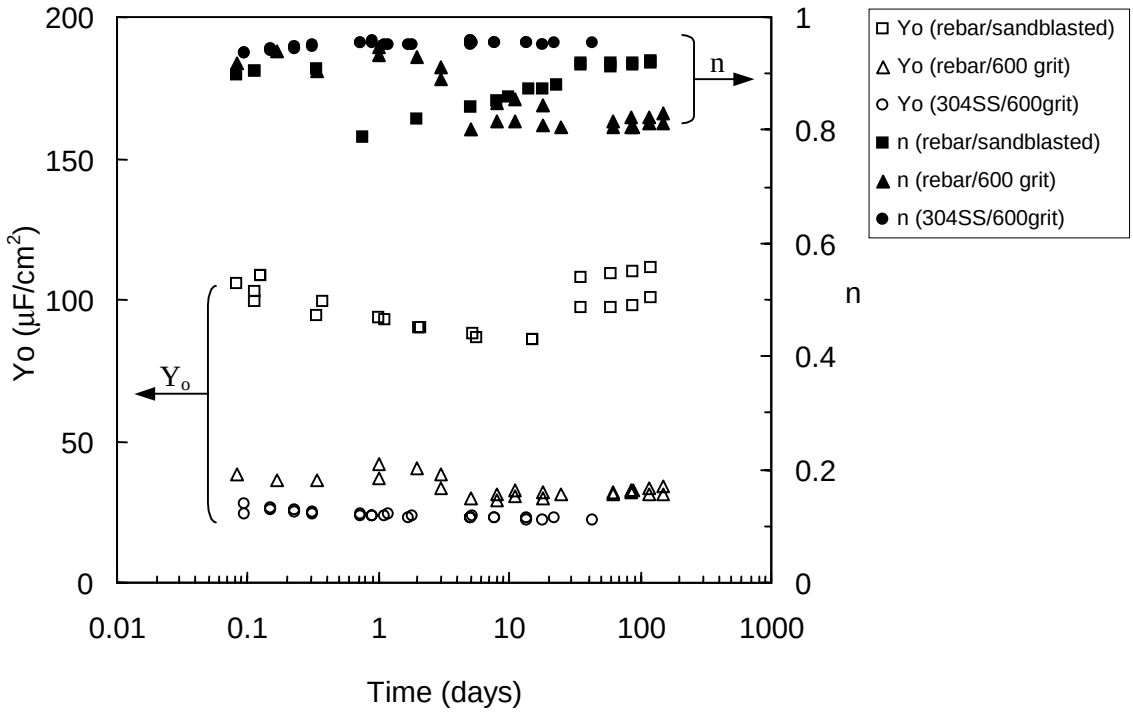

Figure 5.5 Time evolution of Y_o and n values (from EIS) of rebar steel and 304SS in SCS

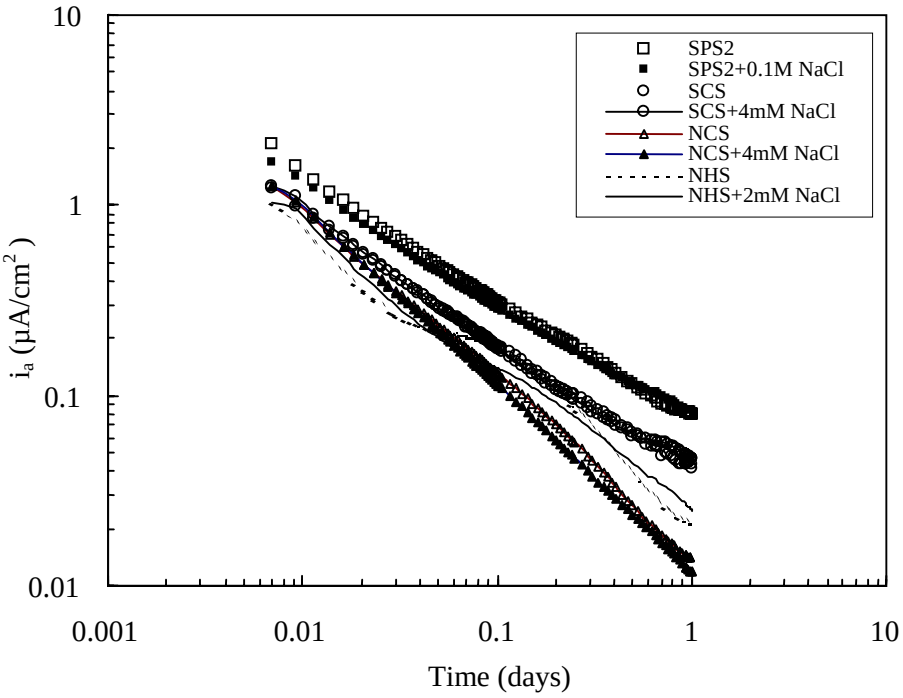

Figure 5.6 Time evolution of anodic current density of rebar steel (600 grit /50 cm^2) under potentiostatic polarization at 0V in alkaline solutions

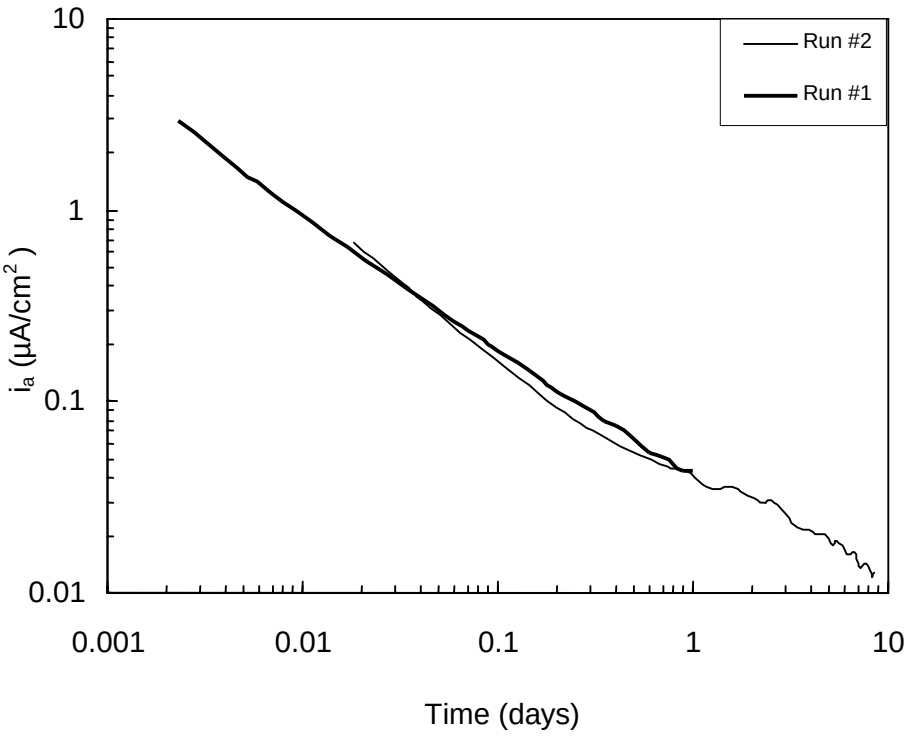

Figure 5.7 Time evolution of anodic current density of rebar steel (600 grit/50 cm^2) under potentiostatic polarization at 0V in SCS

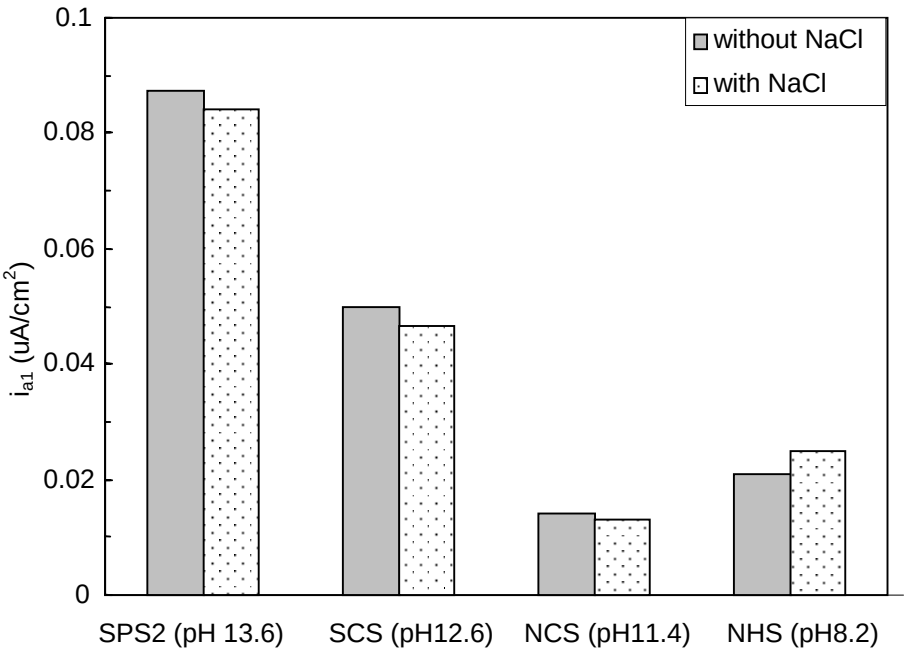

Figure 5.8 Comparison of i_{a1} (average of at least two replicates) measured on 600 grit rebar steel in four types of solutions with and without NaCl (see Figure 5.6 for chloride concentration in each solution)

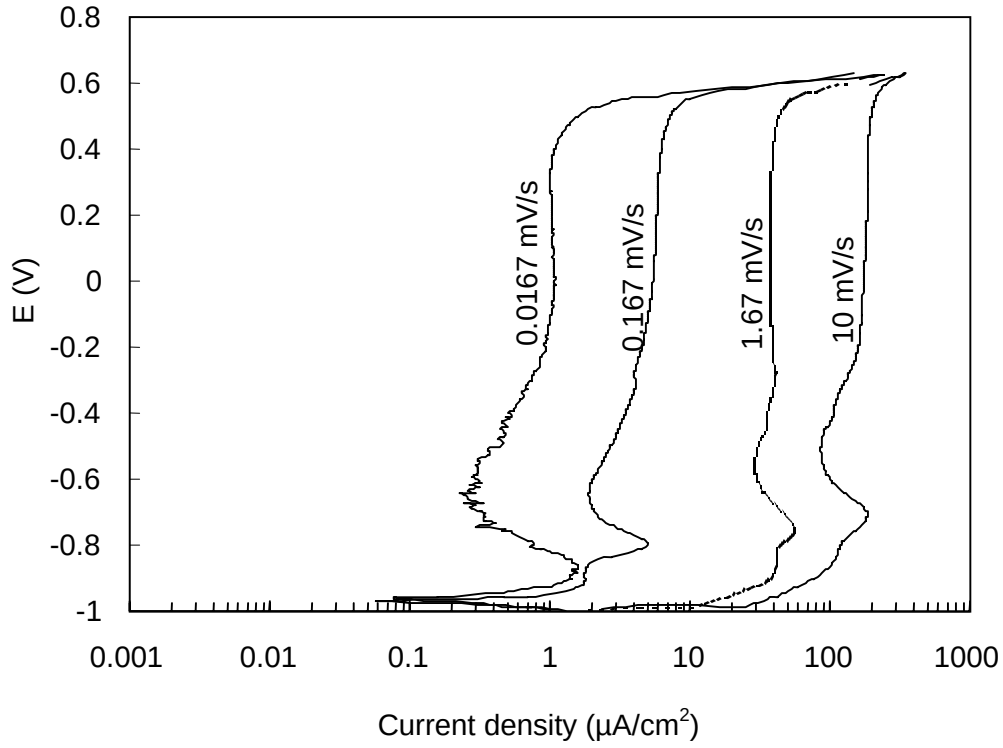

Figure 5.9 Anodic polarization curves of sandblasted rebar steel in SPS2 at different scan rates

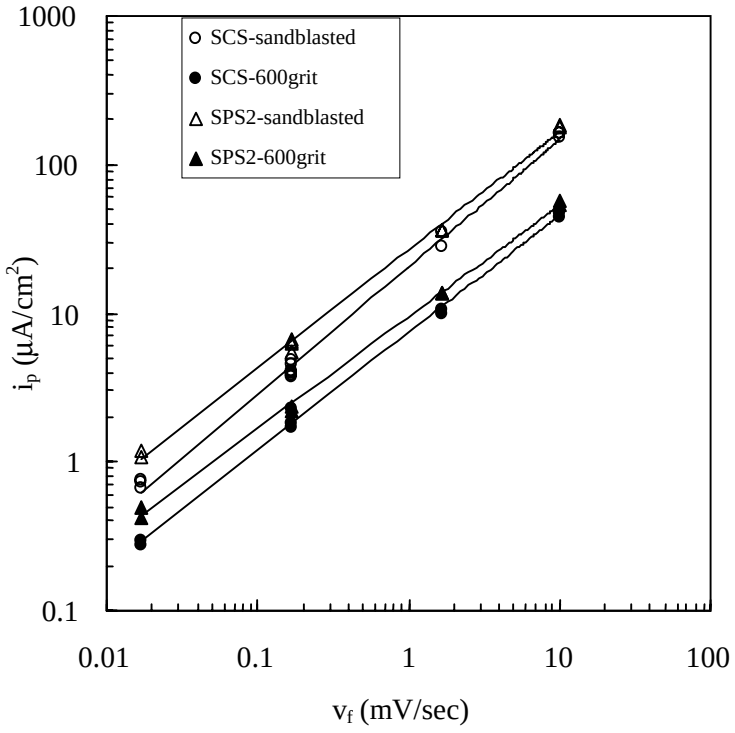

Figure 5.10 Relationship between i_p and v_f in SPS2 and SCS

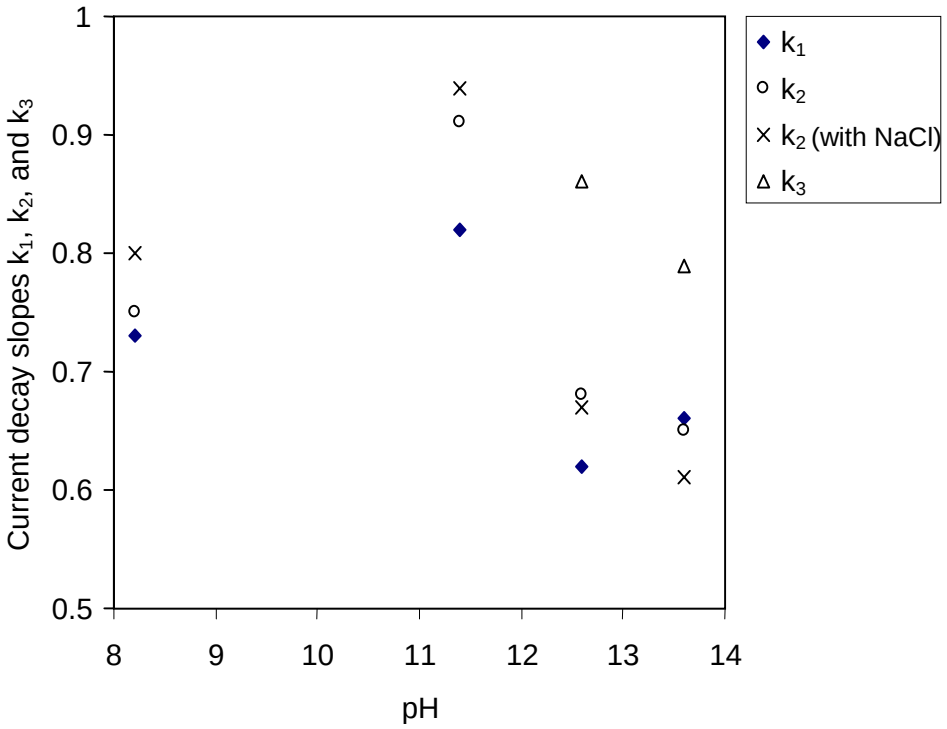

Figure 5.11 Dependence of current decay slopes for sandblasted steel on solution pH

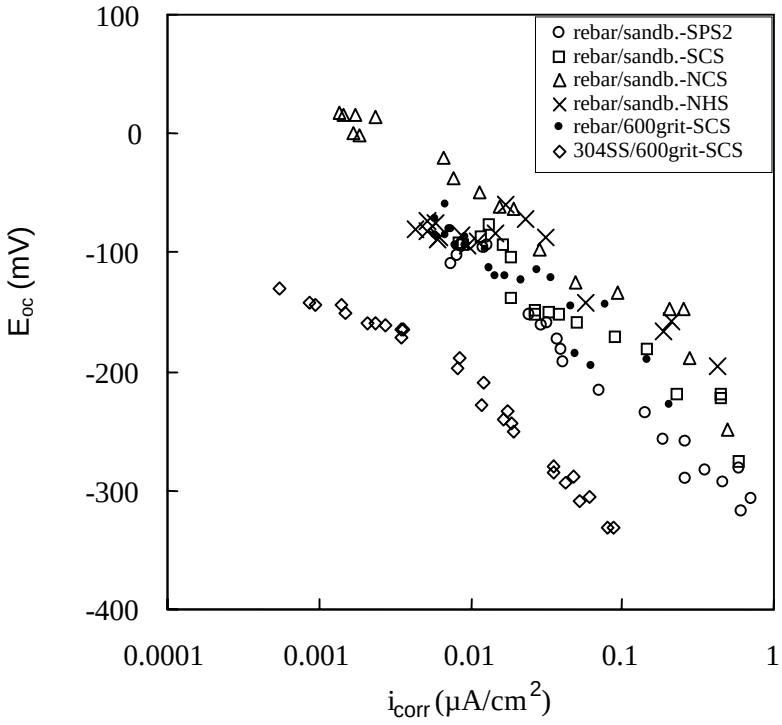

Figure 5.12 Relationship between i_{corr} and E_{oc} in SCS for different test conditions

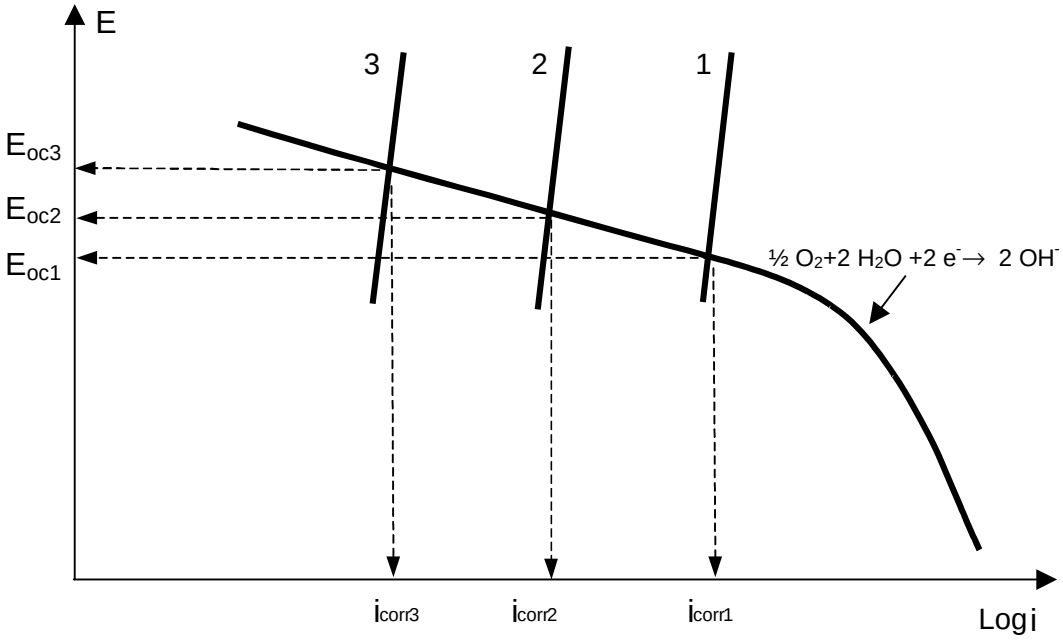

Figure 5.13 Schematic graph showing the relationship between E_{oc} and i_{corr}

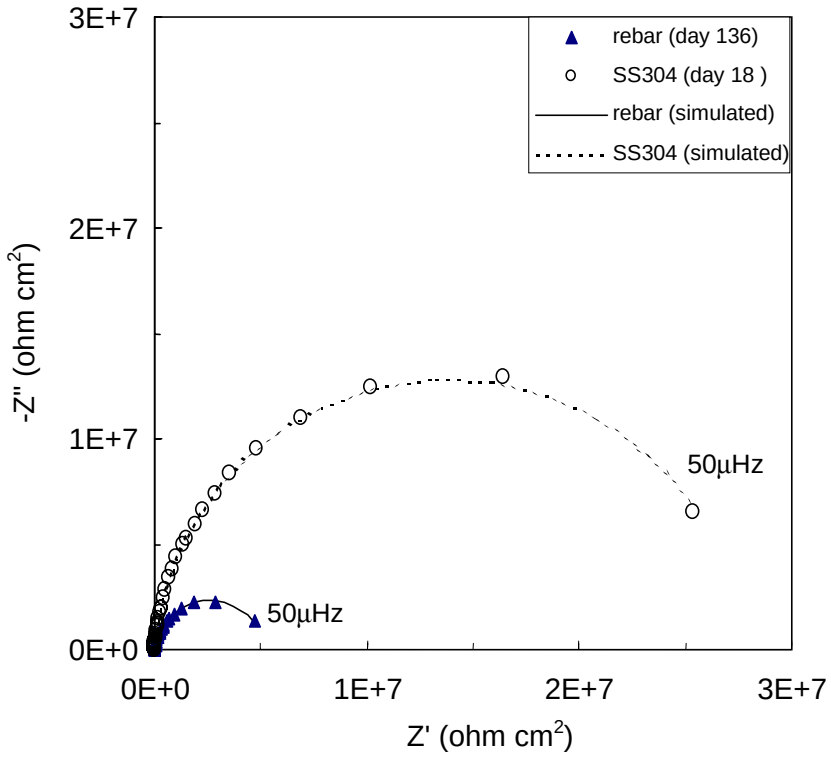

Figure 5.14 Nyquist plots of the EIS response on a sandblasted rebar specimen and a 600 grit SS304 specimen in SCS

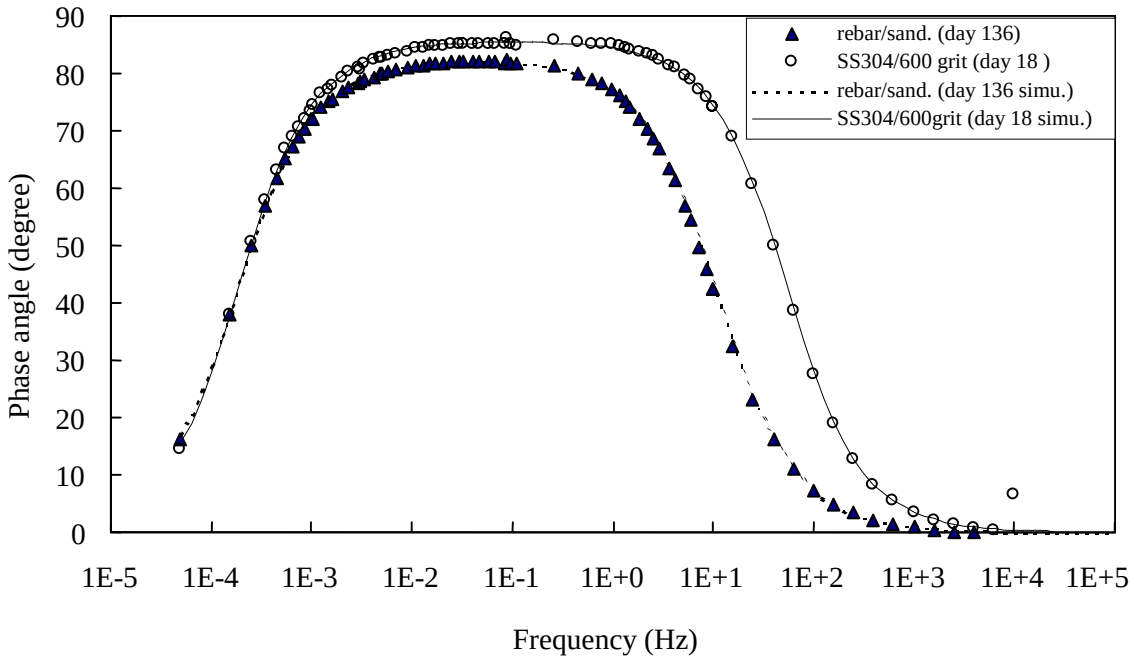

Figure 5.15 Bode phase angle plots of the EIS response on a sandblasted rebar specimen and a 600 grit SS304 specimen in SCS

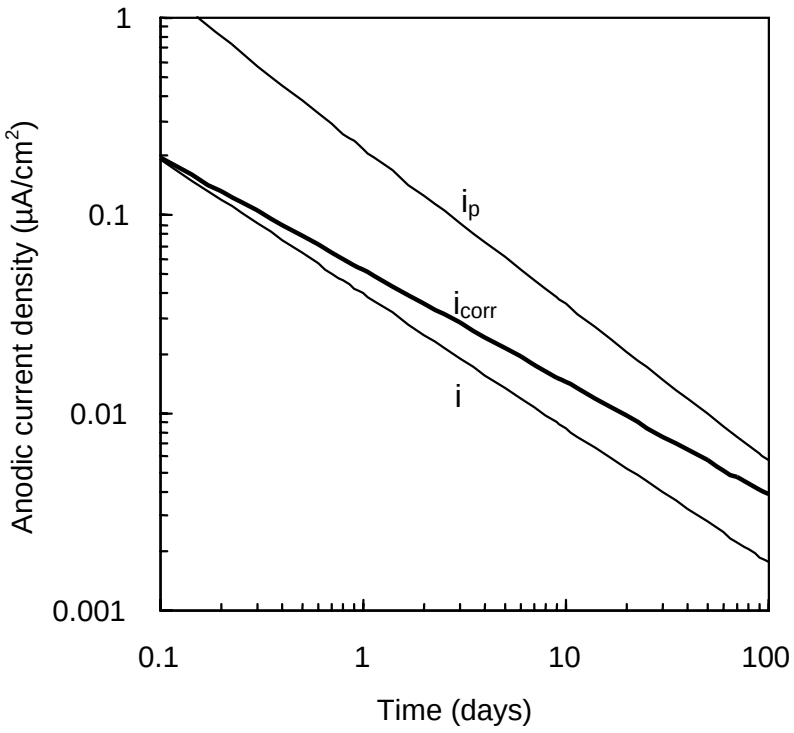

Figure 5.16 A comparison of the time evolution of i_p, i_{corr} and i_a for rebar steel (600 grit) in SCS using regression data in Tables 5.1, 5.2, and 5.3

CONCLUSIONS

1. Several important findings relevant to the pitting initiation and chloride corrosion threshold of reinforced steel in chloride-containing alkaline solutions have been obtained in this investigation. First, using a quasi-static open-circuit immersion method (OCI), the effect of metal surface condition on the chloride corrosion threshold ($[Cl_T]$) was investigated. It was found that removing mill scale or any rust from rebar surface by sandblasting was beneficial in elevating $[Cl^-]_T$. The $[Cl^-]_T$ values for sandblasted steel were about twice those of as-received or prerusted steel in all the solutions (pH12.6 SCS, pH13.3 SPS1, and pH13.6 SPS2) tested. Experimental results revealed that the threshold chloride-to-hydroxide ratio (CR_T) increased with pH, suggesting that the inhibiting effect of hydroxide ions is stronger at higher $[OH^-]$ levels. Estimated ranges of total chloride corrosion threshold in concrete (C_{TT}) based on $[Cl^-]_T$ from liquid solution measurements and on available chloride binding data included C_{TT} values observed in practice.

2. Secondly, using the cyclic polarization technique (CYP), the effect of several factors ($[Cl^-]$, pH, steel surface finish, CYP scan rate, passive film maturity) on the distribution of pitting (E_p) and repassivation (E_r) potentials was studied. It was found that E_p was not a unique function of solution composition or steel surface condition. Therefore, the behavior of E_p was considered using a statistical approach. The variability of E_p tended to decrease at high values of the ratio CR. The average value of E_p ($\underline{E}_p$) for a series of replicate tests decreased with solution $[Cl^-]$ and steel surface roughness but increased with solution $[OH^-]$ and passive film maturity. In contrast, E_r was nearly independent of solution composition and steel surface finish. Instead, E_r was influenced by the severity of corrosion that took place during the return scan of the polarization cycle. The functional form of the distribution of E_p for a given solution and steel surface condition was not clearly apparent. Results from a large series of repeat tests deviated significantly from a simple Gaussian distribution.

3. Thirdly, the effect of specimen size (varied by three orders of magnitude) on the distribution of E_p and E_r was especially studied because of its engineering significance. For most of the conditions examined, $\underline{E}_p$ was found to decrease significantly as the nominal specimen surface area increased; a slope as high as ~0.3V per area decade was observed for 600 grit steel in SCS with 0.1M and 1.0M NaCl. The variability of E_p was not strongly affected by the specimen size but increased with $\underline{E}_p$. However, E_r was independent of specimen surface area. The experimental observations were in reasonable agreement with the prediction of the stochastic pitting initiation theory.

4. Finally, the passivation behavior of reinforcing steel (and to a limited extent that of 304 stainless steel) in alkaline solutions (pH 8.2 to 13.6) was examined using several electrochemical techniques. It was found that the passivation of steel in alkaline media was a gradual process. Regardless of the electrochemical techniques being employed, the logarithm of the anodic current density (i_{corr}, i_a, or i_p) decreased nearly linearly with log(t). The steady-state i_{corr} of rebar steel in alkaline solutions was estimated to be 0.01~0.001 $\mu A/cm^2$. In comparison, the i_{corr} of 304 stainless steel in SCS was about one order of magnitude lower than that of rebar steel. The gradual passivation process of rebar steel in alkaline solutions is in agreement with the observation that E_p increased with prepassivation time.

APPLICATION OF FINDINGS AND RECOMMENDATIONS

FDOT uses the chloride ion corrosion threshold as a key parameter in assessing the time to corrosion initiation in marine substructure. The threshold value is also used to compare against the amount of chloride contamination that may exist in other cementitious media, such as the grout surrounding post-tensioned high strength steel strands. This investigation has contributed to in-depth understanding of the fundamental causes of corrosion initiation in alkaline media, focusing on the effect of the condition of the metal surface and providing ample evidence of the statistical nature of the processes involved. As a result, this work has provided important insight on how the chloride ion threshold should be considered in future design and making decisions for maintenance, repair or rehabilitation of existing structures. The following items summarize pertinent findings and specific recommendations in each case:

1. The investigation showed further evidence that the threshold should not be considered as a single value (even for a given environment, with a given steel surface in the passive condition, and at a fixed potential) but rather as a statistically distributed quantity. It is recommended that projections of time to corrosion for design purposes always include an estimate of the sensitivity of the result to variations in the threshold. Future FDOT service life prediction procedures should incorporate a threshold variability input parameter, properly accounting for amount of surface area per (2) below.

2. Larger specimen area increased the corrosion initiation probability. Future testing to determine the value of the threshold (and its variability) for a given steel and concrete combination should use a representatively large exposed steel surface area in the experiments. Otherwise, unduly optimistic estimates of the threshold may result. It is also recommended that additional work be conducted to establish a practical minimum required steel area for this purpose.

3. Corrosion in test solutions initiated at substantially lower chloride levels in rebar with mill scale (as received or prerusted) than on rebar de-scaled by sandblasting. It is recommended that exploratory cost/benefit analysis of using sandblasted metal in construction be performed

based on these results. If analysis results are favorable, tests in concrete with a sufficiently large rebar assembly should be conducted to ascertain that a threshold advantage is still attained, and that adverse effects (e.g. possible increased corrosion rate after initiation) do not cancel benefits.

4. In bare steel specimens, corrosion initiation was more difficult as the surface roughness decreased. The beneficial effect of surface smoothness should be carefully evaluated for applications where pitting initiation is of critical importance, as in high-strength steel in grout in post tensioned tendons for segmental bridges.

5. The threshold, when expressed as a [Cl-] / [OH-] ratio, was found to decrease as the pH of the medium decreased thus creating a compounded negative effect. It is recommended that concrete modifications that involve high pozzolanic content or very low alkalinity concrete be viewed with renewed caution. Reliable data on pore water pH should be obtained for any new concrete formulations considered by FDOT, and the overall effect on time to corrosion initiation should be evaluated based on combined diffusivity and threshold impact.

6. A potential dependence of the threshold (increased threshold for cathodically polarized steel) was underscored by the results from potentiodynamic testing. Special analysis should be made when attempting to project time to corrosion of portions of the rebar assembly that are significantly cathodically polarized while still passive. Data for estimating threshold change under those conditions are sparse at present but are becoming increasingly available, and should be incorporated in future FDOT procedures.

REFERENCES

1) ACI Committee 318 (1999), Building Code Requirements for Structure Concrete (318-99) and Commentary (318R-99), American Concrete Institute, Farmington Hills, p. 318/318-39

2) Agarwal, P., Crisalle, O.D., and Orazem, M. E., and Garcia-Rubio, L. H. (1995). "Application of Measurement Models to Impedance Spectroscopy, II. Determination of the Stochastic Contribution to the Error Structure ", *J. Electrochem. Soc*., 142(12), 4149-4158

3) Alonso, C, Andrade, C., Izquierdo, M., Nóvoa, X.R. and Pérez, M, C. (1998). "Effect of Protective Oxide Scales in the Macrogalvanic Behavior of Concrete Reinforcements", *Corrosion Science*, 40(8),1379-1398

4) Alvarez, M. G. and Galvele, J.R. (1984). " The Mechanism of Pitting of High Purity Iron in NaCl Solutions", *Corrosion Science*, 24(1), 27-48

5) Andrade, C. and Page, C. L. (1986). "Pore solution chemistry and corrosion in hydrated cement systems containing chloride salts: a study of cation specific effects" *Br. Corros. J*. 21(1), 49-53

6) Andrade, C. and Alonso, M.C. (1994). "Values of corrosion rate of steel in concrete to predict service life of concrete structures," in *Application of Accelerated Corrosion Tests to Service Life Prediction of Materials*, ASTM STP 1194, Eds. G. Cragnolino, N. Sridhar, Philadelphia, p.282

7) Arya, C. and Xu, Y. (1995). "Effect of Cement Type on Chloride Binding and Corrosion of Steel in Concrete", *Cement and Concrete Research*, 25(4), 893-902

8) Aziz, P.M. (1956). "Application of the Statistical Theory of Extreme Values to the Analysis of Maximum Pit Depth Data for Aluminum", *Corrosion*, 12(10), 459t-506t

9) Bakker, R. F. M. (1988). Chapter Three: Initiation Period, in *Corrosion of Steel in Concrete,* Report of the Technical Committee 60-CSC, RILEM*,* Edited by P. Schiessl, Chapman and Hall, London, p.23

10) Bamforth, P.B., and Chapman-Andrews, J.F. (1994). "Long Term Performance of R.C. Elements under U.K. Coastal Exposure Conditions", in "*Corrosion and Corrosion Protection of Steel in Concrete*", edited by R.N. Swamy, Vol. 1, Sheffield Academic Press, Sheffield, 139-156

11) Bard, A. J. and Faulkner, L. R. (1980). *Electrochemical Methods: Fundamental and Applications*, John Wiley & Sons, New York, p.8

12) Baroux, B. (1988). "The Kinetics of Pitting Generation on Stainless Steels", *Corrosion Science*, 28(10), 969-986

13) Barneyback, R. S. and Diamond, S. (1981). "Expression and Analysis of Pore Fluids from Hardened Cement Pastes and Mortars", *Cement and Concrete Research*, 11(2), 279-285

14) Bates, R.G. (1973). *Determination of pH, Theory and Practice*, 2nd edition, John Wiley & Sons

15) Bentur, A., Diamond, S., and Berke, N.S., (1997). *Steel Corrosion in Concrete: Fundeamental and Civil Engineering Practice*, E & FN SPON, London, p29

16) Berke, N. S.(1986). "The Use of Anodic Polarization to Determine the Effectiveness of Calcium Nitrate as an Anodic Inhibitor," in "*Corrosion Effect of Stray Currents and the Techniques for Evaluating Corrosion of Rebars in Concrete*", ASTM STP 906, V. Chaker, Ed., ASTM, Philadelphia, 78-91

17) Berman, H.A.(1975). "Sodium Chloride, Corrosion of Reinforcing Steel, and the pH of Calcium Hydroxide Solution", *ACI Journal*, April 1975, 150-157

18) Boukamp, B. A. (1986). " A Nonlinear Least Squares Fit Procedure for Analysis of Immittance Data of Electrochemical Systems", *Solid State Ionics*, 20, 31-44

19) Boukamp, B. A. (1988). " Equivalent Circuit, Users Manual", second, revised edition, University of Twente

20) Breit, W.(1998). "Critical Chloride Content – Investigation of Steel in Alkaline Chloride Solutions", *Materials and Corrosion*, 49, 539-550

21) British Standards Institution (1985). Structural use of concrete, part I, Code of practice for design and construction, BSI, London, BS8110

22) Broli, A. and Holton, H. (1977). " Determination of Characteristic Pitting Potentials for Aluminum by Use of the Potentiostatic Methods" *Corr. Sci*.,17(1), 59-69

23) Büchler, M, Schmuki, P., Böhni, H.(1997). "Formation and Dissolution of the Passive Film on Iron Studied by a Light Reflectance Technique", J. Electrochem. Soc., 144(7), 2307-2312

24) Burstein, G. T., and Ilevbare, G. O. (1996). " The Effect of Specimen Size on the Measured Pitting Potential of Stainless Steel", *Corrosion Science*, 38(12), 2257-2265

25) Castro, P., Sagüés, A.A, Moreno, E.I. Maldonado, L. and Genescá, J (1996) "Characterization of Activated Titanium Solid Reference Electrodes for Corrosion Testing of Steel in Concrete", *Corrosion*, 52(8), 609-617

26) Constantiner, D. and Diamond, S. (1997). "Pore Solution Analysis: Are There Pressure Effects?," in "*Mechanisms of Chemical Degradation of Cement-based Systems"*, K.L. Scrivener and J.F. Young (Eds.), E & FN SPON, London, 22-29

27) CRC (1973). *Handbook of Chemistry and Physics,* R. C. Weast Editor, CRC Press, Cleveland, p. D-114

28) Dawson, J. L. and Langford, P. E.(1988). "The Electrochemistry of Steel Corrosion in Concrete Compared to Its Response in Pore Solution," *The Use of Synthetic Environments for Corrosion Testing,* Special Technical Publication, 264-273

29) Diamond, S. (1981). "Effects of Two Danish Flyashes on Alkali Contents of Pore Solutions of Cement-Flyash Pastes", *Cement and Concrete Research*, 11(3), 383-394

30) Diamond, S., (1983). “Effects of Microsilica (Silica Fume) on Pore-Solution Chemistry of Cement Pastes”, *Communications of American Ceramic Society*, May,C82-C84

31) Diamond, S. (1986). “Chloride Concentrations in Concrete pore solutions resulting from calcium and sodium chloride admixtures”, *Cement, Concrete, and Aggregates*, CCAGDP, 8(2), 97-102

32) Duchesne, J. and Berube, M.A. (1994). “Evaluation of the Validity of the Pore Solution Expression Method from Hardened Cement Pastes and Mortars”, *Cement and Concrete Research*, 24(3),456-462

33) Dunn, D.S., Cragnolino, G.A., and Sridhar, N. (2000). “An Electrochemical Approach to Predicting Long-term Localized Corrosion of Corrosion-Resistant High-Level Waste Container Materials”, *Corrosion*, 56(1), 90-104

34) Eldredge, G. G. (1957). “ Analysis of Corrosion Pitting by Extreme-Value Statistics and its Application to Oil Well Tubing Caliper Surveys”, *Corrosion*, 13(1), 51t-60t

35) Elsener, B. and Böhni, H.(1986). “Corrosion of Steel in Mortar Studied by Impedance Measurements”, in “*Electrochemical Methods in Corrosion Research*,”, edited by M. Duprat, Vol. 8, Chapter 55, Trans Tech Publications Ltd., Switzerland, 363-372

36) Evans, U. R. (1981). *An Introduction to Metallic Corrosion*, Edward Arnold Ltd., London, p.261

37) Foley, C. L., Kruger, J. and Bechtoldt, C. J. (1967). “Electron Diffraction Studies of Active Passive, and Transpassive Oxide Films Formed on Iron”, *J. Electrochem. Soc*., 114(10), 994-1001

38) Fontana, M. G. (1986). *Corrosion Engineering*, Third Edition, McGraw-Hill, Inc, p72

39) Frankel, G. S. (1998) “Pitting Corrosion of Metals” *J. Electrochem. Soc.,* Vol. 145(6), 2186-2198

40) Ginsberg, H. and Huppatz, W. (1972). “Comparative Current Density/Potential Measurements on the Light Metal Aluminum with Special Consideration of the Passive Behavior of Aluminum and its Alloys”, Metall, 26(6), 565-575

41) Glass, G. K. and Buenfeld, N. R. (1997). “The Presentation of the Chloride Threshold Level for Corrosion of Steel in Concrete”, *Corrosion Science*, 39 (5), 1001-1013

42) Gojkovic, S. L., Zecevic, S. K., Obradovic, M.D., and Drazic, D. M. (1998). “Oxygen Reduction on a Duplex Stainless Steel”, *Corrosion Science*, 40(6), 849-860

43) Goñi, S. and Andrade, C. (1990). “Synthetic concrete pore solution chemistry and rebar corrosion rate in the presence of chlorides”, *Cement and Concrete research,* 20(4), 529-539

44) González, J. A., Otero, E. ,Feliu, S. and Lopez, W. (1993). “Initial Steps of Corrosion in the Steel? Ca(OH)2+Cl- System: The Role of Heterogeneities on the steel surface and Oxygen supply”, *Cement and Concrete Research*, 23(1), 33-40

45) Gouda, V.K.(1970). “Corrosion and Corrosion Inhibition of Reinforcing Steel. I. Immersed in Alkaline Solutions”, *Br. Corrosion. J*., 5(9),198-208

46) Hansson, C.M., and Sorenson, B.(1990). “The Threshold Concentration of Chloride in Concrete for the Initiation of Reinforcement Corrosion”, in “*Corrosion Rates of Steel in Concrete*”, Edited by N.S. Berke, V. Chaker, and D. Witting, ASTM STP 1065, 3-16

47) Haque, M. N. and Kayyali, O.A. (1995) “Free and water Soluble Chloride in Concrete”, *Cement and Concrete Research*, 25(3), 531-542

48) Haruna, T and Macdonald, D. D.(1997). “Theoretical Prediction of the Scan Rate Dependencies of the Pitting Potential and the Probability Distribution in the Induction Time”, *J. Electrochem. Soc*, 144(5), 1574-1581

49) Hausmann, D.A. (1967). “Steel Corrosion in Concrete – how does it occur?”, *Mater. Protection*, 6(11),19-23

50) Hausmann, D.A. (1998). “A probability Model of Steel Corrosion in Concrete”, *Materials Performance,* 37(10), 64-68

51) Henriksen, C.F. (1993). “Chloride Corrosion in Danish Bridge Columns”, in *“ Chloride Penetration into Concrete Structures*”, Nordic Miniseminar, edited by L.-O. Nilsson, Chalmers, Tekniska, Högskola, Göteborg, 166-182

52) Huang, Z. Q., and Ord, J. L.(1985). “An Optical Study of the Iron Electrode in Alkaline Electrolyte”, *J. Electrochem. Soc*., 132(1), pp. 24-28

53) Hussain, S. E., Al-Gahtani, A. S., and Rasheeduzzafar, (1996). “Chloride Threshold for Corrosion of reinforcement in Concrete”, ACI Materials Journal, 94(6), 534-538

54) Ilevbare, G.O., Scully, J. R., Yuan, J., and Kelly, R. G., (2000). “Inhibition of Pitting Corrosion on Aluminum Alloy 2024-T3: Effect of Soluble Chromate Addition vs Chromate Conversion Coating”, *Corrosion,* 56(3), 227-242

55) Joiret, S., Keddam, M., Perrot, H. and Takenouti, H. (1999). “Anodic Behavior of Fe in 1M NaOH in the Presence of Cl^- and NO_2^- ”, 8th International Symposium on Passivity of Metals and Semiconductors, Jasper, Canada, May 1999

56) Kawamura, M., Kayyali, O. A., and Haque, M.N. (1988). “ Effects of a Flyash on Pore Solution Composition in calcium and Sodium Chloride-bearing Mortars”,*Cement and Concrete Research,* 18(5), 763-773

57) Kayyali, O.A. and Haque, M.N. (1990). “Environmental Factor and Concentration of Cl^- and OH^- in Mortars”, *Journal of Materials in Civil Engineering*, 2(1),24-34

58) Kitowski, C.J. and Wheat, H.G.(1997). “Effect of Chlorides on Reinforcing Steel Exposed to Simulated Concrete Solutions”, *Corrosion*, 53(3), 216-226

59) Lambert, P., Page, C.L. and Vassie, P.R.W.(1991). “Investigation of Reinforcement Corrosion. 2. Electrochemical Monitoring of Steel in Chloride-contaminated Concrete”, *Mater. Struct.,* 24(143), 351-358

60) Larbi, J.A., Fraay, A.L. A., and Bijen, J.M.J.M. (1990). “The Chemistry of the Pore Fluid of Silica Fume-Blended cement Systems”, *Cement and Concrete Research*, 20(4), 506-516

61) Larramona, G. and Gutisrrez, C. (1989). " The Passive Film on Iron at pH 1-14", *J. Electrochem. Soc*., 136(8), pp. 2171-2178

62) Larsen, C. K. (1998). "Chloride Binding in Concrete: Effect of Surrounding Environment and Concrete Composition", Ph.D. Thesis, The Norwegian University of Science and Technology, Norway, November, , 24-25

63) Leckie, H. P.(1965). " A Contribution to the Applicability of Critical Pitting Potential", *J. Electrochem. Soc*., 117(9), pp. 1152-1154

64) Levy, A.V. (1991). *Wear-Corrosion Interaction in Liquid Media,* A.A. Sagüés and E.I. Meletis Editors, The Minerals, Metals & Materials Society, Warrendale, p82,

65) Li, L., Sagüés, A. A., and Poor, N. D. (1999 a). "In situ Leaching Investigation of pH and Nitrite Concentration in Concrete Pore Solution," *Cement and Concrete Research,* 29, 315-321

66) Li, L. and Sagüés, A.A. (1999 b). "Effect of Chloride Concentration on the Pitting and Repassivation Potentials of Reinforcing Steel in Alkaline Solutions", Paper No. 567, Corrosion/1999, NACE International, Houston, Texas

67) Li, L. and Sagüés, A.A. (1999 c). "Passive Film Breakdown of Steel in Simulated Concrete Pore Solution" Paper presented on the 8th International Symposium on Passivity of Metals and Semiconductors, Jasper, Alberta, Canada

68) Li, L. and Sagüés, A.A. (2000a). "Effect of the Cation ion Type on the Binding of Chloride and Nitrite in Concrete", to be submitted to *Cement and Concrete Research*

69) Li, L. and Sagüés, A.A. (2000 b). "Effect of Metal Surface Condition on the Chloride Corrosion Threshold of Reinforcing Steel in Alkaline Solutions", Paper No. 801, Corrosion/2000, NACE International, Houston, Texas

70) Li, L. and Sagüés, A.A. (2000 c). "Chloride Corrosion Threshold of Reinforcing Steel in Alkaline Solutions: I. Open-circuit Immersion Tests", Submitted to *Corrosion*

71) Lizlovs, E.A. and Bond, A.P. (1975). "An Evaluation of Some Electrochemical Techniques for the Determination of Pitting Potentials of Stainless Steel", 31(6), 219-222

72) Locke, C.E. and Siman, A. (1980). "Electrochemistry of Reinforcing Steel in Salt Contaminated Concrete", in "*Corrosion of Reinforcing Steel in Concrete*", edited by D.E. Tonini and J.M. Gaidis, ASTM STP 713, 3-16

73) Lukas, W. (1985). "Relationship between Chloride Content in Concrete and Corrosion in Untensioned Reinforcement on Austrian Bridges and Concrete Road Surfacings", *Betonwerk und Fertigteil-Technik*, 51(11),730-734

74) Macdonald, D.D., and Roberts, B. (1978). "A Potentiostatic Transient Study of The Passivation of Carbon Steel in 1M NaOH", *Electrochimica Acta*, 23, 557-564

75) Mammoliti, L. T., Brown, L. C., Hansson, C. M. and Hope. B. B. (1996). "The Influence of Surface Finish of Reinforcing Steel and pH of the Test Solution on the Chloride Threshold

Concentration for Corrosion Initiation in Synthetic Pore Solutions" *Cement and Concrete Research*, 26(4), 545-550

76) Manning, P.E. (1980). "The Effect of Scan Rate on Pitting Potentials of High Performance Alloys in Acidic Chloride Solution", *Corrosion*, 36(9),468-474

77) Manning, P.E., Duquette, D.J. and Savage, W.F.(1979). " The Effect of Test Method and Surface Condition on Pitting Potential of Single and Duplex Phase 304L Stainless Steel", *Corrosion*, 35(4),151-157

78) Mears, R. B. and Brown, R. H. (1937). "Corrosion Probability", *Industrial and Engineering Chemistry*, 29(10), 1087-1091

79) Mehta, P. K. and Monteiro, P. J. M. (1993). *Concrete: Structure, Properties, and Materials*, Second Edition, Prentice-Hall, Inc., Englewood Cliffs, p.24

80) Mindness, S. and Young, J. F. (1981). *Concrete*, Prentice-Hall, Inc., Englewood Cliffs

81) Oranowska, H. and Szklaska-Smialowska, Z. (1981). " An electrochemical and ellipsometric investigation of surface film grown on iron in saturated calcium hydroxide solutions with or without chloride ions", *Corrosion Science*, 21(11), 735-747

82) Orazem, M. E., Wojcik, P. T., Durbha, M., Frateur, I. And Garcia-Rubio, L. H. (1998). "Application of Measurement Models for Interpretation of Impedance Spectra for Corrosion", *Materials Science Forum*, Vols. 298-292, 813-828

83) Page, C.L. and Treadaway, K.W.J.(1982). "Aspects of the Electrochemistry of Steel in Concrete" Nature 297(13), 109-115

84) Page, C. L. and Vennesland, Ø. (1983). "Pore Solution Composition and Chloride Binding Capacity of Silica-fume Cement Pastes", *Mater. Struct*.,16(91),19-25

85) Page, C.L., Short, N.R. and Holden, W.R.(1986). "The Influence of Different Cements on Chloride-Induced Corrosion of Reinforcing Steel", *Cement and Concrete Research*. 16(1), 79-86

86) Pedeferri, P. (1996). "Cathodic protection and cathodic prevention", Construction and Building Materials, 10(5), 391-402

87) Pettersson, K.(1993). "Chloride Threshold Value and Corrosion Rate in Reinforced Concrete", in "*Concrete 2000*", edited by R.K. Dhir and M.R. Jones, Vol. 1, E & FN Spon, London, 461-471

88) Pourbaix, M., Klimzack-Mathieiu, L., Mertens, Ch., Meunier,J., Vanleugenhaghe,Cl., Munick,L., Laureys,J. Needlemans, L., and Warzee, M. (1963). "Potentiokenetic and Corrosimetric Investigations of the Corrosion Behavior of Alloy Steels" *Corrosion Science*, Vol. 3, 239-259,

89) Pourbaix, M. (1966). *Atlas of Electrochemical Equilibria in Aqueous Solutions*, Pergamon Press, Cebelcor, Brussels, 97-105

90) Rasheeduzzafar, Hussain, S. E., and Al-Saadoun, S. S. (1992). "Effect of Tricalcium Aluminate Content of Cement on Chloride Binding and Corrosion of Reinforcing Steel in Concrete", *ACI Materials Journal,* 89 (1), 3-12

91) Ratliff, J. L. and Norman, D.W. (1975). “Corrosion Behavior of Reinforcing Steel in Concrete and Automated Monitoring Systems for Corrosion Detection and Corrosion Control”, Report to The Florida Department of Transportation, University of South Florida

92) Sagüés, A. A. and Li, L. (2000). Unpublished data, University of South Florida

93) Sagüés, A. A., Perez-Duran, H.M. and Powers, R.G. (1991), “Corrosion Performance of Epoxy-coated Reinforcing Steel in Marine Substructure Service”, *Corrosion*, 47(11), 884-893

94) Sagüés, A.A. (1993). “Corrosion Measurement Techniques for Steel in Concrete” Paper No. 353, Corrosion/1993, NACE International, Houston, Texas

95) Sagüés, A. A. (1994). “Performance of Galvanized Rebars in Marine Substructure Service, Project ZE-418-Part 1”, Final Report to International lead and Zinc Research Organization, University of South Florida

96) Salvago, G. and Fumagalli, G. (1995). “The Distribution of the Breakdown Potential of Stainless Steels: Effects of Test Repetition, Specimen Exposure Surfaces and Threshold Current”” *Corrosion Science*, 37(8), 1303-1312

97) Sepa, D. B. and Vojnovic, M. V. (1980). “Kinetics and Mechanism of O_2 Reduction at Pt in Alkaline Solutions”, *Electrochimica Acta*, 25, 1491-1496

98) Schiessl, P. (1988). *Corrosion of Steel in Concrete,* Report for the Technical Committee 60-CSC, RILEM, Chapman and Hall Ltd., London, p.10

99) Schiessl, P. and Raupach, M.(1990). “The Influence of Concrete Composition and Microclimate on the Critical Chloride Content in Concrete”, in “*Corrosion of Reinforcement in Concrete*”, edited by C. L. Page, K.W.J. Treadaway and P.B. Bamforth, Elsevier Applied Science, London, 49-58

100) Schwenk, W. (1964). “Theory of Stainless Steel Pitting” *Corrosion*, 20(4), 129t-137t

101) Shibata, T. and Takeyama, T. (1977). “Stochastic Theory of Pitting Corrosion”, *Corrosion*, 33(7), 243-251

102) Shibata, T. (1982). “Surface Area Dependence of Pitting Potential”, *Boshoku Gijutsu,* 31(10), 643-649

103) Shibata, T. (1996). “1996 W. R. Whitney Award Lecture: Statistical and Stochastic Approaches to Localized Corrosion”, *Corrosion*, 52(11), 813-830

104) Sincich, T. (1996). Business Statistics by Example, 5th edition, Prentice-Hall Inc., New Jersey, 273-275

105) Stern, M. and Geary, A. L. (1957). J*. Electrochem. Soc.,* 104, 56

106) Stewart, J. and Williams, D. E. (1992). “The Initiation of Pitting Corrosion on Austentic Stainless Steel: On the Role and Importance of Sulfide Inclusions”, *Corrosion Science*, 33(3), 457-474

107) Stratful, R.F., Jurkovich, W.J. and Spellman, D.L., (1975). “Corrosion Testing of Bridge Decks”, *Transportation Research Record*, No. 539, 363-372

108) Szauer, T. and Jakobs, J. (1976). “The Pitting Corrosion of Low Alloy And Mild Steels”, *Corrosion Science*, 16, 945-949

109) Szklarska-Smialowska, Z.(1972). “Influence of Sulfide Inclusions on the Pitting Corrosion of Steels”, *Corrosion*, 28(10), 388-396

110) Szklarska-Smialowska, Z.(1986). *Pitting Corrosion of Metals*, National Association of Corrosion Engineers, Houston, Texas

111) Thangavel, K. and Rengaswamy, N. S. (1998). “Relationship between Chloride/ Hydroxide Ratio and Corrosion Rate of Steel in Concrete” *Cement and Concrete Composites*, 20, 283-292

112) Thomas, M.D.A., Matthews, J.D. and Haynes, C.A. (1990). “Chloride Diffusion and Reinforcement Corrosion in Marine exposed Concretes Containing Pulverised fuel Ash”, in “*Corrosion of Reinforcement in Concrete*”, edited by C. L. Page, K.W.J. Treadaway and P.B. Bamforth, Elsevier Applied Science, London, 198-212

113) Thomas, M. (1996). “Chloride Thresholds in Marine Concrete”, *Cement and Concrete Research*, 26 (4), 513-519

114) Thompson, N.G. and Syrett, B.C., (1992). “Relationship between Conventional Pitting and Protection Potentials and a New, Unique Pitting Potential,” *Corrosion*, 48(8), 649-659

115) Transportation Research Board (1991). Highway Deicing: Comparing salt and Calcium Magnesium Acetate, Special Report 235, National Research Council, Washington, DC.

116) Treadaway, K.W.J., Cox, R.N. and Brown, B.L. (1989). “Durability of Corrosion Resisting Steels in Concrete”, *Proc. Inst. Civil Eng. (London)*., Part I, V.86, pt 1, 305-331

117) Tritthart, J. (1989). “Chloride Binding in Concrete. II. The influence of the Hydroxide Concentration in the Pore Solution of Hardened Cement Paste on Chloride Binding”, *Cement and Concrete Research*, 19(5), 683-691

118) Tuutti, K. (1982). *Corrosion of Steel in Concrete*, Swedish Cement and Concrete Research Institute, Document Publisher, Stockholm, 17

119) Tuutti, K.(1993). “Effect of Cement Type and Different Additions on Service Life”, in “*Concrete 2000*”, edited by R.K. Dhir and M.R. Jones, Vol. 2, E & FN Spon, London, 1285-1295

120) Vassie, P. (1984). “Reinforcement Corrosion and the Durability of Concrete Bridges”, in *Proc. Inst. Civil Enginers*., Part I, 76, 713-723

121) Venu, K., Balakrishnan K. and Rajagopalan, K.S. (1965). “A Potentiostatic Polarization Study of the Behavior of Steel in NaOH-NaCl System”, *Corrosion Science*, 5(5), 59-69

122) Videm, K. (1999). “The Anodic Behavior of Iron and Steel in Synthetic Concrete Pore Water and in Cement Mortar”, Corrosion/99, NACE International, Paper No.573

123) Wilde, B.E.(1972). “A critical Appraisal of Some Popular Laboratory Electrochemical Tests for Prediction the Localized Corrosion Resistance of Stainless Alloys in Sea Water”, *Corrosion*, 28(8),283-291

124) Yonezawa, T., Ashworth, V., and Procter, R. P. M. (1988). “Pore Solution Composition and Chloride Effects on the Corrosion of Steel in Concrete”, *Corrosion Science*, 44(7), 489-499

125) Zakroczymski, T., Fan, C., Szklarska-Smialowska, Z. (1985). “ Passive Film Formation on Iron and Film Breakdown in a Sodium Hydroxide Containing Chloride Ions”, *J. Electrochem. Soc.,* 132(12), 2868-2871

126) Zecevic, S., Drazic, D. M., and Gojkovic, S. (1987). “Oxygen reduction on Iron: I. In the Near Neutral Solutions”, *J. Serb. Chem. Soc*., 52(11), 649-660

List of Symbols

ATR	activated titanium reference electrode
B	Stern-Geary constant
C_T	total chloride content in paste, mortar, or concrete (wt% of cement)
C_{TT}	threshold total chloride in paste, mortar, or concrete (by wt% of cement)
CR	chloride-to-hydroxide ratio (=$[Cl^-]/[OH^-]$)
CR_T	threshold chloride-to-hydroxide ratio (=$[Cl^-]_T/[OH^-]$)
$[Cl^-]$	chloride concentration in solution (mol/L)
$[Cl^-]_f$	chloride concentration in pore water of concrete, mortar, or paste (mol/L)
$[Cl^-]_T$	threshold chloride concentration in solution (mol/L)
CPE	constant phase-angle element
CYP	cyclic polarization
E	potential (mV, or V vs. SCE)
E_{OE}	oxygen evolution potential (mV, or V vs. SCE)
E_{oc}	open-circuit potential (mV, or V vs. SCE)
$\underline{E}_{oc}$	average of open-circuit potential (mV, or V vs. SCE)
E_p	pitting potential (mV, or V vs. SCE)
$\underline{E}_p$	average of pitting potential (mV, or V vs. SCE)
E_{pl}	limiting pitting potential (mV, or V vs. SCE)
E_r	repassivation potential (mV, or V vs. SCE)
$\underline{E}_r$	average of repassivation potential (mV, or V vs. SCE)
EIS	electrochemical impedance spectroscopy
g(t)	pitting generation rate per unit area and unit time
i	current density ($\mu A/cm^2$)
i_{corr}	nominal corrosion current density ($\mu A/cm^2$)
i_{corr1}	projected i_{corr} value at t = 1 day ($\mu A/cm^2$)

i_a	anodic current density during potentiostatic polarization ($\mu A/cm^2$)
i_{a1}	projected i_a value at t = 1 day ($\mu A/cm^2$)
i_p	plateau passive current density ($\mu A/cm^2$)
i_{p1}	projected i_p value at t = 1 day ($\mu A/cm^2$)
k_1	decay slope of i_{corr} with time
k_2	decay slope of i_a with time
k_3	decay slope of i_p with time
k_w	dissociation constant of water
LPR	linear polarization resistance
M	molar concentration of species in solution (mol/L)
NCS	0.1M Na_2CO_3 solution (pH = 11.4)
NHS	0.2M $NaHCO_3$ solution (pH = 8.2)
OCI	open-circuit immersion
$[OH^-]$	hydroxide concentration in solution (mol/L)
p	pitting probability
P	survival probability
PDP	potentiodynamic polarization
PP	cumulative pitting probability
PSP	potentiostatic polarization
R_p	polarization resistance ($\Omega \cdot cm^2$)
R_s	solution resistance (Ω)
RP	cumulative repassivation probability
S	nominal exposed surface area of a specimen (cm^2)
SCE	saturated calomel electrode
SCS	saturated calcium hydroxide solution

SPS	simulated concrete pore solution
SPS1	simulated concrete pore solution of pH13.3
SPS2	simulated concrete pore solution of pH13.6
SPS3	simulated concrete pore solution of pH13.1
SPS4	simulated concrete pore solution of pH11.6
SS	sum of the weighted squares of errors
t	time (day, hour, or second)
t_{pp}	prepassivation time (day)
v_f	anodic polarization scan rate, in mV/sec
w/c	water-to-cement ratio
Z	electrochemical impedance
|Z|	magnitude of electrochemical impedance
Z’	real part of electrochemical impedance
Z”	imaginary part of electrochemical impedance
γ	activity coefficients of OH^- ions
$\omega(t)$	elementary pitting probability
σ	standard deviation of E_p (mV or V)

CONVERSION FACTORS, US CUSTOMARY TO METRIC UNITS

Multiply	*by*	*to obtain*
inch	25.4	mm
foot	0.3048	meter
square inches	645	square mm
cubic yard	0.765	cubic meter
pound/cubic yard	0.593	kg/cubic meter
gallon/cubic yard	4.95	liter/cubic meter
standard cubic feet/hour	466.67	ml/minute
ounces	28.35	gram
pound	0.454	kilogram
pound (lb)	4.448	newtons
kip (1000 lb)	4.448	kilo Newton (kN)
pound/in^2	0.0069	MPa
kip/in^2	6.895	MPa
ft-kip	1.356	kN-m
in-kip	0.113	kN-m